White Rose Research Online

eprints@whiterose.ac.uk
https://eprints.whiterose.ac.uk
Universities of Leeds, Sheffield and York

Deposited via The University of Sheffield.

White Rose Research Online URL for this paper:
https://eprints.whiterose.ac.uk/id/eprint/201830/

Version: Published Version

Article:
Aad, G., Abbott, B., Abbott, D.C. et al. (2023) Inclusive and differential cross-sections for dilepton tt¯ production measured in s√ = 13 TeV pp collisions with the ATLAS detector. Journal of High Energy Physics, 2023. 141.

https://doi.org/10.1007/jhep07(2023)141

Reuse
This article is distributed under the terms of the Creative Commons Attribution (CC BY) licence. This licence allows you to distribute, remix, tweak, and build upon the work, even commercially, as long as you credit the authors for the original work. More information and the full terms of the licence here:
https://creativecommons.org/licenses/

Takedown
If you consider content in White Rose Research Online to be in breach of UK law, please notify us by emailing eprints@whiterose.ac.uk including the URL of the record and the reason for the withdrawal request.

UNIVERSITY OF LEEDS
University of Sheffield
UNIVERSITY of York

Published for SISSA by Springer

Received: March 28, 2023
Accepted: June 9, 2023
Published: July 17, 2023

Inclusive and differential cross-sections for dilepton $t\bar{t}$ production measured in $\sqrt{s} = 13\,\text{TeV}$ pp collisions with the ATLAS detector

The ATLAS collaboration

E-mail: atlas.publications@cern.ch

Abstract: Differential and double-differential distributions of kinematic variables of leptons from decays of top-quark pairs ($t\bar{t}$) are measured using the full LHC Run 2 data sample collected with the ATLAS detector. The data were collected at a pp collision energy of $\sqrt{s} = 13\,\text{TeV}$ and correspond to an integrated luminosity of $140\,\text{fb}^{-1}$. The measurements use events containing an oppositely charged $e\mu$ pair and b-tagged jets. The results are compared with predictions from several Monte Carlo generators. While no prediction is found to be consistent with all distributions, a better agreement with measurements of the lepton p_{T} distributions is obtained by reweighting the $t\bar{t}$ sample so as to reproduce the top-quark p_{T} distribution from an NNLO calculation. The inclusive top-quark pair production cross-section is measured as well, both in a fiducial region and in the full phase-space. The total inclusive cross-section is found to be

$$\sigma_{t\bar{t}} = 829 \pm 1\,(\text{stat}) \pm 13\,(\text{syst}) \pm 8\,(\text{lumi}) \pm 2\,(\text{beam})\ \text{pb},$$

where the uncertainties are due to statistics, systematic effects, the integrated luminosity and the beam energy. This is in excellent agreement with the theoretical expectation.

Keywords: Hadron-Hadron Scattering, Top Physics

ArXiv ePrint: 2303.15340

Open Access, Copyright CERN,
for the benefit of the ATLAS Collaboration.
Article funded by SCOAP^3.

https://doi.org/10.1007/JHEP07(2023)141

JHEP07(2023)141

Contents

1 Introduction **2**

2 ATLAS detector **3**

3 Data and simulated event samples **3**
- 3.1 $t\bar{t}$ signal samples 4
- 3.2 Wt samples 5
- 3.3 Other background samples 5

4 Object reconstruction and event selection **6**

5 Data-driven background estimates and efficiency corrections **8**

6 Cross-section determination **12**
- 6.1 Differential fiducial cross-sections 13
- 6.2 Total fiducial cross-section 14
- 6.3 Total inclusive cross-section 15
- 6.4 Validation of the analysis method 16

7 Systematic and statistical uncertainties **16**
- 7.1 Detector-related uncertainties 17
- 7.2 Top-quark pair modelling uncertainties 17
- 7.3 Background modelling uncertainties 18
- 7.4 Luminosity and beam energy 19

8 Results **21**
- 8.1 Total inclusive cross-section 21
- 8.2 Differential cross-section 21
- 8.3 Comparison with predictions 31

9 Conclusion **32**

A Tables with detailed results **35**

The ATLAS collaboration **58**

JHEP07(2023)141

1 Introduction

The top quark is the heaviest known elementary particle and studying its properties is a major goal of the ATLAS experiment [1–3] at the Large Hadron Collider (LHC). Precise measurements of top-quark pair production in high-energy proton-proton (pp) collisions provide sensitive probes of quantum chromodynamics (QCD), particularly parton distribution functions (PDFs). For the measurement of the top-quark pair production cross-section, the decay channel $t\bar{t} \to W^+W^-b\bar{b}$ with subsequent leptonic decays of the W bosons is of particular interest since, compared to the hadronic channels, it is minimally affected by QCD modelling uncertainties. Previous ATLAS measurements of lepton cross-sections based on events containing an $e\mu$ pair with opposite electric charges and one or two b-tagged jets (jets likely to originate from a b-quark) include measurements using pp collision events at centre-of-mass energies $\sqrt{s} = 7$–8 TeV [4, 5] and $\sqrt{s} = 13$ TeV [6]. The latter measurement was based on data collected during 2015–16, corresponding to an integrated luminosity of 36 fb^{-1}. The same analysis technique is applied here to the entire 13 TeV data sample from LHC Run 2, corresponding to an integrated luminosity of 140 fb^{-1}. Similar measurements have also been performed by the CMS Collaboration at $\sqrt{s} = 13$ TeV [7–9].

The large integrated luminosity of the Run 2 data sample allows the lepton differential distributions to be measured over a wider range and with finer granularity than in ref. [6]. The differential distributions of eight kinematic variables of the two leptons are studied:

- p_{T}^{ℓ}, the single-lepton transverse momentum[1] ($\ell = e$ or μ);
- $|\eta^{\ell}|$, the single-lepton pseudorapidity;
- $m^{e\mu}$, the $e\mu$ system invariant mass;
- $p_{\mathrm{T}}^{e\mu}$, the $e\mu$ system transverse momentum;
- $|y^{e\mu}|$, the $e\mu$ system rapidity;
- $E^{e} + E^{\mu}$, the sum of lepton energies;
- $p_{\mathrm{T}}^{e} + p_{\mathrm{T}}^{\mu}$, the scalar sum of lepton transverse momenta;
- $|\Delta\phi^{e\mu}|$, the azimuthal angular separation of the leptons.

Both the absolute differential cross-sections and the normalised distributions of these variables, defined at particle level, are presented in a fiducial region given by $p_{\mathrm{T}}^{\ell} > 27$ (25) GeV for the leading (sub-leading) lepton and $|\eta^{\ell}| < 2.5$ after applying the overlap removal procedure described in section 4. Four double-differential distributions are measured as well: $|y^{e\mu}|$ in bins of $m^{e\mu}$, and $|\Delta\phi^{e\mu}|$ in bins of $m^{e\mu}$, $p_{\mathrm{T}}^{e\mu}$ and $E^{e} + E^{\mu}$.

[1] ATLAS uses a right-handed coordinate system with its origin at the nominal interaction point (IP) in the centre of the detector and the z-axis along the beam pipe. The x-axis points from the IP to the centre of the LHC ring, and the y-axis points upwards. Cylindrical coordinates (r, ϕ) are used in the transverse plane, ϕ being the azimuthal angle around the z-axis. The pseudorapidity is defined in terms of the polar angle θ as $\eta = -\ln\tan(\theta/2)$. Angular distance is measured in units of $\Delta R \equiv \sqrt{(\Delta\eta)^2 + (\Delta\phi)^2}$.

JHEP07(2023)141

The differential and double-differential distributions are compared with predictions from various models of top-quark production in pp collisions and can later be used to constrain model parameters, such as the strong coupling constant α_s, the top-quark mass m_t or the PDFs [6, 8].

The inclusive cross-section for the production of top-quark pairs decaying into an oppositely charged $e\mu$ pair in the fiducial region is also measured, as well as the total inclusive $t\bar{t}$ cross-section. These measurements make use of recent updates to the luminosity determination and a significant reduction in the luminosity uncertainty at Run 2 [10].

2 ATLAS detector

The ATLAS experiment at the LHC is a multipurpose particle detector with a forward-backward symmetric cylindrical geometry and a near 4π coverage in solid angle. It consists of an inner tracking detector surrounded by a thin superconducting solenoid providing a 2 T axial magnetic field, electromagnetic and hadron calorimeters, and a muon spectrometer.

The inner tracking detector covers the pseudorapidity range $|\eta| < 2.5$. It consists of silicon pixel, silicon microstrip, and transition radiation tracking detectors.

Lead/liquid-argon (LAr) sampling calorimeters provide electromagnetic (EM) energy measurements with high granularity. A steel/scintillator-tile hadron calorimeter covers the central pseudorapidity range ($|\eta| < 1.7$). The endcap and forward regions are instrumented with LAr calorimeters for both the EM and hadronic energy measurements up to $|\eta| = 4.9$.

The muon spectrometer surrounds the calorimeters and is based on three large superconducting air-core toroidal magnets with eight coils each. The field integral of the toroids ranges between 2.0 and 6.0 T m across most of the detector. The muon spectrometer includes a system of precision tracking chambers, and fast detectors for triggering.

A two-level trigger system is used to select events. The first-level trigger is implemented in hardware and uses a subset of the detector information to accept events at a rate below 100 kHz. This is followed by a software-based trigger that reduces the accepted event rate to 1 kHz on average depending on the data-taking conditions. An extensive software suite [11] is used in data simulation, in the reconstruction and analysis of real and simulated data, in detector operations, and in the trigger and data acquisition systems of the experiment.

3 Data and simulated event samples

For this analysis, proton-proton collision events collected during Run 2 of the LHC (2015–2018) with the ATLAS detector are required to pass the single-electron or single-muon triggers [12–14], which are highly efficient for leptons with $p_{\mathrm{T}}^{\ell} > 27$ GeV. After all quality criteria [15] have been applied, the data recorded in Run 2 correspond to an integrated luminosity of 140 fb^{-1} with an uncertainty of 0.83% [10].

To aid the analysis, simulated Monte Carlo (MC) samples were produced using either the full ATLAS detector simulation [16] based on the GEANT4 framework [17] or, for the estimation of some of the systematic uncertainties, a faster simulation with parameterised showers in the calorimeters [18].

JHEP07(2023)141

The effect of multiple interactions in the same and neighbouring bunch crossings (pileup) was modelled by overlaying each hard-scattering event with inelastic pp collisions generated with Pythia 8.186 [19] using the NNPDF2.3 set of PDFs [20] and the A3 set of tuned parameters [21]. The EvtGen 1.6.0 program [22] is used for properties of the bottom and charm hadron decays.

3.1 $t\bar{t}$ signal samples

The nominal sample used to model $t\bar{t}$ events was produced using the next-to-leading-order (NLO) matrix element generator Powheg Box [23–26] with the NNPDF3.0 PDF set [27], interfaced to Pythia 8.230 [28, 29] with the A14 tune [30] and the NNPDF2.3 PDF sets [20] for the underlying event, parton shower and fragmentation. The h_{damp} parameter was set to $1.5 \cdot m_t$ [31], with m_t set to 172.5 GeV, and both the renormalisation scale $\mu_{\text{r}}^{\text{default}}$ and the factorization scale $\mu_{\text{f}}^{\text{default}}$ were set equal to the top-quark transverse mass.[2]

Several modifications of Powheg+Pythia 8.230 are used to assess systematic uncertainties arising from assumptions in the simulation. Variations in the level of initial-state radiation (ISR) are performed by using the internal "Var3cUp" ("Var3cDown") weight [30] together with the renormalisation (μ_{r}) and factorisation (μ_{f}) scales set to half (twice) the default values. In two additional samples, the same configurations adopted for the ISR variation sample are used together with a change in the h_{damp} parameter (doubled to be $3.0 \cdot m_t$) [32]. These new samples are labelled "Rad up" and "Rad down" and used only in the generator-data comparison. Final-state radiation (FSR) is varied by changing the $\alpha_{\text{s}}^{\text{FSR}}$ parameter, controlling the FSR emissions in Pythia 8.230. The PDF uncertainties are estimated with the 30 components of the Hessian PDF4LHC15 error set [33–35].

The uncertainty associated with the matrix element generation is estimated using MadGraph5_aMC@NLO [36] interfaced with Pythia 8.230 as an alternative generator, with the A14 tune and the NNPDF2.3 set of PDFs for the underlying event, parton shower and fragmentation. Since the "matrix element correction" (MEC) in Pythia 8.230 is switched off in this simulation [37], a sample of Powheg+Pythia 8.230 events with MEC switched off, with the same PDF sets as the nominal Powheg+Pythia 8.230 generator, was also produced for comparison with MadGraph5_aMC@NLO. In order to estimate the uncertainty associated with the modelling of fragmentation and parton showering, a sample was generated with Powheg interfaced with Herwig 7.0.4 [38, 39] with the H7UE tune [40] and the NNPDF3.0 PDF set.

Additional samples using alternative generators were produced for comparison with data. These include Powheg interfaced with Herwig 7.1.3 [41], MadGraph5_aMC@NLO interfaced with Herwig 7.1.3, and Powheg+Pythia 8.230 with the PDF4LHC15_nnlo_mc set [33, 42]. Finally, a reweighted Powheg+Pythia 8.230 sample was generated. The reweighting is performed on the top-quark p_{T} variable, using the kinematics of the top quarks in the MC sample after initial- and final-state radiation. The prediction for the top-quark p_{T} spectrum is calculated to next-to-next-to-leading order (NNLO) in QCD with NLO EW corrections [43, 44] with the NNPDF3.0 QED PDF

[2] $\mu_{\text{r}} = \mu_{\text{f}} = \sqrt{(m_t^2 + (p_{\text{T},t}^2 + p_{\text{T},\bar{t}}^2)/2}$ where $p_{\text{T},t/\bar{t}}$ is the transverse momentum of the top (anti-top) quark.

JHEP07(2023)141

set using dynamic renormalisation and factorisation scales $m_{\mathrm{T},t}/2$, i.e. half the top-quark transverse mass,[3] for the top-quark p_{T} as proposed in ref. [43], with $m_t = 173.3$ GeV. The reweighting was applied such that at the end of the procedure the reweighted MC sample is in good agreement with the higher-order prediction for the reweighted variable [45]. This sample is referred to as being reweighted to the NNLO prediction in the remainder of the document.

The measurements are sensitive to the fraction of $t\bar{t}$ events produced together with extra heavy-flavour quarks, which is not well modelled. This extra production of heavy flavour, relative to the prediction, is studied with a modified Powheg+Pythia 8.230 sample in which the fraction of events with at least three b-jets at generator level is increased by 30% to reproduce the rate of events in data with three b-tagged jets, as discussed in ref. [6].

When comparing simulation with data, the $t\bar{t}$ samples are normalised to the inclusive cross-section prediction calculated at NNLO accuracy in the strong coupling constant α_{s}, including the resummation of next-to-next-to-leading logarithmic (NNLL) soft gluon terms, $\sigma_{t\bar{t},\mathrm{pred}} = 832^{+20}_{-29}(\mathrm{scale})^{+35}_{-35}(\mathrm{PDF}+\alpha_{\mathrm{s}})$ pb, obtained using the Top++ 2.0 program [46–50].

3.2 Wt samples

In order to describe the dominant background from the single-top Wt channel, samples were produced with Powheg+Pythia 8.230 with the same parameter values as used for the nominal $t\bar{t}$ sample. The interference between the $t\bar{t}$ and Wt amplitudes is modelled using the diagram removal scheme [51, 52]. To estimate the systematic uncertainties from this source, an alternative sample is used, where the interference is modelled with the diagram subtraction scheme [51].

The same variations of Powheg Box that were performed for the nominal $t\bar{t}$ sample were also carried out for the Wt sample. The same alternative generators are also used to estimate the hard-scattering matrix element and parton shower plus hadronisation uncertainties in the Wt background.

3.3 Other background samples

The background from diboson events (WW, WZ and ZZ) was simulated using the Sherpa 2.2.2 [53–55] generator with the NNPDF3.0 PDF set. These simulations are accurate to NLO for up to one additional parton and accurate to leading order (LO) for up to three additional parton emissions.

Another background contribution comes from $Z+$jets with the Z boson decaying into two τ-leptons, which then decay to an electron and a muon. Those samples were simulated with the Sherpa 2.2.1 generator with the NNPDF3.0 PDF set. They are accurate to NLO for up to two additional partons and accurate to LO for up to four additional partons, and so are the $Z(\to ee)+$jets and $Z(\to \mu\mu)+$jets samples which are used to extract a factor to scale the $Z(\to \tau\tau)+$jets background to data; see section 5 for details. To study systematic uncertainties in the $Z+$jets modelling, alternative $Z+$jets samples were generated with Powheg+Pythia 8.230.

[3] The transverse mass of the top quark is denoted by $m_{\mathrm{T},t} = \sqrt{m_t^2 + p_{\mathrm{T},t}^2}$.

JHEP07(2023)141

Backgrounds from $t\bar{t}W$ and $t\bar{t}Z$ are described by samples simulated with the MadGraph5_aMC@NLO generator at NLO interfaced with Pythia 8.210 with the A14 tune and the NNPDF2.3 PDF set. The minor background coming from $t\bar{t}H$ was also simulated with the MadGraph5_aMC@NLO NLO generator with the A14 tune and the NNPDF2.3lo PDF set, and the minor single-top contribution from t-channel exchange was simulated with the Powheg+Pythia 8.230 generator with the NNPDF3.0nlo_4f PDF set.

For the estimation of the misidentified-lepton backgrounds, the above samples, in which a dileptonic filter is applied, are complemented by top-quark samples and diboson samples containing at least one hadronic top-quark or boson decay, respectively, together with $W+$jets samples generated with the same set-up as the $Z+$jets samples.

4 Object reconstruction and event selection

The events used in this analysis must contain a reconstructed electron, a reconstructed muon and either one or two b-tagged jets. All reconstructed objects are required to have $|\eta| < 2.5$ and $p_{\mathrm{T}} > 25$ GeV. For electrons, the pseudorapidity region is reduced to $|\eta| < 1.37$ and $1.52 < |\eta| < 2.47$ to exclude the transition region between the barrel and endcap calorimeters.

Electron candidates are reconstructed from energy clusters in the electromagnetic calorimeter matched to tracks reconstructed in the inner tracking detector [56]. The candidates are required to satisfy "tight" selection criteria. In addition, the candidates are subject to an isolation requirement allowing no more than a certain fraction of the electron energy to be carried by particles measured in the vicinity of the electron candidate. The requirement is passed by 90% of the electrons from $Z \to ee$ decays, at $p_{\mathrm{T}} = 25$ GeV. The candidates are also required to originate from the primary event vertex [57], defined as the reconstructed vertex with the highest sum of p_{T}^2 for the tracks associated with it. The candidate track must satisfy a requirement on the transverse impact parameter significance of $|d_0|/\sigma_{d_0} < 5$ and on the longitudinal impact parameter, z_0, of $|z_0 \sin(\theta)| < 0.5$ mm, where θ is the polar angle of the track.

Muon candidates are reconstructed by combining tracks reconstructed in the inner tracking detector and the muon spectrometer. They are required to have $|\eta| < 2.5$, to satisfy "medium" selection criteria [58] and an isolation requirement which has an efficiency of ∼85% for muons with $p_{\mathrm{T}} = 25$ GeV, increasing gradually to 98% for muons with $p_{\mathrm{T}} > 100$ GeV. Furthermore, the muon candidate tracks must originate from the primary vertex, ensured by requiring $|d_0|/\sigma_{d_0} < 3$ and $|z_0 \sin(\theta)| < 0.5$ mm.

Jets are reconstructed from topological cell clusters [59] in the calorimeters using the anti-k_t algorithm [60, 61] with a radius parameter $R = 0.4$. After calibration of the jet energy scale [62] using information from both data and simulation, the jets are required to have $p_{\mathrm{T}} > 25$ GeV and $|\eta| < 2.5$. In order to reduce contamination from pileup, jets with $p_{\mathrm{T}} < 120$ GeV and $|\eta| < 2.4$ must pass a primary vertex association requirement using the "jet vertex tagger" (JVT) [63], which has an efficiency of 87% for jets with $p_{\mathrm{T}} = 25$ GeV, increasing to 95% for jets with $p_{\mathrm{T}} = 60$ GeV.

JHEP07(2023)141

Jets likely to contain b-hadrons are tagged with the MV2c10 algorithm [64] using jet and track variables sensitive to b- and c-hadron masses, lifetimes and decay topologies. A working point with an average efficiency of 70% was used, with rejection factors for c-quark jets, τ-leptons and light-quark jets of 8, 13 and 313, respectively. These values are estimated using the $t\bar{t}$ simulation.

To avoid double counting, an overlap removal procedure is applied. First, any electron candidates that share a track with a muon candidate are removed. Subsequently, jets within $\Delta R = 0.2$ of an electron are removed, and afterwards, electrons within a region $0.2 < \Delta R < 0.4$ around any remaining jet are rejected. Jets that have fewer than three tracks and are within $\Delta R = 0.2$ of a muon candidate are removed, and muons within $\Delta R = 0.4$ of any remaining jet are discarded.

Events are retained if they contain exactly one electron and exactly one muon satisfying the selection criteria detailed above, where at least one of the two leptons is matched to an electron or muon trigger object, which implies a minimum p_{T} of 27 GeV. The events with opposite-charge $e\mu$ pairs (opposite-sign, OS) are used for the measurement of the $t\bar{t}$ signal, while the same-charge $e\mu$ pairs (same-sign, SS) are used to estimate the background from misidentified leptons. Furthermore, the events must contain either exactly one or exactly two b-tagged jets.

The selected events containing OS leptons are shown as a function of the number of b-tagged jets in figure 1. The mismodelling of the number of events with three or more b-tagged jets is taken into account using the $t\bar{t}$ sample with an enriched rate of events with at least three b-jets at generator level, as described in section 3.1. The reconstructed transverse momentum and $|\eta|$ distributions of the OS leptons in the selected data sample are shown in figures 2 and 3 together with signal and background predictions. The data and simulated distributions generally agree well, but the lepton transverse momentum distribution observed in data is softer than in the nominal signal and background simulation, as has also been observed in previous measurements at $\sqrt{s} = 13\,\mathrm{TeV}$ [6, 7].

In addition to the reconstructed objects, "particle-level" objects are also defined. These are a collection of stable particles (with lifetime larger than 30 ps) from the full matrix element and parton shower generators, without any simulation of the interaction of these particles with the detector components.

Simulated events with an $e\mu$ pair located in a fiducial region, given for both leptons by $p_{\mathrm{T}}^{\ell} > 27$ (25) GeV for the leading (sub-leading) lepton and $|\eta^{\ell}| < 2.5$ at particle-level, are used to extrapolate the observed event rate to a fiducial cross-section. The four-momentum of each charged lepton is taken after final-state radiation and it is summed with the four-momenta of any radiated photons within a cone of size $\Delta R = 0.1$ around the lepton direction. Particle-level jets are reconstructed using stable particles in the event (excluding charged leptons and neutrinos that do not originate from hadron decays) using the anti-k_t algorithm with a R parameter of $R = 0.4$. They are required to have $p_{\mathrm{T}} > 25$ GeV and $|\eta| < 2.5$. Particle-level electrons and muons that overlap with particle jets with $\Delta R < 0.4$ are removed from the event. No electron-muon overlap removal is applied at the particle level.

JHEP07(2023)141

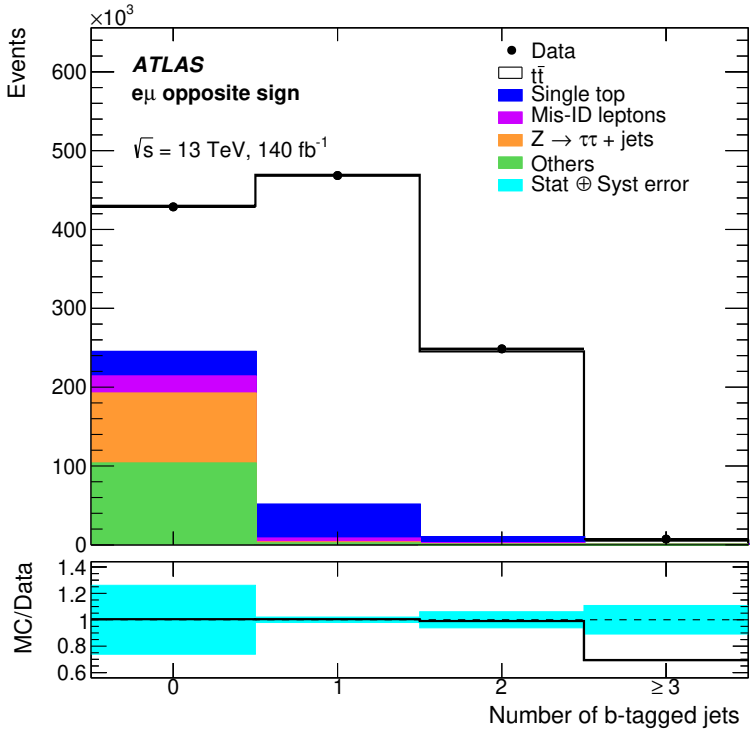

Figure 1. Distribution of the number of b-tagged jets in selected opposite-sign $e\mu$ events. The coloured distributions show the breakdown of the predicted background contributions from single top quarks (Wt and t-channel), misidentified leptons, $Z(\rightarrow \tau\tau)+\text{jets}$ and other sources of background (diboson, $t\bar{t}W$, $t\bar{t}Z$, and $t\bar{t}H$). The bottom panel shows the ratio of the prediction to the data with an uncertainty band covering both the statistical and systematic uncertainties, except for $t\bar{t}$ generator uncertainties.

5 Data-driven background estimates and efficiency corrections

The simulated backgrounds from misidentified leptons and the backgrounds from $Z(\rightarrow \tau\tau)+\text{jets}$ are corrected using data-driven methods. These two backgrounds amount to 1% and 0.2%, respectively, of the total selected event sample.

The misidentified-lepton background is composed of five different categories treated together, as shown in the SS regions in figures 4 and 5. The major contribution is due to $t\bar{t}$ dilepton events where the electron stems from the conversion of a photon radiated from a prompt electron. Three more categories are due to an electron or muon coming from the semileptonic decay of heavy-flavour hadrons or one lepton with a wrongly reconstructed charge. The final category, labelled as "Others", includes all the other cases, e.g. a muon from an in-flight decay of a pion or kaon.

JHEP07(2023)141

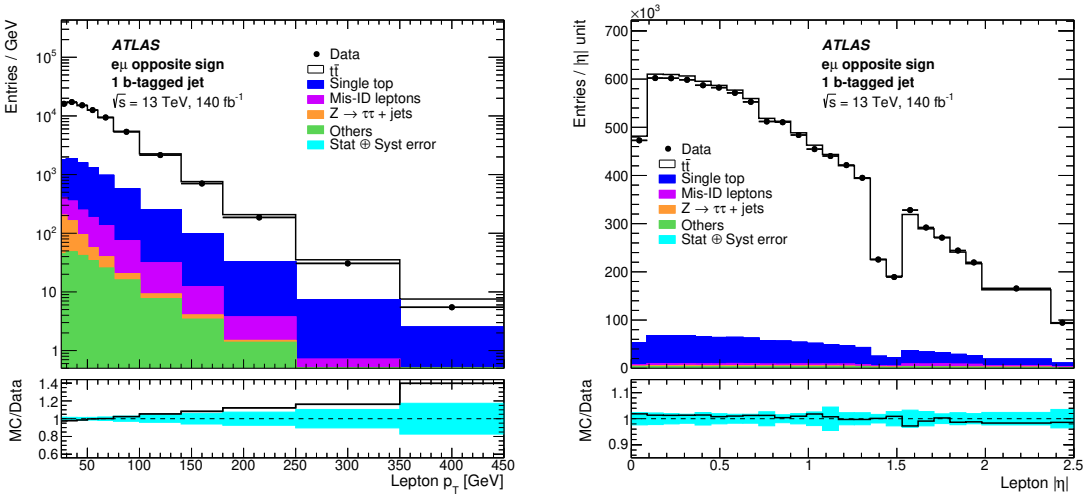

(a) **(b)**

Figure 2. Distributions of lepton p_{T} (left) and $|\eta|$ (right) in opposite-sign $e\mu$ events with one b-tagged jet. The data (dots) are compared with the combined prediction from signal and background processes (line). The simulated event samples are normalised to the integrated luminosity of the data. The coloured distributions show the breakdown of the predicted background contributions from single top quarks (Wt and t-channel), misidentified leptons, $Z(\rightarrow \tau\tau)+\mathrm{jets}$ and other sources of background (diboson, $t\bar{t}W$, $t\bar{t}Z$, and $t\bar{t}H$). The bottom panel shows the ratio of the prediction to the data with an uncertainty band covering both the statistical and systematic uncertainties, except for $t\bar{t}$ generator uncertainties. The last bin of the p_{T} distribution includes overflow events.

JHEP07(2023)141

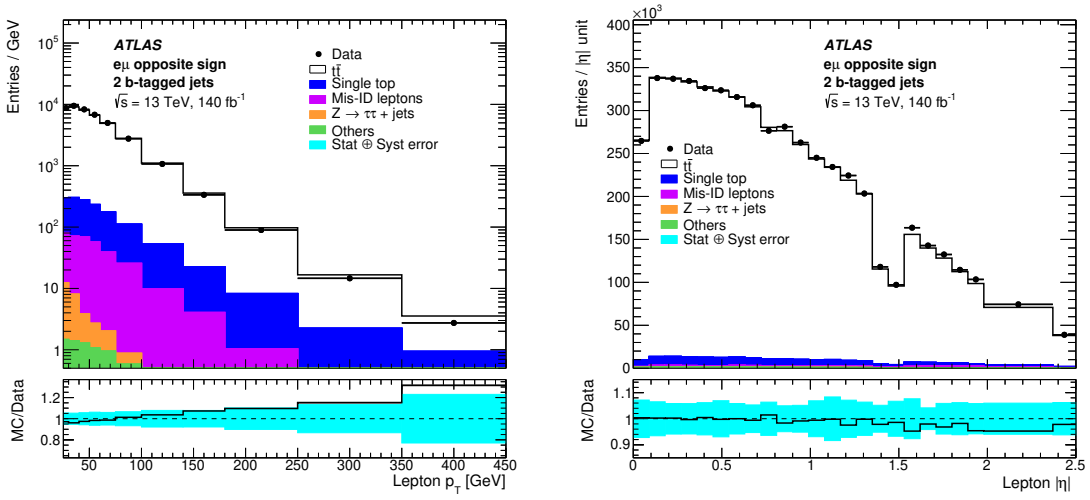

(a) **(b)**

Figure 3. Distributions of lepton p_{T} (left) and $|\eta|$ (right) in opposite-sign $e\mu$ events with two b-tagged jets. The data (dots) are compared with the combined prediction from signal and background processes (line). The simulated event samples are normalised to the integrated luminosity of the data. The coloured distributions show the breakdown of the predicted background contributions from single top quarks (Wt and t-channel), misidentified leptons, $Z(\rightarrow \tau\tau)+$jets and other sources of background (diboson, $t\bar{t}W$, $t\bar{t}Z$, and $t\bar{t}H$). The bottom panel shows the ratio of the prediction to the data with an uncertainty band covering both the statistical and systematic uncertainties, except for $t\bar{t}$ generator uncertainties. The last bin of the p_{T} distribution includes overflow events.

JHEP07(2023)141

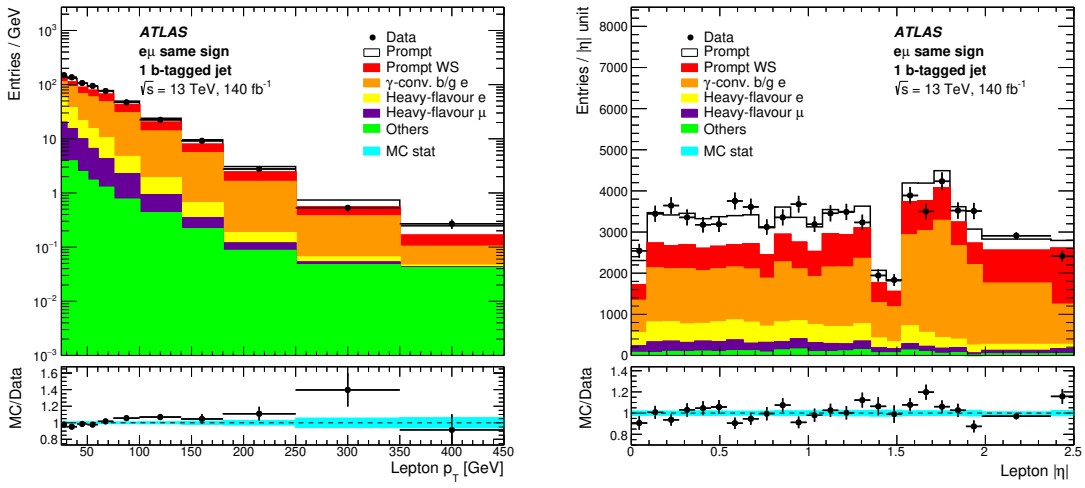

(a) **(b)**

Figure 4. Distribution of lepton p_{T} (left) and $|\eta|$ (right) in same-sign $e\mu$ events with one b-tagged jet. The data (dots) are compared with the combined prediction from signal and background processes (line). The coloured distributions show the breakdown of the predicted contributions: wrong-sign (WS) prompt leptons, where the lepton charge is mismeasured; background electrons from photon conversions; electrons or muons from heavy-flavour decays; and other sources of fake leptons. The bottom panel shows the ratio of the predictions to the data with an uncertainty band covering the MC statistical uncertainty. The last bin of the p_{T} distribution includes overflow events.

The simulated contribution of prompt leptons to the SS $e\mu$ sample is subtracted and the result is scaled by the ratio of OS to SS misidentified leptons in the simulation. These data-driven estimates differ from the MC predictions by less than 10%, as shown in figure 4 and 5.

The background from $Z(\rightarrow \tau\tau)+\text{jets}$ events predicted by the simulation (see section 3.3) is rescaled by the ratio of measured to predicted $Z \rightarrow \mu\mu$ and $Z \rightarrow ee$ events accompanied by b-tagged jets in the Run 2 sample. The $\mu^+\mu^-$ and e^+e^- invariant mass spectra in data are each fitted with a linear combination of two templates, one for leptons from Z boson decays and one for background processes (including misidentified leptons), with both templates taken from simulation. The two Z scale factors obtained from the events with two electrons or two muons are averaged to obtain a weight to be applied to the Z boson events in the $e\mu$ sample. The simulated background from $Z(\rightarrow \tau\tau)+\text{jets}$ events is found to require a scale factor of 1.180 ± 0.001 if the Z boson candidate is accompanied by one b-tagged jet and 1.313 ± 0.006 if the Z boson candidate is accompanied by two b-tagged jets. This result agrees within uncertainties with an earlier result [65] based on a data sample corresponding to an integrated luminosity of 36 fb^{-1}. The errors quoted for the scale factors are purely statistical; the systematic uncertainty is discussed in section 7.3. The lepton correction factors described below have been applied before computing these scale factors.

The lepton trigger, reconstruction and selection efficiencies from simulation receive small corrections derived from measurements of $Z \rightarrow \ell\ell$ events in the data [13, 14, 56, 58]. However, a dedicated *in situ* measurement of the lepton isolation efficiencies is made for

JHEP07(2023)141

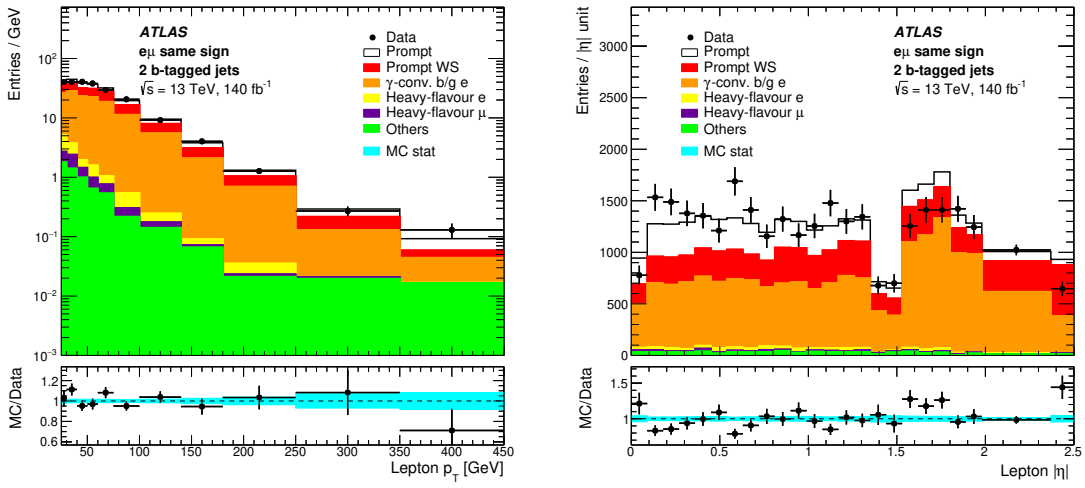

(a) **(b)**

Figure 5. Distribution of lepton p_{T} (left) and $|\eta|$ (right) in same-sign $e\mu$ events with two b-tagged jets. The data (dots) are compared with the combined prediction from signal and background processes (line). The coloured distributions show the breakdown of the predicted contributions: wrong-sign (WS) prompt leptons, where the lepton charge is mismeasured; background electrons from photon conversions; electrons or muons from heavy-flavour decays; and other sources of fake leptons. The bottom panel shows the ratio of the predictions to the data with an uncertainty band covering the MC statistical uncertainty. The last bin of the p_{T} distribution includes overflow events.

this analysis. This ensures that the efficiencies correspond to those in $t\bar{t}$ events, which have larger hadronic activity than in $Z \to \ell\ell$ events, and it also significantly reduces the dependence on the $t\bar{t}$ and pileup modelling. Opposite-sign $e\mu$ events are selected with the isolation requirement only applied to one of the two leptons. The inefficiency of the isolation requirement is given by the fraction of signal events in which the other lepton fails the requirement. The contribution of the prompt-leptons from background sources is subtracted using simulation, the contribution from isolated misidentified leptons is determined from same-sign $e\mu$ pairs as described above, and the contribution from non-isolated misidentified leptons is determined from leptons in data that fail the requirement on the transverse impact parameter significance $|d_0|/\sigma_{d_0}$. This yields a scale factor that multiplies the simulated isolation efficiency and is binned in p_{T} and $|\eta|$. These scale factors deviate from unity by less than 1% in all bins and are evaluated individually for each $t\bar{t}$ generator and applied consistently.

6 Cross-section determination

The total and differential $t\bar{t}$ production cross-sections are measured in the $e\mu$ channel of the $t\bar{t}$ decay in a fiducial region given by $|\eta^{\ell}| < 2.5$ and $p_{\mathrm{T}}^{\ell} > 27$ (25) GeV for the leading (sub-leading) lepton after applying the overlap removal procedure described in section 4. The event selection detailed in section 4 targets $t\bar{t} \to W^+W^-b\bar{b}$ where one of the W bosons

JHEP07(2023)141

decays to an electron and the other to a muon, either directly or via the decay to a τ-lepton which subsequently decays leptonically. When defined in this way, the probability of having an electron and a muon coming from the $t\bar{t}$ process is around 3%.

6.1 Differential fiducial cross-sections

The events used in the analysis are required to contain either exactly one or exactly two b-tagged jets, thereby reducing backgrounds to the 11% or 4% level in the two regions, respectively, and allowing the simultaneous determination of the $t\bar{t}$ cross-section and the combined jet selection and b-tagging efficiency. In each bin i of the lepton kinematic variables listed in section 1, these parameters are evaluated by solving the equations

$$\begin{aligned} N_1^i &= \mathcal{L}\sigma_{t\bar{t}}^i G_{e\mu}^i 2\epsilon_b^i(1-\epsilon_b^i C_b^i) + N_{1,\mathrm{bkg}}^i \\ N_2^i &= \mathcal{L}\sigma_{t\bar{t}}^i G_{e\mu}^i (\epsilon_b^i)^2 C_b^i + N_{2,\mathrm{bkg}}^i \end{aligned} \tag{6.1}$$

where

- N_1^i and N_2^i are the numbers of selected data events with either one b-tagged jet or two b-tagged jets in the reconstructed bin i,
- $N_{1,\mathrm{bkg}}^i$ and $N_{2,\mathrm{bkg}}^i$ are the numbers of predicted background events with either one b-tagged jet or two b-tagged jets in reconstructed bin i,
- $\mathcal{L}$ is the integrated luminosity of the data,
- $\sigma_{t\bar{t}}^i$ is the cross-section for $t\bar{t}$ production resulting in an opposite-sign $e\mu$ pair in the MC generator-level (i.e. particle-level) fiducial region defined by bin i,
- $G_{e\mu}^i$ is the reconstruction efficiency, defined in the simulated $t\bar{t}$ sample as the number of selected $e\mu$ pairs (without any jet requirements) reconstructed in bin i divided by the total number of $e\mu$ pairs generated in bin i. It has an average value of 0.6 and falls to as low as 0.3 for the lowest-energy $e\mu$ pairs,
- ϵ_b^i is the combined probability for a b-jet coming from a top-quark decay to be reconstructed as a jet, to fall within the detector and selection acceptance and be tagged as a b-jet,
- C_b^i is the b-tagging correlation coefficient that corrects the probability of tagging the second jet after having tagged the first one. This coefficient is determined by simulation and is found to be close to unity in most kinematic bins, differing by a maximum of 2%.

The two unknown variables in these equations, the cross-section and the combined selection and b-tagging efficiency, are determined with a log-likelihood fit, as in refs. [4, 6].

The binning is chosen so that more than 90% of $e\mu$ pairs originating in bin i at particle level are usually measured in bin i at detector level. A bin-by-bin unfolding procedure is used where the $G_{e\mu}^i$ efficiency accounts for both the accuracy of lepton reconstruction and the impact of bin migration, which refers to the situation where events categorized in bin

JHEP07(2023)141

j at the particle level are observed in a different bin $i \neq j$ during reconstruction. The large LHC Run 2 dataset allows the chosen binning to be finer than in the previous 13 TeV analysis [6] and the measurements to be made in an extended energy range. It also allows the distribution of one leptonic kinematic variable to be measured in bins of another one. The variable pairs chosen are those deemed most useful for the testing and tuning of MC generators, namely the following four double-differential distributions:

- $|y^{e\mu}|$ in five bins of $m^{e\mu}$;
- $|\Delta\phi^{e\mu}|$ in five bins of $m^{e\mu}$;
- $|\Delta\phi^{e\mu}|$ in three bins of $p_{\mathrm{T}}^{e\mu}$;
- $|\Delta\phi^{e\mu}|$ in five bins of $E^e + E^\mu$.

The cross-section in each two-dimensional bin is determined in the same way as for the one-dimensional distributions and the binning is again chosen so that at least 90% of the events populate the diagonal elements of the migration matrix relating the particle-level variables to the detector-level variables. The chosen binning is sufficiently fine to capture the observed differences between the differential cross-section distributions predicted by a range of event generators.

The normalised differential or double-differential cross-sections profit from a large reduction of systematic effects that are correlated across the distributions. These cross-sections are defined for each bin i as

$$\sigma^{i}_{t\bar{t},\mathrm{norm}} = \frac{\sigma^{i}_{t\bar{t}}}{\sum_j \sigma^{j}_{t\bar{t}}} ,$$

where the denominator sums the absolute differential cross-sections over the distribution in question. However, the normalisation introduces new bin-to-bin correlations which are evaluated by "bootstrapping" pseudo-experiments as explained in section 6.4.

6.2 Total fiducial cross-section

The observed number of selected events in data, together with the predicted backgrounds and their associated statistical uncertainties, are presented in table 1. The MC contributions are normalised to the integrated luminosity of the data and corrections to the MC predictions are implemented as explained in section 5. The observed and predicted yields agree within 1%–2%.

In order to determine the total fiducial $t\bar{t}$ cross-section, eq. (6.1) is solved with bin i taken as the entire fiducial region. An $e\mu$ reconstruction efficiency of $G_{e\mu} = (57.06 \pm 0.02)\%$ and a b-tagging correlation coefficient of $C_b = 1.0058 \pm 0.0005$ are calculated with the nominal $t\bar{t}$ Powheg+Pythia 8.230 $e\mu$ sample, where the quoted uncertainties are from MC statistics only.

JHEP07(2023)141

	OS		SS	
	N_1	N_2	N_1	N_2
$t\bar{t}$	418780 ± 130	235937 ± 95	—	—
Single t	42944 ± 77	7295 ± 31	—	—
Z + jets	1552 ± 66	96.5 ± 7.5	—	—
Diboson	1406.1 ± 9.5	49.9 ± 1.1	223.0 ± 2.4	10.58 ± 0.30
Charge-misid. lepton	1.90 ± 0.14	0.614 ± 0.061	858 ± 11	364.0 ± 7.1
Misidentified lepton	4880 ± 100	1990 ± 67	2550 ± 57	906 ± 35
Other	1192.6 ± 4.1	807.1 ± 3.3	407.0 ± 1.7	238.3 ± 1.3
Total MC prediction	470760 ± 190	246180 ± 120	4039 ± 58	1519 ± 36
Data events	468450	248560	3995	1501
Data/MC	0.995 ± 0.002	1.010 ± 0.002	0.989 ± 0.021	0.988 ± 0.035

Table 1. Observed number of events in data and expected number of events for each process. N_1 and N_2 are the numbers of events with one b-tagged jet and two b-tagged jets, respectively, for the opposite-sign (OS) and same-sign (SS) regions. The $t\bar{t}+X$ ($X = W$, Z, H) contributions are included in "Other". Misidentified lepton events in this table are divided in two categories: "Charge-misid. lepton" refers to the number of events with one wrong-charge reconstructed lepton while "Misidentified lepton" refers to the other four categories combined, estimated as explained in section 5 and shown in figures 4 and 5. The dashes mean that the expected number of events for that process is compatible with zero (given the statistical power of the prediction used). The uncertainties in the ratios of data to MC events are purely statistical. The sum of the individual contributions may differ from the "Total MC prediction" due to rounding.

6.3 Total inclusive cross-section

In order to obtain the inclusive cross-section, the reconstruction efficiency $G_{e\mu}$ in eq. (6.1) is replaced by $E_{e\mu} = A_{e\mu} \cdot G_{e\mu}$. The acceptance $A_{e\mu}$ is defined as

$$A_{e\mu} = \frac{N_{e\mu}^{t\bar{t},\text{fiducial}}}{N^{t\bar{t}}}, \tag{6.2}$$

where $N_{e\mu}^{t\bar{t},\text{fiducial}}$ is the number of particle-level opposite-sign $e\mu$ events found in the fiducial region in a simulated $t\bar{t}$ sample and $N^{t\bar{t}}$ is the total number of $t\bar{t}$ pairs produced by the $t\bar{t}$ generator. The acceptance factor is taken from the same MC $t\bar{t}$ sample used to calculate the reconstruction efficiency and it is corrected for each generator to conform with the W branching ratio predicted by the Standard Model per lepton flavour, $B(W \to \ell\nu) = 10.82\%$ [66]. The value of $E_{e\mu}$ calculated with the nominal $t\bar{t}$ Powheg+Pythia 8.230 sample is $E_{e\mu} = (0.7251 \pm 0.0003)\%$, while the value of the acceptance $A_{e\mu}$ calculated with the same sample is $A_{e\mu} = (1.2708 \pm 0.0004)\%$, where the uncertainties are purely statistical.

JHEP07(2023)141

6.4 Validation of the analysis method

The method used to solve eq. (6.1) for each leptonic kinematic bin i is validated by replacing the data sample by 1000 pseudo-experiments [67] fluctuating N_1^i and N_2^i within their statistical uncertainties in various simulated event samples with known $t\bar{t}$ cross-sections, σ_{true}^i. In practice, this is done with a "bootstrapping method" [68], assigning to each event a set of 1000 weights obtained from fluctuations of a Poisson distribution with a mean value of one.

In all such validations, the parameters of the equation, $G_{e\mu}^i$, C_b^i and the background contributions, are taken from the nominal signal and background samples. The mean of the 1000 cross-sections derived from eq. (6.1) is then compared with the true $t\bar{t}$ cross-section of the simulated event sample in order to check for possible biases in the method. The following simulated event samples are used for validation:

- The nominal $t\bar{t}$ Powheg+Pythia 8.230 sample. The mean measured cross-section equals the true cross-section within the statistical error on the mean in any bin i.
- Half the nominal $t\bar{t}$ Powheg+Pythia 8.230 sample. Here the parameters of eq. (6.1) are evaluated with the other half of the sample. No bias is seen beyond the expected statistical fluctuations.
- Two $t\bar{t}$ Powheg+Pythia 8.230 samples with the top-quark mass changed to 176 GeV and 169 GeV. In the case of $m_t = 169$ GeV, biases of 1%–2% are seen in some kinematic bins, but in general the biases are smaller than the expected statistical uncertainties of the data and hence neglected.
- The nominal $t\bar{t}$ Powheg+Pythia 8.230 sample reweighted to produce the same N_1^i and N_2^i as in the data. As in the other tests, no significant bias away from the true cross-section is seen.

The bootstrapping method is also applied to both the data and simulated event samples in order to construct the covariance matrices of statistical uncertainties of the measurements. The matrices include non-zero off-diagonal elements between different variables and, in the case of normalised differential distributions, also between bins in the same distribution.

7 Systematic and statistical uncertainties

Uncertainties due to theoretical assumptions and detector modelling affect the parameters $\mathcal{L}$, $G_{e\mu}^i$, C_b^i, $N_{1,\text{bkg}}^i$ and $N_{2,\text{bkg}}^i$ of eq. (6.1). Uncertainties associated with generators are evaluated by changing the values of parameters in the simulations or by using alternative generators. Some background uncertainties are evaluated by using data-driven uncertainty estimates, as explained in section 7.3. For each variation, eq. (6.1) is solved and the change with respect to the baseline sample is assigned as the impact of the uncertainty on the cross-section measurement. Effects of finite data and MC sample sizes are evaluated by the bootstrapping method described in section 6.4 and summarised in a covariance matrix covering all measured kinematic bins. The individual sources of systematic uncertainty are discussed in the following subsections and a summary of their impact in the measured fiducial and total inclusive cross-sections is given in table 3.

JHEP07(2023)141

7.1 Detector-related uncertainties

Uncertainties on the trigger [13, 14], reconstruction and selection efficiency [56, 58] for the leptons are estimated using $Z \to ee$ and $Z \to \mu\mu$ events in data. They are expressed as uncertainties in scale factors for the MC predictions, described in section 5. By varying the scale factors, their uncertainties are propagated to $G^i_{e\mu}$ and C^i_b, as well as the number of background events, and eq. (6.1) is solved for each variation. The "up" and "down" variations are applied coherently to all bins of a given kinematic variable, except for the electron efficiency, where this approach overestimates the uncertainties [56]. The latter variations are carried out separately in two $|\eta|$ bins and nine p_{T} bins and their effects are combined, taking measured bin-to-bin correlations into account. The up and down variations of the lepton isolation efficiency scale factors are calculated using $t\bar{t} \to WbWb \to e\nu b\mu\nu b$ events. These variations take into account uncertainties in the isolation efficiencies for data and MC. The uncertainty on the isolation efficiency for data depends on the estimation of events with a misidentified lepton and on the statistical uncertainty, while the uncertainty for the MC depends on the simulated sample size.

The uncertainty on the jet energy scale (JES) and the jet energy resolution (JER) affect ϵ^i_b, C^i_b and the number of background events, mainly from Wt production. The jet-related uncertainties are evaluated using the $Z+$jets, $\gamma+$jet and multijet samples at $\sqrt{s} = 13$ TeV for both real and simulated data [69]. A total of 20 uncorrelated nuisance parameters affecting the JES and five parameters affecting the JER are varied up and down. The difference between the energy response for reconstructed b-jets and that for other jets is varied separately [69] and the maximum possible variation is applied to the flavour composition of the jets (the mixture of quarks and gluons). The modelling of pileup also affects the jet energy, and the associated uncertainty is found by varying the jet energy up and down by the uncertainty in this effect. The jet vertex association efficiency uncertainty affects the C^i_b coefficient. This is evaluated by changing the JVT scale factor up and down within its uncertainty.

A b-tagging efficiency scale factor for the chosen working point is derived from $t\bar{t}$ events [70] and applied to the Monte Carlo events used in the present analysis. The uncertainties are related to the b-jet tagging calibration for b-jets, c-jets and light-jets, and comprise nine, four and five eigenvector variations to the tagging efficiencies, respectively, and two components for the MC-based extrapolation to jets with very high p_{T}.

7.2 Top-quark pair modelling uncertainties

Uncertainties related to the modelling of $t\bar{t}$ events have an impact on $G^i_{e\mu}$ and C^i_b in eq. (6.1) and on the acceptance factor in eq. (6.2). These uncertainties are calculated with alternative $t\bar{t}$ samples or by reweighting the nominal sample or increasing by 30% the fraction of events with at least three b-jets, as described in section 3.1. The effect on $E_{e\mu}$, $G_{e\mu}$ and C_b in the selected sample is summarised in table 2 and the change in the central value is taken as the uncertainty from each source.

As shown in section 8.2, the Powheg+Pythia 8.230 generator does not give a good description of the lepton transverse momentum, which is believed to be a reflection of the

JHEP07(2023)141

Systematic uncertainty name	$\Delta C_b/C_b$ [%]	$\Delta G_{e\mu}/G_{e\mu}$ [%]	$\Delta E_{e\mu}/E_{e\mu}$ [%]
Matrix element	-0.10 ± 0.22	0.25 ± 0.11	0.29 ± 0.12
h_{damp}	-0.06 ± 0.08	-0.05 ± 0.04	-0.05 ± 0.05
Parton shower and hadronisation	0.16 ± 0.08	-0.26 ± 0.04	0.04 ± 0.05
Top p_{T} reweighting	0.03 ± 0.08	0.22 ± 0.04	0.61 ± 0.05
$t\bar{t}$ + heavy flavour	-0.33 ± 0.08	0.01 ± 0.04	0.01 ± 0.05
ISR (high)	-0.01 ± 0.08	0.06 ± 0.04	0.35 ± 0.05
ISR (low)	0.04 ± 0.08	-0.13 ± 0.04	-0.35 ± 0.05
FSR (high)	0.05 ± 0.09	-0.07 ± 0.04	-0.12 ± 0.05
FSR (low)	-0.09 ± 0.15	0.10 ± 0.07	0.16 ± 0.09
PDF	0.02 ± 0.08	0.04 ± 0.04	0.42 ± 0.05

Table 2. Differences in the total b-tagging correlation coefficient, total reconstruction efficiency and total preselection efficiency between the baseline $e\mu$ POWHEG+PYTHIA 8.230 sample and the corresponding $t\bar{t}$ systematic uncertainty samples. The PDF row refers to the sum in quadrature of the differences derived from the 30 eigenvectors and the baseline. All uncertainties shown are due to the limited MC sample size.

top-quark transverse momentum spectrum. Therefore, the difference with respect to the sample where the top-quark transverse momentum is reweighted to the NNLO predicted spectrum is considered as an additional uncertainty in all measurements. This effect is relevant mostly for the extrapolation of the fiducial cross-section to the total phase-space.

The effect of changing the top-quark mass in the $t\bar{t}$ and Wt simulations is not included in table 2 since by convention the inclusive cross-section is quoted at a fixed $m_t = 172.5$ GeV. However, samples with different top-quark masses (from $m_t = 169$ GeV to $m_t = 176$ GeV) are used for validation tests and to study the combined effect on the fiducial cross-section ($\sigma_{t\bar{t}}^{\text{fid}}$) and the total inclusive cross-section. This is found to be

$$\frac{1}{\sigma_{t\bar{t}}^{\text{fid}}}\frac{d\sigma_{t\bar{t}}^{\text{fid}}}{dm_t} = -(0.004 \pm 0.003)\%/\text{GeV}$$
$$\frac{1}{\sigma_{t\bar{t}}}\frac{d\sigma_{t\bar{t}}}{dm_{\text{t}}} = -(0.379 \pm 0.005)\%/\text{GeV}$$

7.3 Background modelling uncertainties

The contribution from Wt is varied up and down by the relative uncertainty in the total cross-section, which is 5.3%, as derived to approximate NNLO for $\sqrt{s} = 13$ TeV using the calculation in ref. [71]. In addition, the nominal Wt generator is varied as described in section 3.2 and the results are propagated to the cross-section in each lepton kinematic bin. In particular, the uncertainty due to the interference between the $t\bar{t}$ and Wt amplitudes is taken as the change in the result when replacing the diagram removal scheme [51, 52] with

JHEP07(2023)141

the diagram subtraction scheme [51]. The uncertainties in the matrix element, fragmentation and parton showering, and those related to the extra initial- and final-state radiation in the Wt background process are evaluated together with the signal process, considering these uncertainties to be correlated between $t\bar{t}$ and Wt.

The uncertainties in the size of the diboson background are assessed by doubling and halving the factorisation and renormalisation scales in the Sherpa 2.2.2 samples and by comparing the nominal Sherpa 2.2.2 samples with those generated with Powheg+Pythia 8.210. A further 40% normalisation uncertainty is added to cover the uncertainties due to heavy-flavour jets produced in association with the diboson pairs as discussed in ref. [72].

An uncertainty of 5% on the scale factors for the $Z \to \tau\tau$ contribution derived in section 5 is considered. The uncertainty from the fit amounts to less than 1%. In order to take into account small differences between the same-flavour ee and $\mu\mu$ control regions and the $e\mu$ measurement region, such as lepton efficiencies, a conservative systematic uncertainty of 5% is assigned, both in the one b-jet and the two b-jets regions. An additional uncertainty due to the shape of the $Z+$jets background is estimated by using the Powheg+Pythia 8.186 sample instead of the nominal Sherpa 2.2.1 sample.

The uncertainty assigned to the $t\bar{t}V$ (where V is W or Z) cross-sections is 13%, following ref. [73].

In order to cover possible mismodelling of the electron charge misidentification and the misidentified-lepton composition in the nominal simulation, the ratio of OS to SS misidentified leptons is varied up and down by 25% in the 1-b-jet region and by 50% in the 2-b-jet region, as discussed in ref. [6]. The uncertainties in the predicted cross-sections for the $t\bar{t}V$ and diboson processes also have a non-negligible impact on the number of SS prompt leptons. A conservative uncertainty of 50% is therefore assigned to those contributions [6].

7.4 Luminosity and beam energy

The uncertainty in the combined 2015–2018 integrated luminosity is 0.83% [10], obtained using the LUCID-2 detector [74] for the primary luminosity measurements, complemented by measurements using the inner tracking detector and calorimeters. This is propagated to the cross-sections via eq. (6.1). Including the effect of the luminosity uncertainty on the predicted background contribution, the fiducial and inclusive cross-sections receive a total uncertainty of 0.93% from the measured luminosity.

The uncertainty in the LHC beam energy is evaluated to be 0.1% [75], which is found to contribute an uncertainty of 0.23% to the measured total fiducial and inclusive cross-sections at $\sqrt{s} = 13$ TeV. The effect of a 0.1% uncertainty in the LHC beam energy is also propagated to the differential measurements by reweighting the PDFs using the LHAPDF library [76]. The effect is generally small but increases in the highest-energy kinematic bins, reaching a maximum contribution of 0.1%

JHEP07(2023)141

Source of uncertainty	$\Delta\sigma_{t\bar{t}}^{\text{fid}}/\sigma_{t\bar{t}}^{\text{fid}}$ [%]	$\Delta\sigma_{t\bar{t}}/\sigma_{t\bar{t}}$ [%]
Data statistics	0.15	0.15
MC statistics	0.04	0.04
Matrix element	0.12	0.16
h_{damp} variation	0.01	0.01
Parton shower	0.08	0.22
$t\bar{t}$ + heavy flavour	0.34	0.34
Top p_{T} reweighting	0.19	0.58
Parton distribution functions	0.04	0.43
Initial-state radiation	0.11	0.37
Final-state radiation	0.29	0.35
Electron energy scale	0.10	0.10
Electron efficiency	0.37	0.37
Electron isolation (in situ)	0.51	0.51
Muon momentum scale	0.13	0.13
Muon reconstruction efficiency	0.35	0.35
Muon isolation (in situ)	0.33	0.33
Lepton trigger efficiency	0.05	0.05
Vertex association efficiency	0.03	0.03
Jet energy scale & resolution	0.10	0.10
b-tagging efficiency	0.07	0.07
$t\bar{t}/Wt$ interference	0.37	0.37
Wt cross-section	0.52	0.52
Diboson background	0.34	0.34
$t\bar{t}V$ and $t\bar{t}H$	0.03	0.03
$Z+$jets background	0.05	0.05
Misidentified leptons	0.32	0.32
Beam energy	0.23	0.23
Luminosity	0.93	0.93
Total uncertainty	1.6	1.8

Table 3. Breakdown of systematic uncertainties in the measured fiducial and inclusive cross-sections.

JHEP07(2023)141

8 Results

8.1 Total inclusive cross-section

The cross-section for the fiducial region is measured with the full Run 2 dataset to be

$$\sigma_{t\bar{t}}^{\text{fid}} = 10.53 \pm 0.02\ (\text{stat}) \pm 0.13\ (\text{syst}) \pm 0.10\ (\text{lumi}) \pm 0.02\ (\text{beam})\ \text{pb}$$

and the total inclusive cross-section is

$$\sigma_{t\bar{t}} = 829 \pm 1\ (\text{stat}) \pm 13\ (\text{syst}) \pm 8\ (\text{lumi}) \pm 2\ (\text{beam})\ \text{pb},$$

where the uncertainties are due to statistics, theoretical and experimental systematic effects, the integrated luminosity and the beam energy. The fiducial region is defined as $p_{\text{T}}^{\ell} > 27$ (25) GeV for the leading (sub-leading) lepton and $|\eta^{\ell}| < 2.5$ after applying the overlap removal procedure described in section 4 for both leptons from $t\bar{t}$ decays producing an $e\mu$ pair. The total relative uncertainties in $\sigma_{t\bar{t}}^{\text{fid}}$ and $\sigma_{t\bar{t}}$ are 1.6% and 1.8%, respectively, where the breakdown of the various sources is shown in table 3.

This measurement is compatible with the earlier ATLAS result at $\sqrt{s} = 13$ TeV using an integrated luminosity of 36 fb^{-1} [6] but is significantly more precise, due to a reduction in the luminosity uncertainty [10]. It is the most precise measurement of the inclusive $t\bar{t}$ cross-section to date.

The predicted NNLO+NNLL value of the total inclusive cross-section at $\sqrt{s} = 13$ TeV, for a top-quark mass of 172.5 GeV, is $\sigma_{t\bar{t},\text{pred}} = 832^{+20}_{-29}\ (\text{scale})^{+23}_{-23}\ (m_t)^{+35}_{-35}\ (\text{PDF}+\alpha_{\text{s}})$ pb [46–50], which is in excellent agreement with this measurement.

8.2 Differential cross-section

The differential cross-section is measured as a function of several lepton kinematic variables: p_{T}^{ℓ}, $|\eta^{\ell}|$, $m^{e\mu}$, $p_{\text{T}}^{e\mu}$, $|y^{e\mu}|$, $E^{e} + E^{\mu}$, $p_{\text{T}}^{e} + p_{\text{T}}^{\mu}$ and $|\Delta\phi^{e\mu}|$. The absolute differential cross-sections in the fiducial region are presented in figures 6 and 7, as well as in tables 6–13 in the appendix. The absolute double-differential cross-sections are presented in figures 8 and 9, as well as in tables 14–17 in the appendix. The luminosity gives the largest contribution to the cross-section uncertainty in most bins, resulting in a typical uncertainty of 1% out of a total uncertainty around 2%. An uncertainty of around 1% is expected since it affects both the signal and background yields in equation (6.1) and the final impact on the measured cross-section is subject to background fluctuations, having a relative impact on the measurement ranging between 0.9% and 1.1%. However, uncertainties related to the modelling of the $t\bar{t}$ process, those affecting the reconstruction of leptons and those affecting the modelling of the background processes also have a significant contribution in all bins of the distributions. The statistical uncertainty increases with increasing transverse momentum, combined mass or energy, but is overtaken by the uncertainty related to the interference between $t\bar{t}$ and Wt amplitudes that dominates the uncertainty in the high mass or energy bins.

However, in the normalised differential cross-section the uncertainty due to the luminosity largely cancels out. This results in a typical uncertainty of 1%, except in the highest

JHEP07(2023)141

energy bins. These results are presented in figures 10 and 11, as well as in tables 18–25 in the appendix. Instead of the luminosity, the interference between $t\bar{t}$ and Wt amplitudes becomes the most important source of uncertainty, especially for high values of variables with dimensions of energy. The $t\bar{t}$ modelling uncertainties are also important, while other uncertainties are very small in the normalised distributions.

Due to differences in the fiducial region definition, these results are not directly comparable to the previous results from ref. [6]. The lepton p_{T} requirement in this analysis, $p_{\mathrm{T}}^{\ell} > 27$ (25) GeV for the leading (sub-leading) lepton, differs from that in the $36\,\mathrm{fb}^{-1}$ analysis [6], in which the minimum lepton p_{T} was 20 GeV whilst requiring at least one lepton to be above the lepton trigger threshold of $21 - 27$ GeV.

The gain in precision from using the full Run 2 sample is especially significant in the normalised double-differential cross-sections, allowing the binning to have finer granularity than in the previous analysis. The obtained double-differential cross-section measurements as a function of $|y^{e\mu}|$ in bins of $m^{e\mu}$, $|\Delta\phi^{e\mu}|$ in bins of $m^{e\mu}$, $|\Delta\phi^{e\mu}|$ in bins of $p_{\mathrm{T}}^{e\mu}$, and $|\Delta\phi^{e\mu}|$ in bins of $E^{e} + E^{\mu}$ are presented in figures 12 and 13 and in tables 26–29 in the appendix.

JHEP07(2023)141

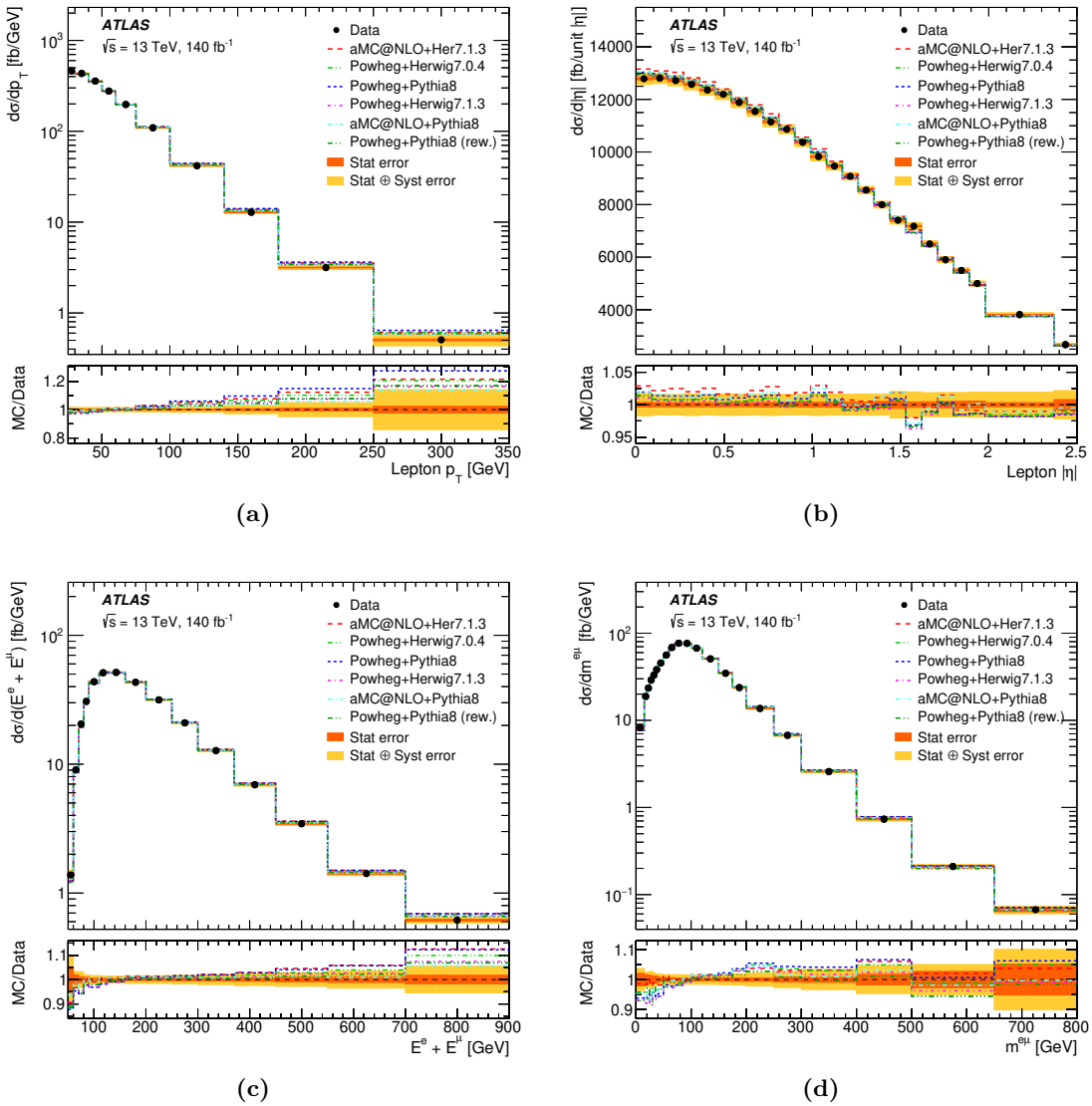

Figure 6. Absolute differential cross-sections as a function of (a) p_{T}^{ℓ}, (b) $|\eta^{\ell}|$, (c) $E^{e} + E^{\mu}$ and (d) $m^{e\mu}$ with statistical (orange) and statistical plus systematic uncertainties (yellow). The data points are placed at the centre of each bin. The results are compared with the predictions from different Monte Carlo generators normalised to the Top++ prediction: the baseline Powheg+Pythia 8.230 $t\bar{t}$ sample (blue), MadGraph5_aMC@NLO+Herwig 7.1.3 (red), Powheg+Herwig 7.0.4 (green), Powheg+Herwig 7.1.3 (purple), MadGraph5_aMC@NLO+Pythia 8.230 (cyan) and Powheg+Pythia 8.230 rew. (dark green), which refers to Powheg+Pythia 8.230 reweighted according to the top-quark p_{T}. The lower panel shows the ratios of the predictions to data, with the bands indicating the statistical and systematic uncertainties. The last bin in (a), (c) and (d) also contains overflow events.

JHEP07(2023)141

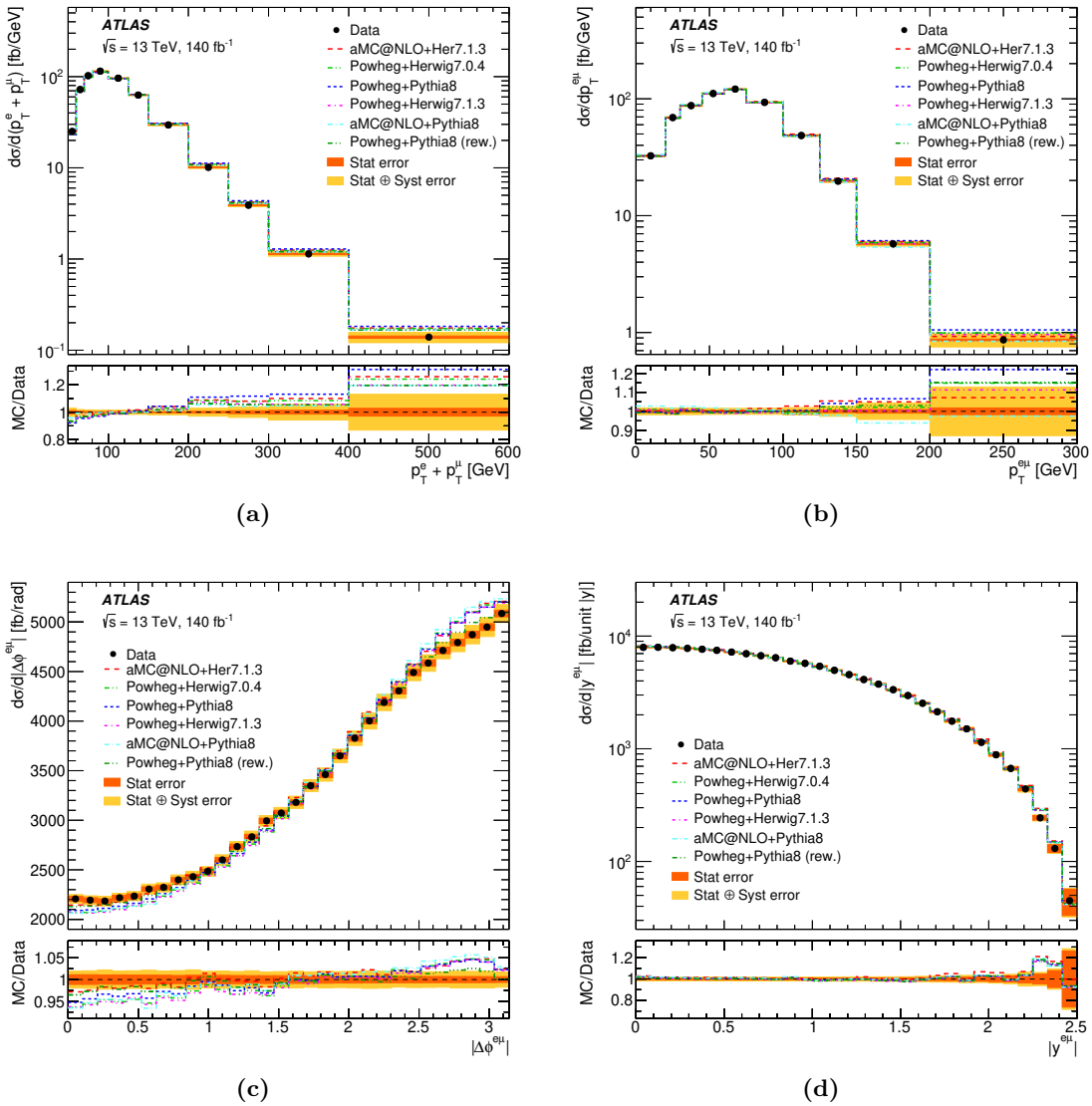

Figure 7. Absolute differential cross-sections as a function of (a) $p_{\mathrm{T}}^{e} + p_{\mathrm{T}}^{\mu}$, (b) $p_{\mathrm{T}}^{e\mu}$, (c) $|\Delta\phi^{e\mu}|$ and (d) $|y^{e\mu}|$ with statistical (orange) and statistical plus systematic uncertainties (yellow). The data points are placed at the centre of each bin. The results are compared with the predictions from different Monte Carlo generators normalised to the Top++ prediction: the baseline Powheg+Pythia 8.230 $t\bar{t}$ sample (blue), MadGraph5_aMC@NLO+Herwig 7.1.3 (red), Powheg+Herwig 7.0.4 (green), Powheg+Herwig 7.1.3 (purple), MadGraph5_aMC@NLO+Pythia 8.230 (cyan) and Powheg+Pythia 8.230 rew. (dark green), which refers to Powheg+Pythia 8.230 reweighted according to the top-quark p_{T}. The lower panel shows the ratios of the predictions to data, with the bands indicating the statistical and systematic uncertainties. The last bin in (a) and (b) also contains overflow events.

JHEP07(2023)141

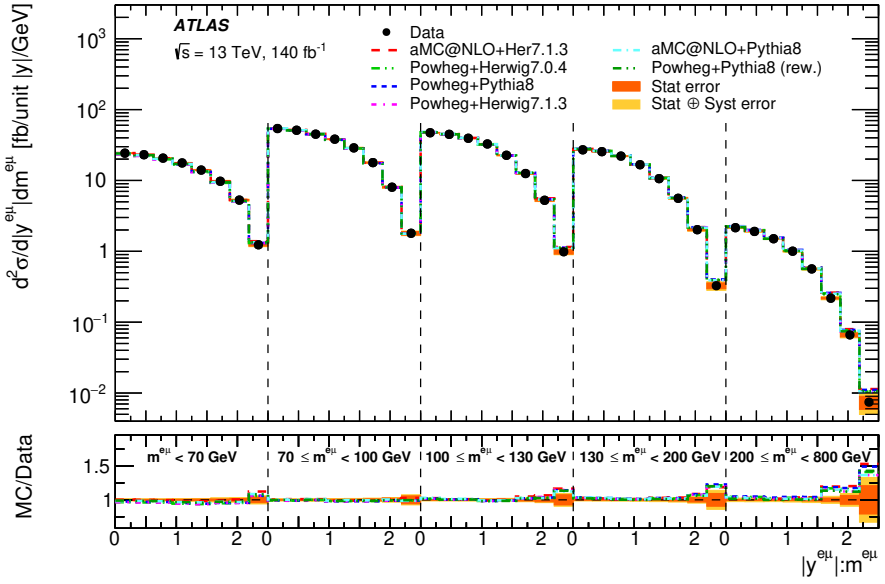

(a)

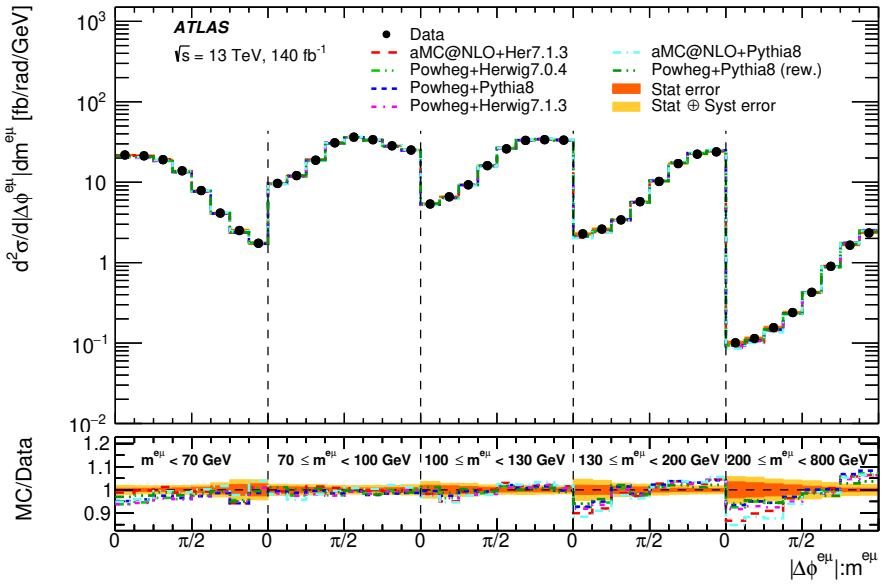

(b)

Figure 8. Absolute double-differential cross-sections as a function of (a) $|y^{e\mu}|$ in bins of $m^{e\mu}$ and (b) $|\Delta\phi^{e\mu}|$ in bins of $m^{e\mu}$ with statistical (orange) and statistical plus systematic uncertainties (yellow). The data points are placed at the centre of each bin. The results are compared with the predictions from different Monte Carlo generators normalised to the Top++ prediction: the baseline Powheg+Pythia 8.230 $t\bar{t}$ sample (blue), MadGraph5_aMC@NLO+Herwig 7.1.3 (red), Powheg+Herwig 7.0.4 (green), Powheg+Herwig 7.1.3 (purple), MadGraph5_aMC@NLO+Pythia 8.230 (cyan) and Powheg+Pythia 8.230 rew. (dark green), which refers to Powheg+Pythia 8.230 reweighted according to the top-quark p_{T}. The lower panel shows the ratios of the predictions to data, with the bands indicating the statistical and systematic uncertainties. The highest invariant mass bin of the two distributions contains the overflows.

JHEP07(2023)141

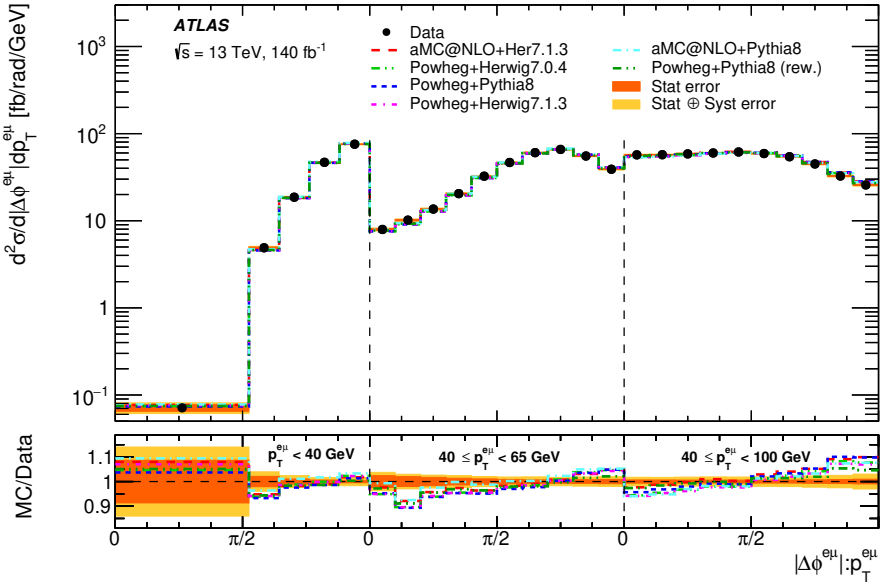

(a)

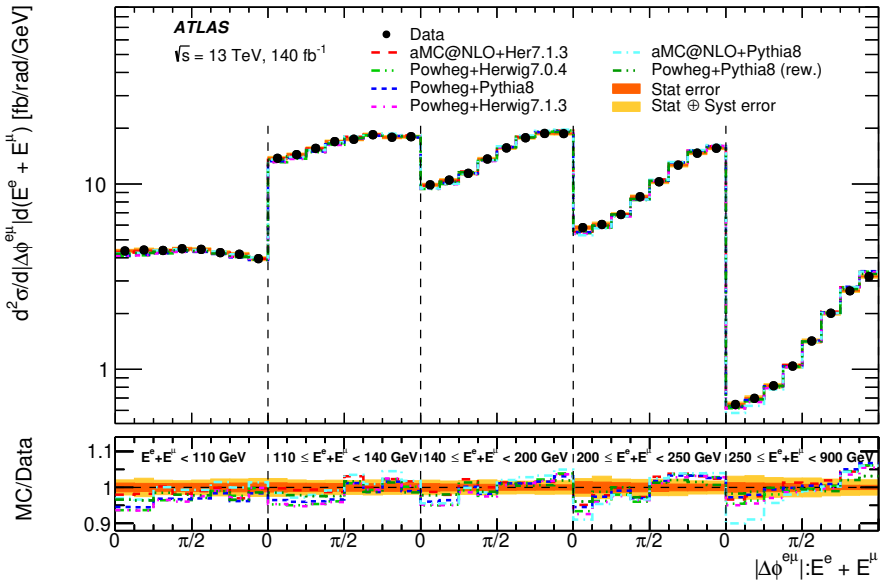

(b)

Figure 9. Absolute double-differential cross-sections as a function of (a) $|\Delta\phi^{e\mu}|$ in bins of $p_{\mathrm{T}}^{e\mu}$ and (b) $|\Delta\phi^{e\mu}|$ in bins of $E^e + E^\mu$ with statistical (orange) and statistical plus systematic uncertainties (yellow). The data points are placed at the centre of each bin. The results are compared with the predictions from different Monte Carlo generators normalised to the Top++ prediction: the baseline Powheg+Pythia 8.230 $t\bar{t}$ sample (blue), MadGraph5_aMC@NLO+Herwig 7.1.3 (red), Powheg+Herwig 7.0.4 (green), Powheg+Herwig 7.1.3 (purple), MadGraph5_aMC@NLO+Pythia 8.230 (cyan) and Powheg+Pythia 8.230 rew. (dark green), which refers to Powheg+Pythia 8.230 reweighted according to the top-quark p_{T}. The lower panel shows the ratios of the predictions to data, with the bands indicating the statistical and systematic uncertainties. The highest $E^e + E^\mu$ and p_{T} bin contains the overflows.

JHEP07(2023)141

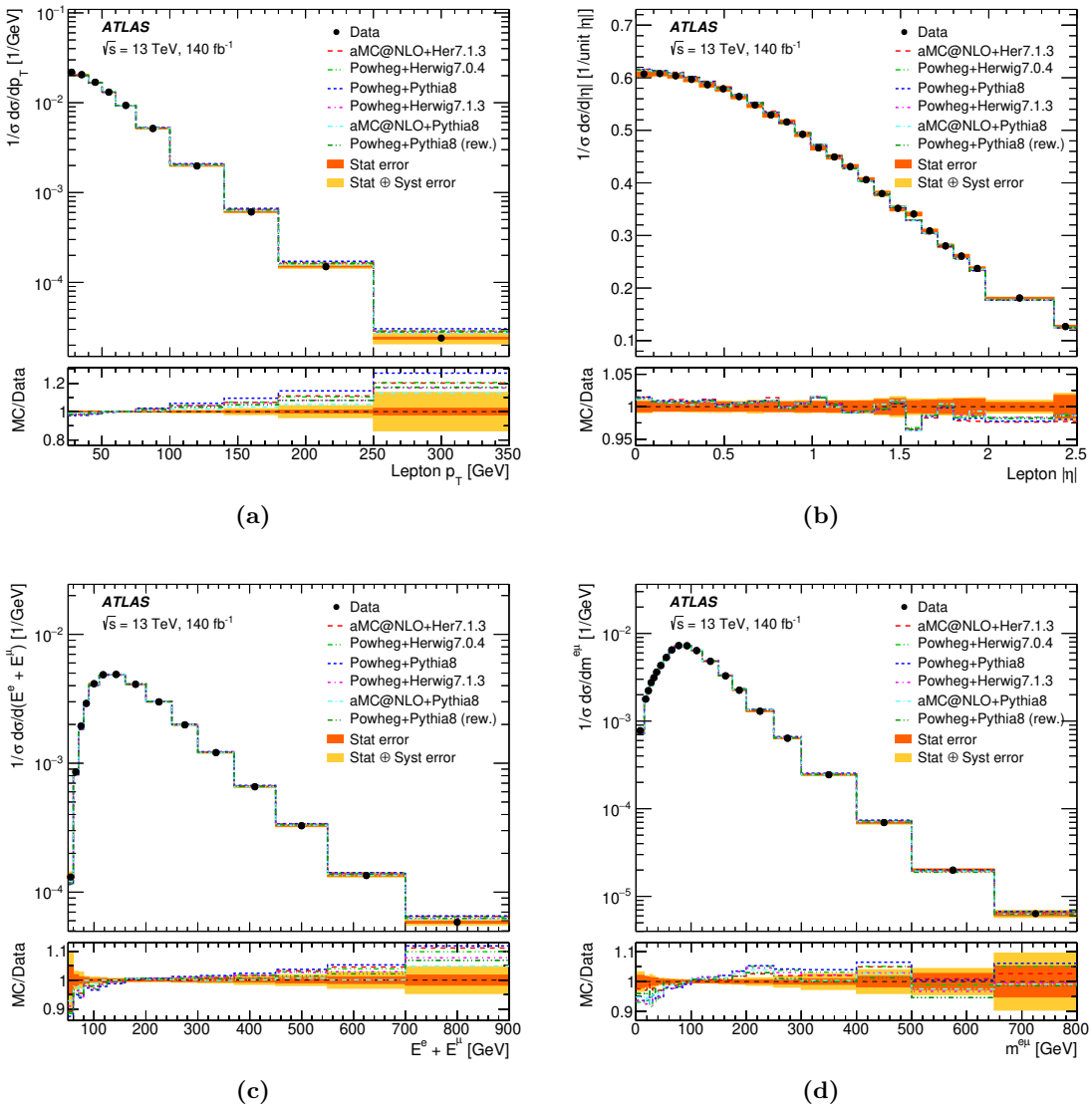

Figure 10. Normalised differential cross-sections as a function of (a) p_{T}^{ℓ}, (b) $|\eta^{\ell}|$, (c) $E^{e} + E^{\mu}$ and (d) $m^{e\mu}$ with statistical (orange) and statistical plus systematic uncertainties (yellow). The data points are placed at the centre of each bin. The results are compared with the predictions from different Monte Carlo generators normalised to the Top++ prediction: the baseline Powheg+Pythia 8.230 $t\bar{t}$ sample (blue), MadGraph5_aMC@NLO+Herwig 7.1.3 (red), Powheg+Herwig 7.0.4 (green), Powheg+Herwig 7.1.3 (purple), MadGraph5_aMC@NLO+Pythia 8.230 (cyan) and Powheg+Pythia 8.230 rew. (dark green), which refers to Powheg+Pythia 8.230 reweighted according to the top-quark p_{T}. The lower panel shows the ratios of the predictions to data, with the bands indicating the statistical and systematical uncertainties. The last bin in (a), (c) and (d) also contains overflow events.

JHEP07(2023)141

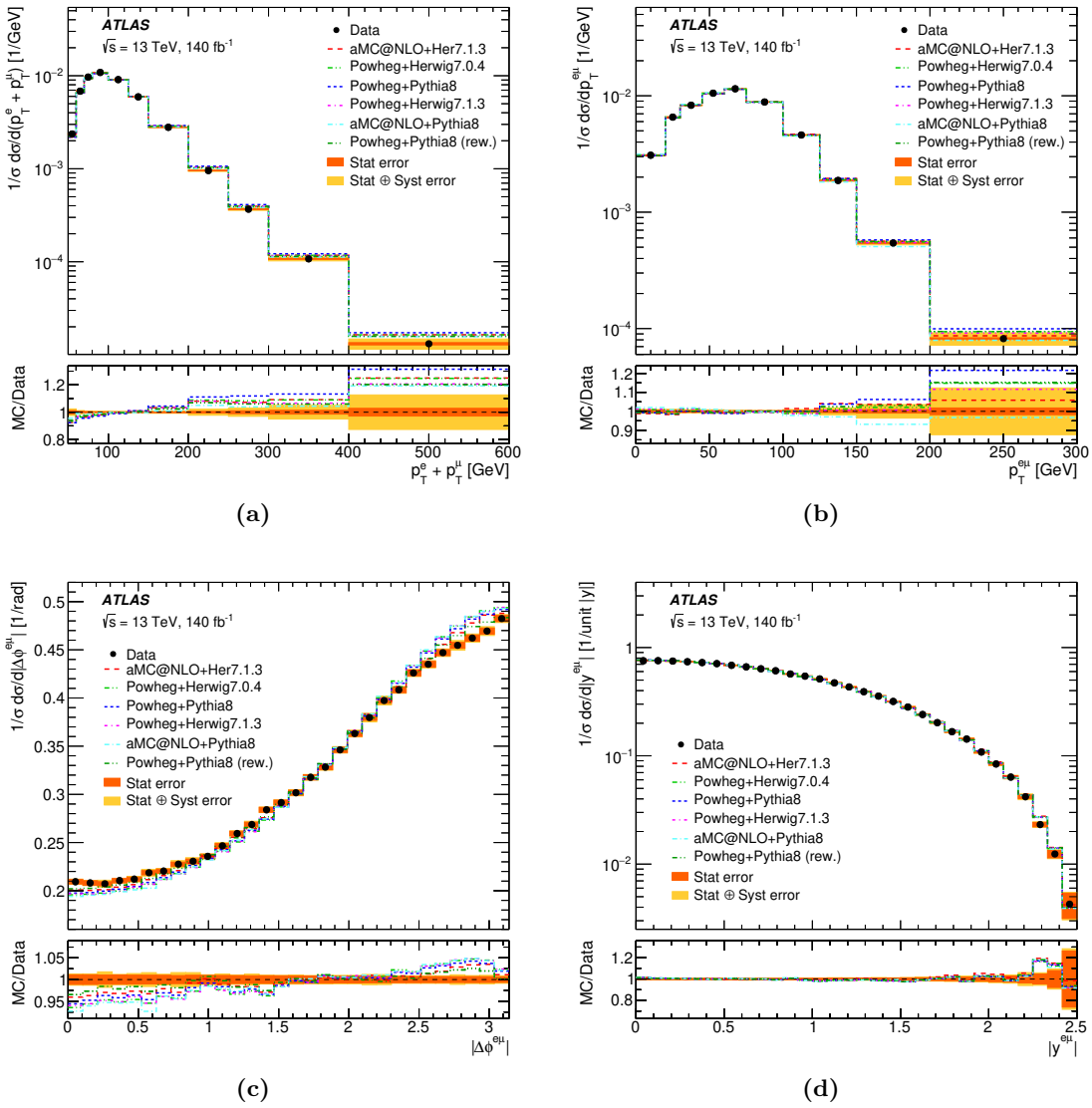

Figure 11. Normalised differential cross-sections as a function of (a) $p_{\mathrm{T}}^{e} + p_{\mathrm{T}}^{\mu}$, (b) $p_{\mathrm{T}}^{e\mu}$, (c) $|\Delta\phi^{e\mu}|$ and (d) $|y^{e\mu}|$ with statistical (orange) and statistical plus systematic uncertainties (yellow). The data points are placed at the centre of each bin. The results are compared with the predictions from different Monte Carlo generators normalised to the Top++ prediction: the baseline Powheg+Pythia 8.230 $t\bar{t}$ sample (blue), MadGraph5_aMC@NLO+Herwig 7.1.3 (red), Powheg+Herwig 7.0.4 (green), Powheg+Herwig 7.1.3 (purple), MadGraph5_aMC@NLO+Pythia 8.230 (cyan) and Powheg+Pythia 8.230 rew. (dark green), which refers to Powheg+Pythia 8.230 reweighted according to the top-quark p_{T}. The lower panel shows the ratios of the predictions to data, with the bands indicating the statistical and systematic uncertainties. The last bin in (a) and (b) also contains overflow events.

JHEP07(2023)141

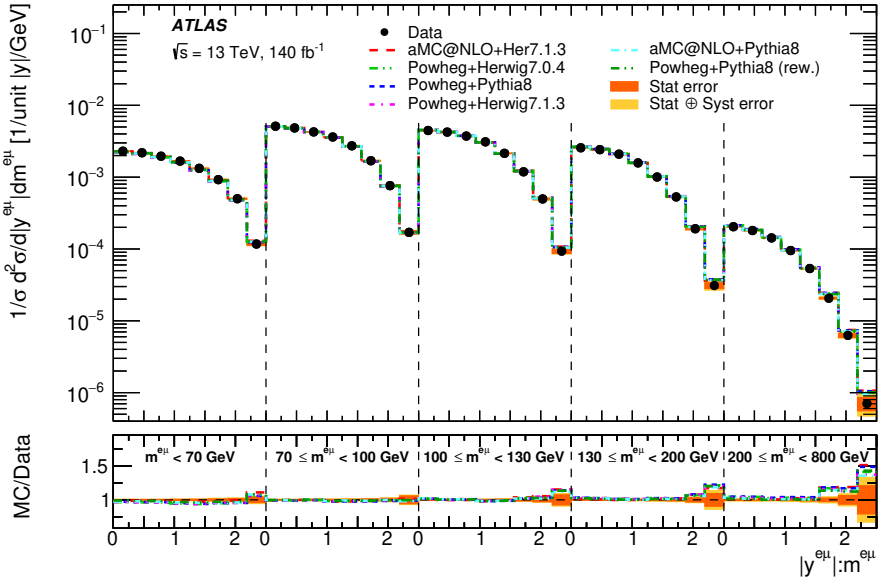

(a)

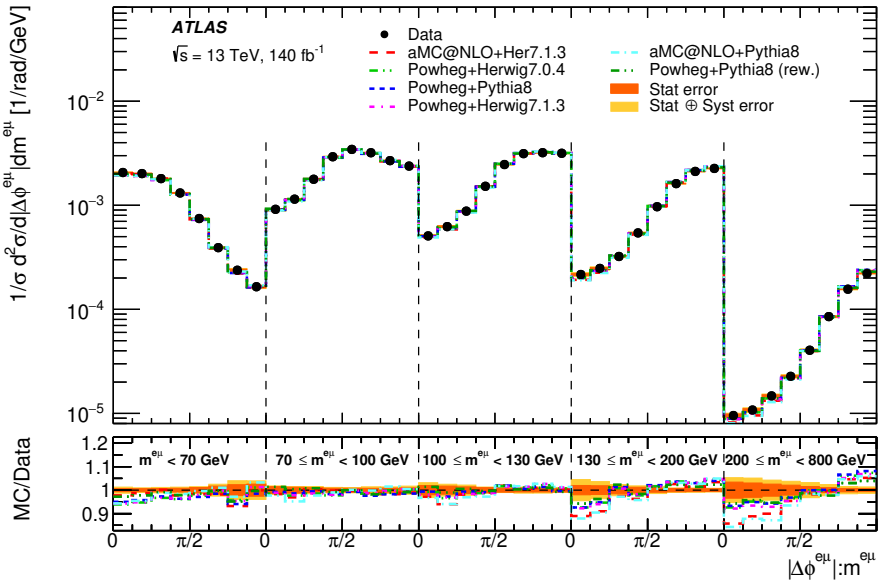

(b)

Figure 12. Normalised double-differential cross-sections as a function of (a) $|y^{e\mu}|$ in bins of $m^{e\mu}$ and (b) $|\Delta\phi^{e\mu}|$ in bins of $m^{e\mu}$ with statistical (orange) and statistical plus systematic uncertainties (yellow). The data points are placed at the centre of each bin. The results are compared with the predictions from different Monte Carlo generators normalised to the Top++ prediction: the baseline Powheg+Pythia 8.230 $t\bar{t}$ sample (blue), MadGraph5_aMC@NLO+Herwig 7.1.3 (red), Powheg+Herwig 7.0.4 (green), Powheg+Herwig 7.1.3 (purple), MadGraph5_aMC@NLO+Pythia 8.230 (cyan) and Powheg+Pythia 8.230 rew. (dark green), which refers to Powheg+Pythia 8.230 reweighted according to the top-quark p_{T}. The lower panel shows the ratios of the predictions to data, with the bands indicating the statistical and systematic uncertainties. The highest invariant mass bin of the two distributions contains the overflows.

JHEP07(2023)141

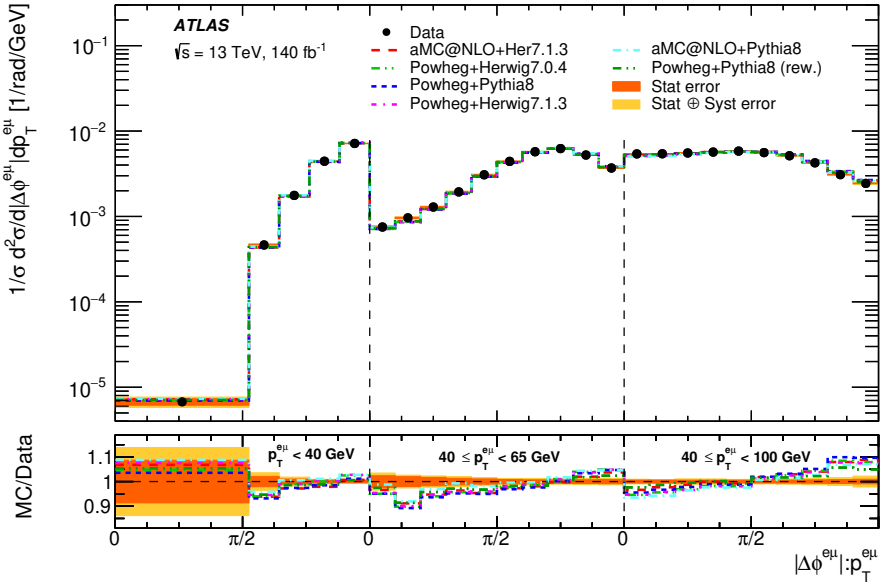

(a)

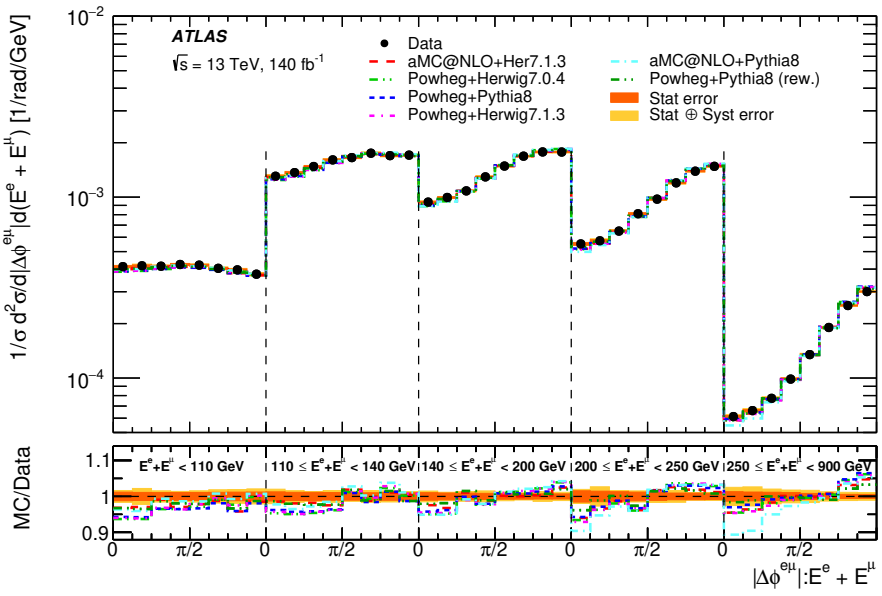

(b)

Figure 13. Normalised double-differential cross-sections as a function of (a) $|\Delta\phi^{e\mu}|$ in bins of $p_{\mathrm{T}}^{e\mu}$ and (b) $|\Delta\phi^{e\mu}|$ in bins of $E^e + E^\mu$ with statistical (orange) and statistical plus systematic uncertainties (yellow). The data points are placed at the centre of each bin. The results are compared with the predictions from different Monte Carlo generators normalised to the Top++ prediction: the baseline Powheg+Pythia 8.230 $t\bar{t}$ sample (blue), MadGraph5_aMC@NLO+Herwig 7.1.3 (red), Powheg+Herwig 7.0.4 (green), Powheg+Herwig 7.1.3 (purple), MadGraph5_aMC@NLO+Pythia 8.230 (cyan) and Powheg+Pythia 8.230 rew. (dark green), which refers to Powheg+Pythia 8.230 reweighted according to the top-quark p_{T}. The lower panel shows the ratios of the predictions to data, with the bands indicating the statistical and systematic uncertainties. The highest $E^e + E^\mu$ and p_{T} bin contains the overflows.

JHEP07(2023)141

8.3 Comparison with predictions

Defining a vector V_b as the difference between the measured and predicted values for an absolute differential cross-section in b kinematic bins, the compatibility of the data and predictions is assessed by using a χ^2 test with b degrees of freedom

$$\chi^2 = V_b^T \cdot \mathrm{Cov}_{b\times b}^{-1} \cdot V_b \tag{8.1}$$

The covariance matrix $\mathrm{Cov}_{b\times b}$ is a sum of several terms. The statistical covariance matrices for both the data and the simulated event sample are calculated with the method described in section 6.4. Each systematic uncertainty contributes another term, where the uncertainties are assumed to be fully correlated between bins, except for the statistical uncertainties of the misidentified-lepton estimate. No uncertainty was assigned to the theoretical prediction.

The normalised differential cross-sections have one less degree of freedom and the χ^2 is calculated by simply dropping one bin in eq. (8.1)

$$\chi^2 = V_{(b-1)}^T \cdot \mathrm{Cov}_{(b-1)\times(b-1)}^{-1} \cdot V_{(b-1)}$$

The statistical covariance matrix terms are constructed using the same method as for the absolute differential cross-sections, and the systematic covariance matrix contributions are propagated to the normalised differential cross-sections. The resulting combined χ^2 for each variable and each $t\bar{t}$ generator set-up are shown in table 4, while those for each double-differential distribution are shown in table 5. The results show that no generator describes all distributions with a χ^2 probability larger than 1% . However, some interesting features stand out and were also observed in the earlier ATLAS results at $\sqrt{s} = 13$ TeV [6]:

- All generators, except for the MadGraph5_aMC@NLO+Pythia 8.230 sample, predict a spectrum for the variables p_{T}^{ℓ}, $E^e + E^\mu$ and $p_{\mathrm{T}}^e + p_{\mathrm{T}}^\mu$ which is harder than in the data. Among the various combinations of matrix element and shower generators, Powheg+Pythia 8.230 gives the poorest agreement with these distributions, while MadGraph5_aMC@NLO+Pythia 8.230 provides acceptable matches to the measured normalised distributions, in particular for the $E^e + E^\mu$ and $p_{\mathrm{T}}^e + p_{\mathrm{T}}^\mu$ differential cross-sections.

- The $m^{e\mu}$ distribution is well represented by MadGraph5_aMC@NLO+Herwig 7.1.3, while the $p_{\mathrm{T}}^{e\mu}$ distribution is better represented by Powheg+Pythia 8.230, especially the sample with the top-quark transverse momentum reweighted.

- All generators fail to reproduce the $|\eta^{\ell}|$ distribution because of a 2% deficit for $|\eta^{\ell}| > 1.5$. The $|y^{e\mu}|$ distribution is best represented by Powheg+Pythia 8.230 with the PDF4LHC15_nnlo_mc set, while other generators predict a surplus of events for $|y^{e\mu}| > 2.2$, especially at high $m^{e\mu}$.

- All generators predict a different trend than seen in data for the distribution of $|\Delta\phi^{e\mu}|$. The data tend to be higher than the predictions at low $|\Delta\phi^{e\mu}|$, whereas they

JHEP07(2023)141

Generator	p_{T}^{ℓ}	$\lvert\eta^{\ell}\rvert$	$p_{\mathrm{T}}^{e\mu}$	$p_{\mathrm{T}}^{e}+p_{\mathrm{T}}^{\mu}$	$E^{e}+E^{\mu}$	$m^{e\mu}$	$\lvert\Delta\phi^{e\mu}\rvert$	$\lvert y^{e\mu}\rvert$
N_{dof}	9	23	9	10	14	20	29	29
Powheg+Pythia 8	196	132	12.0	130	33	102	193	47
Powheg+Pythia 8 - top p_{T} rew.	51	114	7.8	42	20.4	53	65	45.2
Powheg+Pythia 8 - $h_{\mathrm{damp}} \times 2$	228	139	26	167	38	97	121	45.3
Powheg+Pythia 8 - PDF4LHC	186	100	11.5	125	32	93	185	33.6
Powheg+Pythia 8 - ISR up	149	111	17.3	120	34	79	66	50
Powheg+Pythia 8 - ISR down	216	159	10.6	131	30	113	311	44.5
Powheg+Pythia 8 - Rad up	164	115	27	139	38	78	49	47.6
Powheg+Pythia 8 - Rad down	216	159	10.6	131	30	113	311	44.5
Powheg+Pythia 8 - FSR up	216	132	12.5	143	35	106	194	46.8
Powheg+Pythia 8 - FSR down	171	139	9.5	118	30	98	185	49
Powheg+Pythia 8 - MEC off	42	136	41	37	16.5	83	181	42.7
aMC@NLO+Pythia 8	16.5	126	48	14.4	14.3	89	300	50
aMC@NLO+Herwig 7.0.4	98	137	24	74	24.1	29.1	110	54
Powheg+Herwig 7.0.4	113	104	28	82	28	135	271	45.8
Powheg+Herwig 7.1.3	101	107	31	75	25.5	138	259	45.5

Table 4. χ^2 values for the comparison of the normalised measured differential cross-sections with different $t\bar{t}$ simulation samples. N_{dof} is the number of degrees of freedom. The χ^2 values are displayed to one decimal place if the corresponding χ^2 probability is greater than 1%, and rounded to integers otherwise.

are generally lower in the high $|\Delta\phi^{e\mu}|$ region. This trend was observed in various previous measurements [6, 7, 77].

9 Conclusion

The production of $t\bar{t}$ pairs in pp collisions at $\sqrt{s} = 13$ TeV is measured using opposite-sign $e\mu$ events in association with one or two b-tagged jets in the LHC Run 2 (2015–2018) data collected by the ATLAS experiment with an integrated luminosity of 140 fb^{-1}.

The inclusive fiducial and total cross-sections for $t\bar{t}$ production are measured. The total inclusive cross-section is measured to be

$$\sigma_{t\bar{t}} = 829 \pm 1\ (\mathrm{stat}) \pm 13\ (\mathrm{syst}) \pm 8\ (\mathrm{lumi}) \pm 2\ (\mathrm{beam})\ \mathrm{pb},$$

where the uncertainties are due to statistics, theoretical and experimental systematic effects, the integrated luminosity and the beam energy. This result is in excellent agreement with theoretical expectations. It is the most precise measurement of the inclusive $t\bar{t}$ cross-section to date.

The $t\bar{t}$ absolute and normalised differential cross-sections are measured as functions of eight different variables ($p_{\mathrm{T}}^{e\mu}$, $p_{\mathrm{T}}^{e}+p_{\mathrm{T}}^{\mu}$, p_{T}^{ℓ}, $E^{e}+E^{\mu}$, $m^{e\mu}$, $|\eta^{\ell}|$, $|\Delta\phi^{e\mu}|$ and $|y^{e\mu}|$). Furthermore, four double-differential cross-sections are measured as a function of $|y^{e\mu}|$ in bins of $m^{e\mu}$, and as a function of $|\Delta\phi^{e\mu}|$ in bins of $m^{e\mu}$, $p_{\mathrm{T}}^{e\mu}$ and $E^{e}+E^{\mu}$. These distributions are

JHEP07(2023)141

Generator	$\lvert y^{e\mu}\rvert : m^{e\mu}$	$\lvert\Delta\phi^{e\mu}\rvert : m^{e\mu}$	$\lvert\Delta\phi^{e\mu}\rvert : p_{\mathrm{T}}^{e\mu}$	$\lvert\Delta\phi^{e\mu}\rvert : E^{e} + E^{\mu}$
N_{dof}	39	39	24	39
Powheg+Pythia 8	131	364	264	263
Powheg+Pythia 8 - top p_{T} rew.	82	140	81	96
Powheg+Pythia 8 - $h_{\mathrm{damp}} \times 2$	129	250	182	183
Powheg+Pythia 8 - PDF4LHC	114	351	252	253
Powheg+Pythia 8 - ISR up	108	153	105	112
Powheg+Pythia 8 - ISR down	143	562	413	409
Powheg+Pythia 8 - Rad up	109	130	90	104
Powheg+Pythia 8 - Rad down	143	562	413	409
Powheg+Pythia 8 - FSR up	137	374	271	268
Powheg+Pythia 8 - FSR down	122	349	247	255
Powheg+Pythia 8 - MEC off	107	276	219	237
aMC@NLO+Pythia 8	108	436	363	386
aMC@NLO+Herwig 7.0.4	95	270	154	162
Powheg+Herwig 7.0.4	151	400	334	345
Powheg+Herwig 7.1.3	147	392	318	336

Table 5. χ^2 values for the comparison of the normalised measured double-differential cross-sections with different $t\bar{t}$ simulation samples. N_{dof} is the number of degrees of freedom. The χ^2 values are displayed to one decimal place if the corresponding χ^2 probability is greater than 1%, and rounded to integers otherwise.

confined to the fiducial region $p_{\mathrm{T}}^{\ell} > 27$ (25) GeV for the leading (sub-leading) lepton and $|\eta^{\ell}| < 2.5$ for both leptons.

The precision of the measurements is typically 2% for the absolute differential cross-sections and at the 1% level for the normalised differential cross-sections, except in the highest energy bins where the $t\bar{t}/Wt$ interference uncertainty contribution increases. The measurements are compared with a wide range of models for $t\bar{t}$ production in pp collisions. No model can describe all measured distributions within their uncertainties.

Acknowledgments

We thank CERN for the very successful operation of the LHC, as well as the support staff from our institutions without whom ATLAS could not be operated efficiently.

We acknowledge the support of ANPCyT, Argentina; YerPhI, Armenia; ARC, Australia; BMWFW and FWF, Austria; ANAS, Azerbaijan; CNPq and FAPESP, Brazil; NSERC, NRC and CFI, Canada; CERN; ANID, Chile; CAS, MOST and NSFC, China; Minciencias, Colombia; MEYS CR, Czech Republic; DNRF and DNSRC, Denmark; IN2P3-CNRS and CEA-DRF/IRFU, France; SRNSFG, Georgia; BMBF, HGF and MPG, Germany; GSRI, Greece; RGC and Hong Kong SAR, China; ISF and Benoziyo Center, Israel; INFN, Italy; MEXT and JSPS, Japan; CNRST, Morocco; NWO, Netherlands; RCN, Norway; MEiN, Poland; FCT, Portugal; MNE/IFA, Romania; MESTD, Serbia; MSSR, Slovakia; ARRS and MIZŠ, Slovenia; DSI/NRF, South Africa; MICINN, Spain; SRC

JHEP07(2023)141

and Wallenberg Foundation, Sweden; SERI, SNSF and Cantons of Bern and Geneva, Switzerland; MOST, Taiwan; TENMAK, Türkiye; STFC, United Kingdom; DOE and NSF, United States of America. In addition, individual groups and members have received support from BCKDF, CANARIE, Compute Canada and CRC, Canada; PRIMUS 21/SCI/017 and UNCE SCI/013, Czech Republic; COST, ERC, ERDF, Horizon 2020 and Marie Skłodowska-Curie Actions, European Union; Investissements d'Avenir Labex, Investissements d'Avenir Idex and ANR, France; DFG and AvH Foundation, Germany; Herakleitos, Thales and Aristeia programmes co-financed by EU-ESF and the Greek NSRF, Greece; BSF-NSF and MINERVA, Israel; Norwegian Financial Mechanism 2014-2021, Norway; NCN and NAWA, Poland; La Caixa Banking Foundation, CERCA Programme Generalitat de Catalunya and PROMETEO and GenT Programmes Generalitat Valenciana, Spain; Göran Gustafssons Stiftelse, Sweden; The Royal Society and Leverhulme Trust, United Kingdom.

The crucial computing support from all WLCG partners is acknowledged gratefully, in particular from CERN, the ATLAS Tier-1 facilities at TRIUMF (Canada), NDGF (Denmark, Norway, Sweden), CC-IN2P3 (France), KIT/GridKA (Germany), INFN-CNAF (Italy), NL-T1 (Netherlands), PIC (Spain), ASGC (Taiwan), RAL (U.K.) and BNL (U.S.A.), the Tier-2 facilities worldwide and large non-WLCG resource providers. Major contributors of computing resources are listed in ref. [78].

A Tables with detailed results

p_{T}^{ℓ} bins [GeV]	$d\sigma/dp_{\mathrm{T}}^{\ell}$ [fb/GeV]	Data stat. [%]	MC stat. [%]	$t\bar{t}$ mod. [%]	Lep. [%]	Jets/ b-tag. [%]	Bkg. [%]	Lumi + E_{beam} [%]	Total unc. [%]
25.0–30.0	461.6	0.38	0.11	0.48	1.09	0.11	0.71	0.93	1.72
30.0–40.0	433.1	0.27	0.08	0.56	0.87	0.11	0.67	0.93	1.57
40.0–50.0	357.0	0.30	0.07	0.66	0.74	0.11	0.66	0.92	1.54
50.0–60.0	277.2	0.33	0.07	0.53	0.74	0.12	0.68	0.92	1.51
60.0–75.0	197.2	0.29	0.07	0.59	0.74	0.13	0.67	0.92	1.52
75.0–100.0	109.2	0.30	0.07	0.69	0.82	0.15	0.85	0.93	1.69
100.0–140.0	41.79	0.40	0.09	0.65	0.96	0.17	1.25	0.94	2.00
140.0–180.0	12.85	0.69	0.17	0.71	1.42	0.20	2.22	0.97	2.99
180.0–250.0	3.16	1.02	0.28	1.04	1.86	0.26	4.25	1.01	4.98
250.0–350.0	0.51	2.35	0.66	2.54	4.24	0.41	12.97	1.15	14.15

Table 6. Absolute differential cross-section for p_{T}^{ℓ}.

$\lvert\eta^{\ell}\rvert$ bins -	$d\sigma/d\lvert\eta^{\ell}\rvert$ [pb/units of η]	Data stat. [%]	MC stat. [%]	$t\bar{t}$ mod. [%]	Lep. [%]	Jets/ b-tag. [%]	Bkg. [%]	Lumi + E_{beam} [%]	Total unc. [%]
0.00–0.09	12.79	0.36	0.12	0.67	1.01	0.12	0.72	0.93	1.74
0.09–0.18	12.81	0.32	0.12	0.49	0.81	0.13	0.77	0.93	1.58
0.18–0.27	12.72	0.32	0.11	0.62	0.76	0.13	0.74	0.93	1.58
0.27–0.36	12.57	0.30	0.12	0.81	0.76	0.13	0.76	0.93	1.67
0.36–0.45	12.36	0.30	0.12	0.60	0.76	0.13	0.75	0.93	1.57
0.45–0.54	12.19	0.32	0.11	0.84	0.76	0.14	0.68	0.93	1.65
0.54–0.63	11.88	0.31	0.12	0.74	0.76	0.13	0.75	0.93	1.64
0.63–0.72	11.54	0.33	0.12	0.59	0.76	0.13	0.82	0.93	1.61
0.72–0.81	11.15	0.34	0.13	0.75	0.76	0.12	0.78	0.93	1.66
0.81–0.90	10.86	0.34	0.12	0.54	0.76	0.12	0.78	0.93	1.58
0.90–0.99	10.37	0.35	0.12	0.60	0.76	0.12	0.72	0.93	1.57
0.99–1.08	9.82	0.37	0.14	0.61	0.77	0.13	0.86	0.93	1.66
1.08–1.17	9.46	0.38	0.13	0.60	0.77	0.16	0.77	0.93	1.61
1.17–1.26	9.08	0.39	0.13	0.55	0.79	0.16	0.78	0.93	1.60
1.26–1.35	8.55	0.39	0.14	0.59	0.78	0.13	0.80	0.93	1.63
1.35–1.44	8.00	0.51	0.19	0.56	0.76	0.14	0.74	0.93	1.62
1.44–1.53	7.41	0.56	0.23	1.17	0.80	0.12	0.96	0.93	2.04
1.53–1.62	7.18	0.42	0.15	1.05	0.97	0.12	0.87	0.93	1.97
1.62–1.71	6.50	0.45	0.18	0.63	0.97	0.10	0.98	0.93	1.85
1.71–1.80	5.90	0.48	0.18	0.66	0.97	0.11	1.00	0.94	1.88
1.80–1.89	5.49	0.53	0.19	0.52	0.95	0.12	1.07	0.94	1.88
1.89–1.98	5.00	0.54	0.20	0.60	0.95	0.11	1.13	0.94	1.94
1.98–2.37	3.81	0.31	0.12	0.78	1.02	0.11	1.03	0.93	1.93
2.37–2.50	2.67	0.79	0.25	0.90	1.17	0.16	0.99	0.93	2.18

Table 7. Absolute differential cross-section for $\lvert\eta^{\ell}\rvert$.

JHEP07(2023)141

$E^e + E^\mu$ bins [GeV]	$d\sigma/d(E^e + E^\mu)$ [fb/GeV]	Data stat. [%]	MC stat. [%]	$t\bar{t}$ mod. [%]	Lep. [%]	Jets/ b-tag. [%]	Bkg. [%]	Lumi + E_{beam} [%]	Total unc. [%]
50.0–60.0	1.38	5.20	3.78	4.20	1.38	1.08	5.61	0.88	9.71
60.0–70.0	9.04	1.93	0.89	1.82	1.10	0.38	1.03	0.94	3.33
70.0–80.0	20.47	1.16	0.38	2.43	0.96	0.14	0.97	0.92	3.18
80.0–90.0	30.69	0.95	0.29	0.79	0.88	0.17	0.65	0.92	1.92
90.0–110.0	43.64	0.52	0.14	0.74	0.80	0.13	0.65	0.92	1.66
110.0–125.0	51.23	0.56	0.13	0.55	0.75	0.12	0.59	0.92	1.55
125.0–160.0	51.53	0.37	0.09	0.46	0.73	0.12	0.59	0.92	1.45
160.0–200.0	43.20	0.37	0.09	0.67	0.74	0.13	0.66	0.92	1.56
200.0–250.0	31.56	0.38	0.09	0.65	0.78	0.11	0.76	0.93	1.62
250.0–300.0	20.93	0.48	0.11	0.56	0.84	0.15	1.02	0.93	1.79
300.0–370.0	12.74	0.54	0.13	0.79	0.93	0.13	1.25	0.94	2.06
370.0–450.0	6.92	0.70	0.16	0.91	1.07	0.15	1.61	0.95	2.45
450.0–550.0	3.45	0.97	0.22	0.70	1.29	0.17	1.92	0.96	2.79
550.0–700.0	1.42	1.19	0.29	1.39	1.61	0.16	2.37	0.96	3.55
700.0–900.0	0.62	1.78	0.44	2.25	2.48	0.27	3.77	1.00	5.46

Table 8. Absolute differential cross-section for $E^e + E^\mu$.

$m^{e\mu}$ bins [GeV]	$d\sigma/dm^{e\mu}$ [fb/GeV]	Data stat. [%]	MC stat. [%]	$t\bar{t}$ mod. [%]	Lep. [%]	Jets/ b-tag. [%]	Bkg. [%]	Lumi + E_{beam} [%]	Total unc. [%]
0.0–15.0	8.21	2.08	0.47	2.38	0.90	0.14	1.31	0.93	3.69
15.0–20.0	18.81	1.71	0.36	0.59	0.85	0.12	0.76	0.92	2.36
20.0–25.0	23.48	1.54	0.33	1.19	0.84	0.12	0.73	0.92	2.45
25.0–30.0	29.02	1.33	0.30	1.72	0.84	0.09	1.07	0.92	2.75
30.0–35.0	33.04	1.24	0.29	1.17	0.85	0.09	0.79	0.92	2.28
35.0–40.0	38.24	1.19	0.26	0.37	0.84	0.09	0.74	0.93	1.93
40.0–50.0	45.49	0.75	0.18	0.75	0.84	0.10	0.80	0.93	1.84
50.0–60.0	56.16	0.70	0.21	0.45	0.85	0.11	0.74	0.93	1.71
60.0–70.0	68.55	0.63	0.20	0.51	0.84	0.11	0.72	0.93	1.67
70.0–85.0	76.71	0.47	0.13	0.67	0.80	0.11	0.70	0.93	1.65
85.0–100.0	76.44	0.47	0.10	0.48	0.77	0.12	0.68	0.92	1.54
100.0–120.0	67.32	0.44	0.09	0.56	0.75	0.13	0.68	0.92	1.55
120.0–150.0	50.78	0.39	0.10	0.65	0.75	0.13	0.76	0.93	1.61
150.0–175.0	34.67	0.51	0.12	0.71	0.78	0.14	0.86	0.93	1.73
175.0–200.0	23.76	0.61	0.15	0.63	0.84	0.17	1.06	0.93	1.87
200.0–250.0	13.68	0.58	0.13	0.83	0.91	0.16	1.38	0.94	2.16
250.0–300.0	6.73	0.83	0.20	1.32	1.08	0.18	1.64	0.94	2.70
300.0–400.0	2.58	0.94	0.23	0.82	1.31	0.21	2.64	0.95	3.36
400.0–500.0	0.73	1.78	0.44	1.14	1.70	0.26	3.65	0.96	4.68
500.0–650.0	0.21	2.74	0.67	1.95	2.22	0.27	2.77	0.96	5.03
650.0–800.0	0.068	5.12	1.26	1.48	3.26	0.39	7.72	1.00	10.07

Table 9. Absolute differential cross-section for $m^{e\mu}$.

JHEP07(2023)141

$p_{\mathrm{T}}^{e}+p_{\mathrm{T}}^{\mu}$ bins [GeV]	$d\sigma/d(p_{\mathrm{T}}^{e}+p_{\mathrm{T}}^{\mu})$ [fb/GeV]	Data stat. [%]	MC stat. [%]	$t\bar{t}$ mod. [%]	Lep. [%]	Jets/ b-tag. [%]	Bkg. [%]	Lumi + E_{beam} [%]	Total unc. [%]
50.0–60.0	25.03	1.25	0.49	2.10	1.36	0.19	0.74	0.93	3.09
60.0–70.0	72.26	0.66	0.22	0.70	1.05	0.16	0.85	0.93	1.92
70.0–80.0	102.4	0.52	0.14	0.70	0.88	0.14	0.65	0.92	1.69
80.0–100.0	114.9	0.33	0.08	0.59	0.79	0.11	0.65	0.92	1.53
100.0–125.0	96.23	0.33	0.07	0.55	0.74	0.12	0.63	0.92	1.49
125.0–150.0	62.80	0.39	0.09	0.66	0.76	0.13	0.74	0.93	1.61
150.0–200.0	29.54	0.41	0.10	0.79	0.87	0.16	1.11	0.94	1.92
200.0–250.0	10.14	0.65	0.17	0.92	1.19	0.20	2.18	0.96	2.91
250.0–300.0	3.90	1.09	0.26	1.09	1.52	0.22	2.97	0.98	3.82
300.0–400.0	1.14	1.43	0.36	2.37	2.06	0.26	4.45	1.00	5.73
400.0–600.0	0.14	2.84	0.82	2.70	3.73	0.44	11.87	1.11	13.13

Table 10. Absolute differential cross-section for $p_{\mathrm{T}}^{e}+p_{\mathrm{T}}^{\mu}$.

$p_{\mathrm{T}}^{e\mu}$ bins [GeV]	$d\sigma/dp_{\mathrm{T}}^{e\mu}$ [fb/GeV]	Data stat. [%]	MC stat. [%]	$t\bar{t}$ mod. [%]	Lep. [%]	Jets/ b-tag. [%]	Bkg. [%]	Lumi + E_{beam} [%]	Total unc. [%]
0.0–20.0	32.51	0.66	0.21	0.87	0.79	0.19	0.67	0.92	1.79
20.0–30.0	69.08	0.64	0.17	0.87	0.78	0.22	0.68	0.92	1.78
30.0–45.0	87.41	0.46	0.11	0.90	0.78	0.18	0.66	0.92	1.72
45.0–60.0	111.0	0.41	0.09	0.71	0.79	0.15	0.64	0.92	1.61
60.0–75.0	121.0	0.38	0.09	0.66	0.79	0.14	0.63	0.92	1.57
75.0–100.0	93.20	0.33	0.07	0.70	0.78	0.12	0.66	0.92	1.59
100.0–125.0	48.51	0.45	0.10	0.97	0.89	0.15	0.99	0.93	1.96
125.0–150.0	19.74	0.70	0.17	0.38	1.20	0.21	1.98	0.95	2.64
150.0–200.0	5.73	0.95	0.23	0.55	1.62	0.28	3.65	1.00	4.28
200.0–300.0	0.86	1.78	0.49	3.39	2.64	0.35	11.88	1.14	12.82

Table 11. Absolute differential cross-section for $p_{\mathrm{T}}^{e\mu}$.

JHEP07(2023)141

$\lvert\Delta\phi^{e\mu}\rvert$ bins [rad]	$d\sigma/d\lvert\Delta\phi^{e\mu}\rvert$ [pb/rad]	Data stat. [%]	MC stat. [%]	$t\bar{t}$ mod. [%]	Lep. [%]	Jets/ b-tag. [%]	Bkg. [%]	Lumi + E_{beam} [%]	Total unc. [%]
0.00–0.10	2.21	1.12	0.24	0.46	0.84	0.11	0.84	0.92	1.95
0.10–0.21	2.19	1.12	0.24	0.73	0.84	0.10	0.83	0.92	2.03
0.21–0.31	2.18	1.05	0.24	1.26	0.84	0.10	0.79	0.92	2.22
0.31–0.42	2.22	1.08	0.23	0.33	0.85	0.08	1.02	0.93	1.99
0.42–0.52	2.23	1.03	0.23	0.93	0.84	0.10	0.78	0.92	2.04
0.52–0.63	2.31	1.02	0.22	1.19	0.84	0.09	0.77	0.92	2.16
0.63–0.73	2.32	1.00	0.22	0.70	0.84	0.12	0.89	0.92	1.98
0.73–0.84	2.40	0.95	0.22	1.11	0.83	0.10	0.72	0.92	2.06
0.84–0.94	2.43	1.01	0.23	1.22	0.83	0.10	0.93	0.93	2.23
0.94–1.05	2.48	0.98	0.22	0.65	0.83	0.11	0.83	0.93	1.92
1.05–1.15	2.60	0.98	0.23	0.88	0.83	0.11	0.75	0.93	1.98
1.15–1.26	2.73	0.93	0.21	0.59	0.82	0.09	0.80	0.93	1.86
1.26–1.36	2.83	0.91	0.20	0.95	0.82	0.10	0.90	0.93	2.03
1.36–1.47	2.99	0.90	0.20	0.37	0.81	0.13	0.78	0.93	1.77
1.47–1.57	3.07	0.90	0.21	0.47	0.81	0.11	0.87	0.93	1.83
1.57–1.68	3.18	0.88	0.20	0.57	0.81	0.12	1.03	0.93	1.93
1.68–1.78	3.35	0.86	0.21	0.57	0.80	0.12	0.78	0.93	1.79
1.78–1.88	3.46	0.85	0.21	0.62	0.80	0.14	1.00	0.93	1.92
1.88–1.99	3.65	0.80	0.21	0.62	0.80	0.13	0.90	0.93	1.85
1.99–2.09	3.83	0.81	0.20	0.86	0.79	0.13	0.82	0.93	1.91
2.09–2.20	4.00	0.75	0.19	1.21	0.79	0.14	0.76	0.93	2.04
2.20–2.30	4.19	0.75	0.20	1.10	0.79	0.17	0.78	0.93	1.98
2.30–2.41	4.31	0.74	0.19	0.60	0.80	0.16	0.72	0.93	1.73
2.41–2.51	4.49	0.73	0.18	0.79	0.80	0.17	0.81	0.93	1.84
2.51–2.62	4.59	0.71	0.19	0.67	0.81	0.16	0.87	0.93	1.82
2.62–2.72	4.71	0.72	0.19	0.60	0.81	0.18	0.82	0.93	1.77
2.72–2.83	4.79	0.70	0.18	0.94	0.82	0.19	0.86	0.94	1.93
2.83–2.93	4.87	0.71	0.19	0.86	0.82	0.20	0.86	0.93	1.90
2.93–3.04	4.95	0.68	0.18	1.03	0.83	0.18	0.75	0.93	1.93
3.04–3.14	5.09	0.66	0.17	0.70	0.83	0.19	0.76	0.93	1.77

Table 12. Absolute differential cross-section for $\lvert\Delta\phi^{e\mu}\rvert$.

JHEP07(2023)141

$\lvert y^{e\mu}\rvert$ bins	$d\sigma/d\lvert y^{e\mu}\rvert$	Data	MC	$t\bar{t}$	Lep.	Jets/	Bkg.	Lumi +	Total
-	[pb/units of y]	stat. [%]	stat. [%]	mod. [%]	[%]	b-tag. [%]	[%]	E_{beam} [%]	unc. [%]
0.00–0.08	7.94	0.59	0.15	0.58	0.77	0.13	0.75	0.92	1.65
0.08–0.17	7.96	0.57	0.14	0.70	0.78	0.13	0.75	0.92	1.69
0.17–0.25	7.89	0.61	0.15	0.43	0.77	0.13	0.69	0.93	1.59
0.25–0.33	7.78	0.56	0.14	0.51	0.78	0.14	0.82	0.93	1.65
0.33–0.42	7.64	0.60	0.14	0.65	0.77	0.12	0.80	0.93	1.71
0.42–0.50	7.47	0.61	0.15	0.81	0.77	0.12	0.89	0.93	1.82
0.50–0.58	7.21	0.64	0.15	0.73	0.77	0.14	0.79	0.93	1.75
0.58–0.67	6.98	0.65	0.15	1.03	0.77	0.13	0.75	0.93	1.88
0.67–0.75	6.70	0.65	0.16	0.85	0.78	0.14	0.79	0.93	1.81
0.75–0.83	6.42	0.66	0.16	0.53	0.78	0.13	0.90	0.93	1.74
0.83–0.92	5.99	0.68	0.17	0.59	0.79	0.14	0.88	0.93	1.77
0.92–1.00	5.73	0.69	0.17	0.68	0.80	0.14	0.73	0.93	1.74
1.00–1.08	5.40	0.76	0.18	0.77	0.81	0.13	0.86	0.93	1.86
1.08–1.17	4.97	0.80	0.20	0.95	0.82	0.13	0.87	0.93	1.98
1.17–1.25	4.55	0.86	0.20	0.94	0.84	0.13	0.89	0.93	2.01
1.25–1.33	4.12	0.89	0.24	0.84	0.86	0.16	0.80	0.93	1.96
1.33–1.42	3.75	1.02	0.24	0.97	0.88	0.11	0.85	0.93	2.10
1.42–1.50	3.34	1.05	0.27	0.74	0.91	0.11	0.91	0.94	2.06
1.50–1.58	2.97	1.15	0.29	0.79	0.95	0.13	0.91	0.94	2.16
1.58–1.67	2.53	1.27	0.36	1.31	1.01	0.14	1.02	0.94	2.53
1.67–1.75	2.13	1.43	0.38	1.40	1.05	0.14	1.29	0.95	2.80
1.75–1.83	1.76	1.58	0.44	1.42	1.11	0.14	1.28	0.95	2.92
1.83–1.92	1.50	1.81	0.43	2.12	1.17	0.12	1.17	0.95	3.41
1.92–2.00	1.14	2.04	0.57	1.26	1.23	0.10	1.29	0.96	3.19
2.00–2.08	0.88	2.54	0.73	1.60	1.30	0.15	1.56	0.96	3.82
2.08–2.17	0.67	2.87	0.76	1.40	1.39	0.32	2.35	0.98	4.39
2.17–2.25	0.44	3.71	1.00	4.70	1.41	0.18	1.71	0.98	6.54
2.25–2.33	0.24	4.63	1.61	2.40	1.50	0.24	2.26	0.99	6.18
2.33–2.42	0.13	7.91	2.26	3.54	1.53	0.29	2.74	1.00	9.55
2.42–2.50	0.045	26.27	3.68	7.40	1.89	0.77	6.60	0.92	28.41

Table 13. Absolute differential cross-section for $\lvert y^{e\mu}\rvert$.

JHEP07(2023)141

$\lvert y^{e\mu}\rvert \times m^{e\mu}$ bins		$d^2\sigma/d\lvert y^{e\mu}\rvert dm^{e\mu}$	Data	MC	$t\bar{t}$	Lep.	Jets/	Bkg.	Lumi +	Total
-		[fb/GeV]	stat. [%]	stat. [%]	mod. [%]	[%]	b-tag. [%]	[%]	E_{beam} [%]	unc. [%]
	0.00–0.31	24.27	0.68	0.20	0.62	0.84	0.11	0.61	0.92	1.68
	0.31–0.62	23.06	0.68	0.18	0.47	0.80	0.09	0.64	0.92	1.62
	0.62–0.94	20.66	0.74	0.20	0.38	0.78	0.12	0.73	0.93	1.66
$0.0 \leq m^{e\mu}$	0.94–1.25	17.66	0.85	0.22	0.62	0.81	0.09	0.87	0.93	1.85
< 70.0 GeV	1.25–1.56	14.01	1.07	0.29	0.65	0.93	0.10	0.81	0.93	2.01
	1.56–1.88	9.74	1.34	0.39	1.86	1.12	0.12	1.43	0.96	3.10
	1.88–2.19	5.28	1.90	0.59	1.61	1.25	0.18	1.60	0.96	3.41
	2.19–2.50	1.24	4.19	1.42	3.25	1.37	0.24	1.95	0.98	6.06
	0.00–0.31	54.03	0.66	0.17	0.87	0.76	0.12	0.60	0.92	1.74
	0.31–0.62	51.12	0.71	0.17	0.57	0.75	0.12	0.63	0.92	1.64
	0.62–0.94	44.99	0.80	0.19	1.31	0.75	0.13	0.68	0.92	2.07
$70.0 \leq m^{e\mu}$	0.94–1.25	38.25	0.85	0.21	0.92	0.78	0.12	0.73	0.93	1.91
< 100.0 GeV	1.25–1.56	28.81	1.06	0.29	0.92	0.85	0.16	0.86	0.93	2.10
	1.56–1.88	17.85	1.45	0.41	1.03	0.98	0.12	1.17	0.94	2.56
	1.88–2.19	8.03	2.40	0.67	0.87	1.14	0.12	1.61	0.95	3.43
	2.19–2.50	1.80	5.87	1.39	3.11	1.28	0.67	2.56	0.99	7.46
	0.00–0.31	47.10	0.70	0.16	0.46	0.72	0.14	0.66	0.92	1.60
	0.31–0.62	44.75	0.74	0.16	0.69	0.72	0.13	0.67	0.92	1.70
	0.62–0.94	39.40	0.83	0.18	0.76	0.73	0.13	0.70	0.92	1.78
$100.0 \leq m^{e\mu}$	0.94–1.25	32.73	0.92	0.22	0.68	0.76	0.13	0.87	0.93	1.89
< 130.0 GeV	1.25–1.56	22.66	1.16	0.26	1.15	0.81	0.11	0.80	0.93	2.22
	1.56–1.88	12.52	1.71	0.40	1.32	0.96	0.13	1.08	0.94	2.80
	1.88–2.19	5.25	2.92	0.67	1.77	1.27	0.17	1.52	0.96	4.12
	2.19–2.50	0.99	7.55	1.93	4.29	1.51	0.37	2.67	0.94	9.47
	0.00–0.31	27.05	0.62	0.14	0.62	0.73	0.15	0.72	0.92	1.65
	0.31–0.62	25.49	0.63	0.15	0.91	0.74	0.14	0.79	0.93	1.82
	0.62–0.94	22.06	0.71	0.16	0.84	0.77	0.15	0.90	0.93	1.87
$130.0 \leq m^{e\mu}$	0.94–1.25	16.67	0.84	0.19	1.19	0.82	0.16	0.98	0.93	2.16
< 200.0 GeV	1.25–1.56	10.61	1.10	0.26	1.75	0.88	0.17	0.96	0.93	2.64
	1.56–1.88	5.60	1.68	0.39	2.05	1.16	0.17	1.10	0.94	3.26
	1.88–2.19	2.02	3.28	0.77	2.48	1.69	0.12	1.41	0.97	4.82
	2.19–2.50	0.33	9.44	2.36	9.34	2.27	0.27	2.97	0.98	14.03
	0.00–0.31	2.15	0.76	0.17	1.01	0.98	0.18	1.81	0.94	2.61
	0.31–0.62	1.91	0.79	0.19	1.20	1.03	0.18	1.96	0.94	2.82
	0.62–0.94	1.50	0.88	0.21	0.53	1.10	0.17	1.93	0.94	2.63
$200.0 \leq m^{e\mu}$	0.94–1.25	1.00	1.16	0.27	1.65	1.23	0.20	1.94	0.95	3.22
$< 800.0+$ GeV	1.25–1.56	0.56	1.71	0.37	2.67	1.48	0.21	1.63	0.95	4.00
	1.56–1.88	0.22	2.74	0.76	3.05	1.92	0.24	2.23	0.97	5.19
	1.88–2.19	0.078	6.53	1.56	5.63	2.67	0.34	1.85	1.00	9.40
	2.19–2.50	0.007	20.92	7.43	23.77	3.91	1.32	3.80	1.00	33.02

Table 14. Double-differential cross-section for $\lvert y^{e\mu}\rvert : m^{e\mu}$. The cross-section measured in the last region includes events with an invariant mass greater than 800 GeV.

JHEP07(2023)141

$\lvert\Delta\phi^{e\mu}\rvert \times m^{e\mu}$ bins [rad]		$d^2\sigma/d\lvert\Delta\phi^{e\mu}\rvert dm^{e\mu}$ [fb/rad GeV]	Data stat. [%]	MC stat. [%]	$t\bar{t}$ mod. [%]	Lep. [%]	Jets/ b-tag. [%]	Bkg. [%]	Lumi + E_{beam} [%]	Total unc. [%]
	0.00–0.39	21.80	0.69	0.15	1.11	0.83	0.09	0.74	0.92	1.96
	0.39–0.79	21.29	0.66	0.15	0.66	0.82	0.09	0.73	0.93	1.72
	0.79–1.18	19.05	0.71	0.16	0.67	0.82	0.10	0.76	0.93	1.76
$0.0 \leq m^{e\mu}$	1.18–1.57	13.86	0.82	0.20	0.72	0.85	0.12	0.75	0.93	1.84
< 70.0 GeV	1.57–1.96	7.88	1.13	0.39	0.72	0.92	0.14	0.79	0.93	2.08
	1.96–2.36	4.13	1.74	0.82	1.49	1.04	0.30	1.04	0.96	3.01
	2.36–2.75	2.51	2.33	1.31	2.69	1.10	0.41	1.49	0.95	4.35
	2.75–3.14	1.74	2.60	1.76	1.50	1.20	0.48	1.97	0.98	4.31
	0.00–0.39	9.66	1.51	0.33	0.53	0.84	0.11	1.23	0.92	2.40
	0.39–0.79	12.09	1.27	0.29	0.83	0.82	0.11	0.90	0.92	2.18
	0.79–1.18	18.78	1.06	0.24	1.21	0.82	0.14	0.86	0.93	2.22
$70.0 \leq m^{e\mu}$	1.18–1.57	30.89	0.83	0.18	0.92	0.78	0.11	0.77	0.93	1.91
< 100.0 GeV	1.57–1.96	36.34	0.81	0.18	0.79	0.77	0.15	0.68	0.93	1.80
	1.96–2.36	33.76	0.80	0.21	1.08	0.80	0.16	0.78	0.92	1.99
	2.36–2.75	28.35	0.89	0.27	0.63	0.83	0.16	0.87	0.93	1.89
	2.75–3.14	25.13	0.98	0.30	1.24	0.84	0.22	0.77	0.92	2.18
	0.00–0.39	5.36	1.98	0.43	2.26	0.88	0.19	1.26	0.92	3.53
	0.39–0.79	6.58	1.74	0.37	1.47	0.90	0.12	1.06	0.92	2.85
	0.79–1.18	9.28	1.41	0.32	1.48	0.86	0.13	1.33	0.92	2.76
$100.0 \leq m^{e\mu}$	1.18–1.57	16.07	1.08	0.24	0.76	0.83	0.15	1.05	0.93	2.12
< 130.0 GeV	1.57–1.96	26.01	0.87	0.20	0.71	0.76	0.13	0.80	0.93	1.85
	1.96–2.36	33.10	0.79	0.18	1.20	0.74	0.15	0.67	0.93	2.00
	2.36–2.75	33.80	0.81	0.17	0.80	0.74	0.17	0.70	0.92	1.80
	2.75–3.14	33.37	0.82	0.19	0.62	0.75	0.15	0.65	0.92	1.72
	0.00–0.39	2.28	1.99	0.41	3.68	0.94	0.17	1.28	0.91	4.59
	0.39–0.79	2.61	1.89	0.40	2.93	0.92	0.11	1.64	0.91	4.09
	0.79–1.18	3.40	1.58	0.35	1.38	0.89	0.14	1.49	0.92	2.90
$130.0 \leq m^{e\mu}$	1.18–1.57	5.73	1.26	0.27	0.98	0.92	0.14	1.27	0.93	2.44
< 200.0 GeV	1.57–1.96	10.23	0.90	0.21	0.90	0.87	0.13	1.26	0.93	2.21
	1.96–2.36	17.05	0.71	0.16	0.92	0.80	0.16	0.79	0.93	1.88
	2.36–2.75	22.33	0.63	0.15	0.78	0.76	0.17	0.74	0.93	1.75
	2.75–3.14	23.86	0.61	0.15	0.79	0.75	0.19	0.69	0.93	1.72
	0.00–0.39	0.10	3.44	0.72	3.19	1.13	0.21	2.80	0.93	5.71
	0.39–0.79	0.11	3.06	0.66	2.29	1.12	0.18	3.59	0.93	5.49
	0.79–1.18	0.16	2.58	0.58	1.97	1.17	0.13	2.95	0.94	4.68
$200.0 \leq m^{e\mu}$	1.18–1.57	0.24	2.13	0.47	1.61	1.08	0.19	2.94	0.94	4.25
$< 800.0+$ GeV	1.57–1.96	0.43	1.56	0.35	1.08	1.13	0.17	3.03	0.94	3.89
	1.96–2.36	0.90	1.08	0.23	1.11	1.12	0.17	2.29	0.94	3.14
	2.36–2.75	1.65	0.75	0.19	0.71	1.10	0.19	1.70	0.95	2.47
	2.75–3.14	2.34	0.67	0.15	0.80	1.10	0.24	1.43	0.94	2.31

Table 15. Double-differential cross-section for $\lvert\Delta\phi^{e\mu}\rvert : m^{e\mu}$. The cross-section measured in the last region includes events with an invariant mass greater than 800 GeV.

JHEP07(2023)141

$\lvert\Delta\Phi^{e\mu}\rvert \times p_{\mathrm{T}}^{e\mu}$ bins		$d^2\sigma/d\lvert\Delta\phi^{e\mu}\rvert dp_{\mathrm{T}}^{e\mu}$	Data	MC	$t\bar{t}$	Lep.	Jets/	Bkg.	Lumi +	Total
[rad]		[fb/rad GeV]	stat. [%]	stat. [%]	mod. [%]	[%]	b-tag. [%]	[%]	E_{beam} [%]	unc. [%]
	0.00–1.65	0.077	8.69	3.11	8.43	2.01	0.29	6.00	0.95	14.04
$0.0 \leq p_{\mathrm{T}}^{e\mu}$	1.65–2.02	4.89	2.11	0.79	2.49	1.15	0.21	1.46	0.93	3.95
< 40.0 GeV	2.02–2.40	18.63	1.05	0.37	1.44	0.91	0.18	0.85	0.93	2.40
	2.40–2.77	46.83	0.63	0.18	0.52	0.78	0.19	0.67	0.92	1.63
	2.77–3.14	75.62	0.49	0.13	0.78	0.77	0.21	0.66	0.92	1.66
	0.00–0.31	7.94	2.39	0.53	2.22	1.18	0.26	0.97	0.91	3.76
	0.31–0.63	10.16	2.00	0.42	1.26	1.13	0.13	0.95	0.91	2.97
	0.63–0.94	13.62	1.71	0.39	0.68	1.08	0.12	1.15	0.91	2.62
	0.94–1.26	20.47	1.35	0.32	1.24	1.01	0.11	0.79	0.92	2.44
$40.0 \leq p_{\mathrm{T}}^{e\mu}$	1.26–1.57	32.47	1.09	0.25	0.88	0.92	0.14	0.70	0.92	2.06
< 65.0 GeV	1.57–1.88	46.63	0.88	0.23	0.80	0.84	0.13	0.65	0.92	1.86
	1.88–2.20	60.45	0.72	0.18	1.08	0.77	0.14	0.69	0.92	1.91
	2.20–2.51	65.85	0.69	0.15	0.66	0.74	0.17	0.71	0.92	1.69
	2.51–2.83	55.33	0.75	0.17	0.93	0.78	0.19	0.69	0.92	1.85
	2.83–3.14	39.00	0.88	0.22	0.97	0.86	0.21	0.70	0.93	1.97
	0.00–0.31	57.04	0.65	0.15	0.61	0.83	0.10	0.82	0.92	1.74
	0.31–0.63	57.25	0.64	0.14	0.34	0.83	0.09	0.88	0.93	1.69
	0.63–0.94	58.49	0.60	0.14	0.74	0.82	0.11	0.90	0.93	1.81
	0.94–1.26	59.96	0.60	0.14	0.99	0.81	0.11	0.84	0.93	1.89
$65.0 \leq p_{\mathrm{T}}^{e\mu}$	1.26–1.57	61.55	0.59	0.13	0.77	0.80	0.13	0.97	0.93	1.85
$< 100.0+$ GeV	1.57–1.88	59.08	0.62	0.14	0.72	0.81	0.14	1.13	0.93	1.93
	1.88–2.20	54.28	0.62	0.15	0.75	0.87	0.15	1.24	0.94	2.04
	2.20–2.51	44.84	0.71	0.17	0.83	1.01	0.19	1.42	0.95	2.28
	2.51–2.83	32.62	0.80	0.21	0.62	1.21	0.18	1.71	0.96	2.53
	2.83–3.14	25.75	0.95	0.23	1.05	1.32	0.24	2.09	0.96	3.02

Table 16. Double-differential cross-section for $|\Delta\phi^{e\mu}| : p_{\mathrm{T}}^{e\mu}$. The cross-section measured in the last region includes events with a p_{T} greater than 100 GeV.

JHEP07(2023)141

$\lvert\Delta\phi^{e\mu}\rvert \times (E^e + E^\mu)$ bins [rad]		$d^2\sigma/d\lvert\Delta\phi^{e\mu}\rvert d(E^e + E^\mu)$ [fb/rad GeV]	Data stat. [%]	MC stat. [%]	$t\bar{t}$ mod. [%]	Lep. [%]	Jets/ b-tag. [%]	Bkg. [%]	Lumi + E_{beam} [%]	Total unc. [%]
$0.0 \leq E^e + E^\mu < 110.0$ GeV	0.00–0.39	4.35	1.21	0.27	0.90	0.85	0.12	0.69	0.91	2.09
	0.39–0.79	4.40	1.13	0.24	1.74	0.85	0.11	0.78	0.91	2.56
	0.79–1.18	4.38	1.08	0.26	0.76	0.85	0.13	0.80	0.91	2.01
	1.18–1.57	4.48	1.13	0.28	0.47	0.85	0.12	0.61	0.92	1.88
	1.57–1.96	4.44	1.12	0.32	0.91	0.85	0.15	0.65	0.92	2.05
	1.96–2.36	4.26	1.15	0.44	1.40	0.86	0.23	0.62	0.93	2.35
	2.36–2.75	4.18	1.21	0.45	1.18	0.85	0.20	0.90	0.92	2.34
	2.75–3.14	3.96	1.24	0.51	1.49	0.85	0.19	0.76	0.92	2.49
$110.0 \leq E^e + E^\mu < 140.0$ GeV	0.00–0.39	13.76	1.28	0.27	1.59	0.77	0.10	0.62	0.91	2.47
	0.39–0.79	14.40	1.16	0.26	0.98	0.77	0.10	0.72	0.91	2.08
	0.79–1.18	15.57	1.15	0.25	0.69	0.76	0.10	0.60	0.92	1.91
	1.18–1.57	16.94	1.08	0.24	1.01	0.75	0.13	0.62	0.92	2.01
	1.57–1.96	17.44	1.06	0.27	0.83	0.75	0.15	0.64	0.92	1.93
	1.96–2.36	18.45	1.03	0.26	1.10	0.74	0.16	0.77	0.92	2.09
	2.36–2.75	17.89	1.09	0.26	0.67	0.74	0.17	0.74	0.92	1.91
	2.75–3.14	18.00	1.04	0.26	0.76	0.75	0.14	0.61	0.92	1.88
$140.0 \leq E^e + E^\mu < 200.0$ GeV	0.00–0.39	9.90	1.07	0.23	0.97	0.81	0.11	0.68	0.92	2.03
	0.39–0.79	10.50	0.96	0.21	0.53	0.79	0.11	0.68	0.92	1.79
	0.79–1.18	11.42	0.93	0.22	0.93	0.78	0.13	0.70	0.92	1.94
	1.18–1.57	13.65	0.87	0.19	1.33	0.75	0.11	0.66	0.92	2.10
	1.57–1.96	15.66	0.80	0.20	0.85	0.74	0.13	0.72	0.93	1.82
	1.96–2.36	17.77	0.76	0.18	0.81	0.72	0.15	0.61	0.92	1.74
	2.36–2.75	18.75	0.75	0.19	1.09	0.72	0.19	0.62	0.92	1.89
	2.75–3.14	18.72	0.72	0.18	0.99	0.72	0.16	0.68	0.92	1.84
$200.0 \leq E^e + E^\mu < 250.0$ GeV	0.00–0.39	5.81	1.59	0.33	0.91	0.88	0.16	0.96	0.92	2.46
	0.39–0.79	6.05	1.48	0.33	2.21	0.88	0.11	0.96	0.92	3.12
	0.79–1.18	6.85	1.32	0.31	0.91	0.86	0.13	1.06	0.93	2.33
	1.18–1.57	8.53	1.20	0.27	0.93	0.82	0.14	1.01	0.93	2.23
	1.57–1.96	10.28	1.13	0.26	1.32	0.79	0.12	0.81	0.93	2.29
	1.96–2.36	12.65	0.94	0.23	1.52	0.77	0.13	0.70	0.93	2.28
	2.36–2.75	14.68	0.94	0.22	0.67	0.76	0.16	0.72	0.93	1.83
	2.75–3.14	15.61	0.88	0.21	0.68	0.75	0.20	0.70	0.93	1.80
$250.0 \leq E^e + E^\mu < 900.0+$ GeV	0.00–0.39	0.65	1.32	0.30	1.54	1.10	0.17	1.84	0.95	3.12
	0.39–0.79	0.70	1.24	0.30	1.52	1.10	0.15	2.14	0.95	3.27
	0.79–1.18	0.81	1.17	0.26	0.96	1.08	0.13	1.75	0.95	2.74
	1.18–1.57	1.04	1.09	0.24	0.67	1.07	0.15	1.75	0.95	2.61
	1.57–1.96	1.42	0.86	0.21	1.03	1.05	0.14	1.74	0.95	2.62
	1.96–2.36	2.01	0.75	0.17	0.96	1.01	0.17	1.41	0.94	2.33
	2.36–2.75	2.65	0.60	0.15	0.74	1.01	0.17	1.38	0.95	2.19
	2.75–3.14	3.17	0.59	0.13	0.85	1.03	0.23	1.20	0.94	2.13

Table 17. Double-differential cross-section for $\lvert\Delta\phi^{e\mu}\rvert : E^e + E^\mu$. The cross-section measured in the last region includes events with a sum of the two energies greater than 900 GeV.

JHEP07(2023)141

p_{T}^{ℓ} bins [GeV]	$1/\sigma\ d\sigma/dp_{\mathrm{T}}^{\ell}$ $\times 10^{-3}$ [1/GeV]	Data stat. [%]	MC stat. [%]	$t\bar{t}$ mod. [%]	Lep. [%]	Jets/ b-tag. [%]	Bkg. [%]	Lumi + E_{beam} [%]	Total unc. [%]
25.0–30.0	21.85	0.34	0.10	0.24	0.55	0.07	0.24	0.01	0.74
30.0–40.0	20.50	0.23	0.06	0.23	0.21	0.04	0.30	0.01	0.49
40.0–50.0	16.90	0.25	0.06	0.37	0.19	0.02	0.27	0.01	0.56
50.0–60.0	13.12	0.28	0.07	0.13	0.23	0.02	0.20	0.01	0.44
60.0–75.0	9.33	0.26	0.06	0.46	0.25	0.02	0.20	0.01	0.62
75.0–100.0	5.17	0.26	0.07	0.34	0.20	0.04	0.15	0.00	0.51
100.0–140.0	1.98	0.37	0.09	0.31	0.43	0.08	0.64	0.02	0.92
140.0–180.0	0.61	0.68	0.17	0.57	0.92	0.13	1.67	0.05	2.11
180.0–250.0	0.15	1.01	0.28	0.86	1.42	0.20	3.74	0.09	4.23
250.0–350.0	0.024	2.34	0.66	2.57	3.90	0.35	12.48	0.24	13.55

Table 18. Normalised differential cross-section for p_{T}^{ℓ}.

$\lvert\eta^{\ell}\rvert$ bins -	$1/\sigma\ d\sigma/d\lvert\eta^{\ell}\rvert$ $\times 10^{-2}$ [1/units of η]	Data stat. [%]	MC stat. [%]	$t\bar{t}$ mod. [%]	Lep. [%]	Jets/ b-tag. [%]	Bkg. [%]	Lumi + E_{beam} [%]	Total unc. [%]
0.00–0.09	60.72	0.78	0.12	0.24	0.40	0.02	0.17	0.01	0.93
0.09–0.18	60.81	0.69	0.11	0.09	0.11	0.02	0.14	0.01	0.73
0.18–0.27	60.38	0.68	0.11	0.24	0.08	0.03	0.12	0.02	0.75
0.27–0.36	59.70	0.65	0.11	0.46	0.08	0.03	0.13	0.01	0.82
0.36–0.45	58.67	0.68	0.11	0.49	0.08	0.02	0.19	0.01	0.87
0.45–0.54	57.91	0.69	0.11	0.49	0.08	0.02	0.22	0.01	0.88
0.54–0.63	56.42	0.68	0.11	0.38	0.09	0.03	0.09	0.01	0.79
0.63–0.72	54.80	0.70	0.11	0.66	0.13	0.02	0.13	0.01	0.99
0.72–0.81	52.92	0.73	0.12	0.41	0.13	0.02	0.11	0.01	0.87
0.81–0.90	51.59	0.74	0.11	0.23	0.13	0.02	0.11	0.01	0.80
0.90–0.99	49.24	0.78	0.12	0.47	0.13	0.02	0.14	0.01	0.94
0.99–1.08	46.65	0.79	0.13	0.28	0.13	0.03	0.16	0.00	0.88
1.08–1.17	44.94	0.83	0.12	0.42	0.12	0.05	0.09	0.00	0.95
1.17–1.26	43.10	0.84	0.13	0.37	0.13	0.05	0.04	0.00	0.94
1.26–1.35	40.61	0.85	0.14	0.43	0.14	0.03	0.04	0.00	0.98
1.35–1.44	37.97	1.09	0.18	0.56	0.11	0.04	0.12	0.01	1.25
1.44–1.53	35.16	1.24	0.22	0.85	0.12	0.05	0.25	0.01	1.54
1.53–1.62	34.08	0.92	0.15	0.69	0.32	0.04	0.16	0.01	1.21
1.62–1.71	30.87	0.99	0.17	0.44	0.31	0.08	0.29	0.02	1.18
1.71–1.80	28.02	1.05	0.18	0.52	0.30	0.05	0.35	0.02	1.27
1.80–1.89	26.08	1.17	0.18	0.33	0.30	0.05	0.39	0.03	1.33
1.89–1.98	23.72	1.19	0.20	0.36	0.31	0.03	0.49	0.03	1.39
1.98–2.37	18.10	0.65	0.11	0.50	0.41	0.03	0.34	0.04	0.98
2.37–2.50	12.68	1.74	0.25	0.71	0.58	0.14	0.45	0.06	2.04

Table 19. Normalised differential cross-section for $|\eta^{\ell}|$.

JHEP07(2023)141

$E^e + E^\mu$ bins [GeV]	$1/\sigma\ d\sigma/d(E^e + E^\mu)$ $\times 10^{-3}$ [1/GeV]	Data stat. [%]	MC stat. [%]	$t\bar{t}$ mod. [%]	Lep. [%]	Jets/ b-tag. [%]	Bkg. [%]	Lumi + E_{beam} [%]	Total unc. [%]
50.0–60.0	0.13	5.19	3.77	3.95	0.92	1.07	5.68	0.06	9.54
60.0–70.0	0.86	1.92	0.88	1.84	0.52	0.40	1.02	0.03	3.05
70.0–80.0	1.94	1.15	0.37	2.25	0.42	0.13	1.14	0.03	2.83
80.0–90.0	2.91	0.93	0.28	0.45	0.35	0.11	0.63	0.03	1.29
90.0–110.0	4.14	0.50	0.13	0.54	0.31	0.07	0.69	0.03	1.07
110.0–125.0	4.86	0.54	0.12	0.30	0.26	0.03	0.58	0.03	0.90
125.0–160.0	4.89	0.33	0.08	0.26	0.22	0.02	0.39	0.02	0.62
160.0–200.0	4.10	0.35	0.08	0.36	0.17	0.02	0.24	0.01	0.59
200.0–250.0	2.99	0.35	0.08	0.30	0.13	0.02	0.06	0.00	0.49
250.0–300.0	1.99	0.46	0.11	0.47	0.17	0.05	0.35	0.01	0.77
300.0–370.0	1.21	0.52	0.13	0.45	0.27	0.04	0.60	0.03	0.96
370.0–450.0	0.66	0.68	0.16	0.74	0.44	0.05	0.99	0.04	1.49
450.0–550.0	0.33	0.95	0.22	0.43	0.73	0.08	1.33	0.06	1.85
550.0–700.0	0.13	1.18	0.28	1.49	1.11	0.08	1.79	0.08	2.85
700.0–900.0	0.058	1.75	0.43	1.97	2.06	0.21	3.18	0.14	4.65

Table 20. Normalised differential cross-section for $E^e + E^\mu$.

$m^{e\mu}$ bins [GeV]	$1/\sigma\ d\sigma/dm^{e\mu}$ $\times 10^{-3}$ [1/GeV]	Data stat. [%]	MC stat. [%]	$t\bar{t}$ mod. [%]	Lep. [%]	Jets/ b-tag. [%]	Bkg. [%]	Lumi + E_{beam} [%]	Total unc. [%]
0.0–15.0	0.78	2.06	0.47	2.18	0.32	0.16	1.21	0.01	3.29
15.0–20.0	1.78	1.70	0.36	0.45	0.18	0.15	0.60	0.01	1.91
20.0–25.0	2.22	1.54	0.32	1.10	0.19	0.14	0.43	0.02	1.98
25.0–30.0	2.75	1.32	0.30	1.52	0.16	0.10	1.15	0.02	2.35
30.0–35.0	3.13	1.23	0.28	1.20	0.17	0.07	0.53	0.01	1.83
35.0–40.0	3.62	1.18	0.25	0.28	0.17	0.08	0.49	0.01	1.35
40.0–50.0	4.31	0.74	0.18	0.60	0.17	0.06	0.62	0.01	1.16
50.0–60.0	5.32	0.68	0.20	0.38	0.19	0.06	0.55	0.01	0.99
60.0–70.0	6.49	0.60	0.19	0.33	0.17	0.06	0.44	0.01	0.85
70.0–85.0	7.26	0.44	0.12	0.46	0.16	0.06	0.31	0.01	0.74
85.0–100.0	7.24	0.44	0.10	0.23	0.16	0.02	0.36	0.01	0.64
100.0–120.0	6.37	0.40	0.09	0.23	0.13	0.03	0.18	0.01	0.53
120.0–150.0	4.81	0.36	0.09	0.41	0.10	0.03	0.07	0.00	0.56
150.0–175.0	3.28	0.49	0.11	0.60	0.13	0.03	0.20	0.01	0.82
175.0–200.0	2.25	0.59	0.15	0.36	0.22	0.06	0.47	0.01	0.88
200.0–250.0	1.30	0.56	0.13	0.68	0.30	0.06	0.83	0.02	1.26
250.0–300.0	0.64	0.81	0.20	1.11	0.53	0.09	1.11	0.03	1.85
300.0–400.0	0.24	0.93	0.23	0.85	0.78	0.11	2.17	0.05	2.64
400.0–500.0	0.07	1.76	0.43	0.95	1.22	0.17	3.18	0.07	3.98
500.0–650.0	0.020	2.72	0.67	1.74	1.79	0.17	2.24	0.08	4.38
650.0–800.0	0.064	5.13	1.25	1.55	2.87	0.30	7.25	0.14	9.55

Table 21. Normalised differential cross-section for $m^{e\mu}$.

JHEP07(2023)141

$p_{\mathrm{T}}^{e}+p_{\mathrm{T}}^{\mu}$ bins [GeV]	$1/\sigma\ d\sigma/d(p_{\mathrm{T}}^{e}+p_{\mathrm{T}}^{\mu})$ $\times 10^{-3}$ [1/GeV]	Data stat. [%]	MC stat. [%]	$t\bar{t}$ mod. [%]	Lep. [%]	Jets/ b-tag. [%]	Bkg. [%]	Lumi + E_{beam} [%]	Total unc. [%]
50.0–60.0	2.36	1.23	0.48	1.76	0.85	0.17	0.55	0.01	2.42
60.0–70.0	6.82	0.62	0.21	0.44	0.43	0.12	0.78	0.01	1.20
70.0–80.0	9.67	0.49	0.13	0.22	0.25	0.09	0.44	0.01	0.76
80.0–100.0	10.85	0.29	0.08	0.31	0.25	0.05	0.46	0.01	0.68
100.0–125.0	9.09	0.29	0.06	0.20	0.22	0.01	0.32	0.01	0.53
125.0–150.0	5.93	0.36	0.08	0.50	0.17	0.04	0.04	0.00	0.64
150.0–200.0	2.79	0.37	0.09	0.34	0.32	0.08	0.53	0.01	0.81
200.0–250.0	0.96	0.63	0.17	1.11	0.72	0.13	1.69	0.04	2.25
250.0–300.0	0.37	1.09	0.26	0.76	1.07	0.14	2.49	0.07	3.03
300.0–400.0	0.11	1.42	0.36	2.08	1.64	0.17	4.00	0.09	5.02
400.0–600.0	0.013	2.84	0.83	2.97	3.38	0.37	11.44	0.20	12.65

Table 22. Normalised differential cross-section for $p_{\mathrm{T}}^{e}+p_{\mathrm{T}}^{\mu}$.

$p_{\mathrm{T}}^{e\mu}$ bins [GeV]	$1/\sigma\ d\sigma/dp_{\mathrm{T}}^{e\mu}$ $\times 10^{-3}$ [1/GeV]	Data stat. [%]	MC stat. [%]	$t\bar{t}$ mod. [%]	Lep. [%]	Jets/ b-tag. [%]	Bkg. [%]	Lumi + E_{beam} [%]	Total unc. [%]
0.0–20.0	3.08	0.64	0.20	0.47	0.29	0.12	0.47	0.01	0.99
20.0–30.0	6.55	0.61	0.16	0.77	0.27	0.17	0.42	0.01	1.13
30.0–45.0	8.29	0.42	0.10	0.47	0.25	0.09	0.47	0.01	0.84
45.0–60.0	10.53	0.37	0.09	0.55	0.17	0.06	0.42	0.01	0.81
60.0–75.0	11.48	0.35	0.08	0.23	0.13	0.03	0.40	0.01	0.60
75.0–100.0	8.84	0.29	0.07	0.24	0.05	0.04	0.19	0.00	0.43
100.0–125.0	4.60	0.43	0.09	0.66	0.30	0.12	0.37	0.00	0.94
125.0–150.0	1.87	0.67	0.16	0.53	0.73	0.21	1.46	0.03	1.86
150.0–200.0	0.54	0.93	0.22	0.73	1.20	0.28	3.13	0.08	3.57
200.0–300.0	0.082	1.78	0.48	3.71	2.24	0.33	11.38	0.22	12.32

Table 23. Normalised differential cross-section for $p_{\mathrm{T}}^{e\mu}$.

JHEP07(2023)141

$\lvert\Delta\phi^{e\mu}\rvert$ bins [rad]	$1/\sigma\ d\sigma/d\lvert\Delta\phi^{e\mu}\rvert$ $\times 10^{-2}$ [1/rad]	Data stat. [%]	MC stat. [%]	$t\bar{t}$ mod. [%]	Lep. [%]	Jets/ b-tag. [%]	Bkg. [%]	Lumi + E_{beam} [%]	Total unc. [%]
0.00–0.10	20.94	1.11	0.24	0.61	0.14	0.13	0.15	0.01	1.31
0.10–0.21	20.81	1.11	0.24	0.59	0.13	0.11	0.26	0.01	1.32
0.21–0.31	20.72	1.04	0.24	1.39	0.13	0.12	0.32	0.01	1.79
0.31–0.42	21.04	1.07	0.22	0.25	0.14	0.10	0.35	0.01	1.19
0.42–0.52	21.20	1.02	0.22	0.90	0.13	0.08	0.12	0.01	1.39
0.52–0.63	21.87	1.01	0.22	1.19	0.12	0.09	0.22	0.01	1.60
0.63–0.73	22.04	0.99	0.22	0.62	0.12	0.10	0.29	0.01	1.24
0.73–0.84	22.76	0.93	0.22	1.26	0.11	0.08	0.32	0.01	1.62
0.84–0.94	23.06	1.00	0.23	1.22	0.11	0.08	0.20	0.00	1.61
0.94–1.05	23.57	0.97	0.22	0.47	0.10	0.06	0.07	0.01	1.11
1.05–1.15	24.66	0.96	0.22	0.82	0.11	0.07	0.24	0.01	1.31
1.15–1.26	25.94	0.92	0.21	0.49	0.09	0.06	0.15	0.01	1.08
1.26–1.36	26.87	0.89	0.20	0.84	0.08	0.07	0.20	0.00	1.26
1.36–1.47	28.40	0.89	0.20	0.42	0.07	0.09	0.14	0.00	1.02
1.47–1.57	29.15	0.88	0.20	0.31	0.06	0.04	0.16	0.00	0.97
1.57–1.68	30.17	0.86	0.20	0.45	0.06	0.03	0.37	0.00	1.06
1.68–1.78	31.77	0.85	0.20	0.32	0.04	0.04	0.07	0.00	0.93
1.78–1.88	32.83	0.83	0.21	0.35	0.03	0.07	0.35	0.00	0.99
1.88–1.99	34.62	0.79	0.20	0.50	0.02	0.03	0.16	0.00	0.97
1.99–2.09	36.31	0.79	0.20	0.51	0.03	0.03	0.10	0.00	0.97
2.09–2.20	37.97	0.74	0.18	0.89	0.03	0.03	0.11	0.00	1.18
2.20–2.30	39.74	0.73	0.20	0.84	0.05	0.06	0.20	0.00	1.15
2.30–2.41	40.84	0.71	0.18	0.21	0.06	0.06	0.38	0.00	0.86
2.41–2.51	42.60	0.71	0.18	0.45	0.08	0.06	0.12	0.00	0.87
2.51–2.62	43.50	0.69	0.19	0.47	0.09	0.08	0.13	0.01	0.87
2.62–2.72	44.70	0.69	0.19	0.47	0.10	0.08	0.14	0.01	0.88
2.72–2.83	45.46	0.68	0.17	0.84	0.12	0.09	0.08	0.01	1.11
2.83–2.93	46.22	0.69	0.18	0.53	0.13	0.09	0.15	0.01	0.92
2.93–3.04	46.94	0.67	0.18	0.64	0.14	0.08	0.19	0.01	0.98
3.04–3.14	48.24	0.65	0.16	0.49	0.14	0.13	0.11	0.01	0.86

Table 24. Normalised differential cross-section for $\lvert\Delta\phi^{e\mu}\rvert$.

JHEP07(2023)141

$\lvert y^{e\mu}\rvert$ bins	$1/\sigma\ d\sigma/d\lvert y^{e\mu}\rvert$	Data	MC	$t\bar{t}$	Lep.	Jets/	Bkg.	Lumi +	Total
-	$\times 10^{-3}$ [1/units of y]	stat. [%]	stat. [%]	mod. [%]	[%]	b-tag. [%]	[%]	E_{beam} [%]	unc. [%]
0.00–0.08	754.8	0.56	0.14	0.27	0.15	0.02	0.18	0.02	0.68
0.08–0.17	756.2	0.55	0.14	0.33	0.15	0.03	0.18	0.02	0.69
0.17–0.25	749.7	0.60	0.14	0.39	0.14	0.02	0.18	0.02	0.76
0.25–0.33	739.6	0.55	0.13	0.14	0.14	0.03	0.26	0.02	0.65
0.33–0.42	726.2	0.59	0.14	0.57	0.13	0.02	0.20	0.02	0.86
0.42–0.50	710.1	0.59	0.14	0.65	0.12	0.03	0.25	0.01	0.93
0.50–0.58	685.2	0.62	0.14	0.53	0.12	0.03	0.20	0.01	0.86
0.58–0.67	663.1	0.64	0.15	0.81	0.11	0.02	0.14	0.01	1.05
0.67–0.75	636.3	0.64	0.16	0.53	0.09	0.02	0.10	0.01	0.86
0.75–0.83	610.2	0.64	0.16	0.33	0.08	0.03	0.23	0.00	0.78
0.83–0.92	569.5	0.67	0.17	0.25	0.07	0.03	0.19	0.00	0.76
0.92–1.00	544.1	0.68	0.16	0.44	0.08	0.04	0.23	0.00	0.86
1.00–1.08	512.9	0.74	0.17	0.56	0.06	0.03	0.16	0.00	0.96
1.08–1.17	472.0	0.79	0.19	0.97	0.08	0.02	0.11	0.01	1.27
1.17–1.25	432.5	0.84	0.20	0.79	0.10	0.05	0.13	0.01	1.18
1.25–1.33	391.0	0.87	0.23	0.65	0.13	0.06	0.11	0.02	1.13
1.33–1.42	356.0	1.00	0.23	0.88	0.17	0.04	0.35	0.02	1.40
1.42–1.50	317.8	1.04	0.26	0.28	0.21	0.07	0.25	0.02	1.16
1.50–1.58	282.1	1.13	0.28	0.61	0.29	0.14	0.35	0.03	1.40
1.58–1.67	240.7	1.25	0.35	1.09	0.36	0.08	0.45	0.03	1.80
1.67–1.75	202.4	1.41	0.37	1.07	0.43	0.06	0.65	0.05	1.98
1.75–1.83	167.1	1.57	0.43	1.21	0.51	0.10	0.85	0.05	2.26
1.83–1.92	142.7	1.79	0.42	1.86	0.59	0.09	0.74	0.05	2.79
1.92–2.00	108.4	2.03	0.56	1.21	0.67	0.10	0.84	0.07	2.66
2.00–2.08	84.03	2.52	0.72	1.44	0.75	0.11	1.31	0.07	3.35
2.08–2.17	63.59	2.86	0.75	1.34	0.86	0.28	1.99	0.09	3.91
2.17–2.25	41.88	3.69	1.00	4.41	0.88	0.19	1.42	0.10	6.07
2.25–2.33	23.18	4.63	1.60	2.39	0.96	0.24	1.94	0.12	5.87
2.33–2.42	12.40	7.90	2.25	3.77	1.01	0.35	2.42	0.15	9.42
2.42–2.50	4.27	26.26	3.66	7.43	1.45	0.69	6.67	0.11	28.37

Table 25. Normalised differential cross-section for $\lvert y^{e\mu}\rvert$.

JHEP07(2023)141

$\lvert y^{e\mu}\rvert \times m^{e\mu}$ bins		$1/\sigma\ d^2\sigma/d\lvert y^{e\mu}\rvert dm^{e\mu}$	Data	MC	$t\bar{t}$	Lep.	Jets/	Bkg.	Lumi +	Total
-		$\times 10^{-3}$ [1/GeV]	stat. [%]	stat. [%]	mod. [%]	[%]	b-tag. [%]	[%]	E_{beam} [%]	unc. [%]
	0.00–0.31	2.30	0.66	0.19	0.48	0.22	0.08	0.57	0.03	1.04
	0.31–0.62	2.19	0.66	0.17	0.27	0.21	0.07	0.52	0.03	0.93
	0.62–0.94	1.96	0.73	0.20	0.30	0.21	0.06	0.54	0.02	1.00
$0.0 \leq m^{e\mu}$	0.94–1.25	1.67	0.82	0.21	0.58	0.19	0.08	0.79	0.01	1.31
< 70.0 GeV	1.25–1.56	1.33	1.05	0.29	0.36	0.29	0.07	0.54	0.01	1.31
	1.56–1.88	0.92	1.33	0.38	1.72	0.55	0.09	1.04	0.04	2.50
	1.88–2.19	0.50	1.89	0.58	1.61	0.72	0.16	1.26	0.06	2.94
	2.19–2.50	0.12	4.18	1.41	3.10	0.84	0.26	1.38	0.10	5.63
	0.00–0.31	5.12	0.65	0.17	0.72	0.21	0.04	0.33	0.03	1.06
	0.31–0.62	4.84	0.70	0.17	0.44	0.21	0.03	0.26	0.02	0.91
	0.62–0.94	4.26	0.78	0.18	1.19	0.19	0.02	0.44	0.02	1.52
$70.0 \leq m^{e\mu}$	0.94–1.25	3.63	0.84	0.20	0.88	0.18	0.03	0.44	0.01	1.32
< 100.0 GeV	1.25–1.56	2.73	1.05	0.29	0.92	0.22	0.17	0.47	0.01	1.53
	1.56–1.88	1.69	1.44	0.41	0.68	0.37	0.09	0.71	0.03	1.83
	1.88–2.19	0.76	2.38	0.67	0.57	0.60	0.11	1.29	0.06	2.91
	2.19–2.50	0.17	5.86	1.39	2.83	0.73	0.69	2.29	0.10	7.11
	0.00–0.31	4.46	0.69	0.16	0.32	0.21	0.04	0.26	0.03	0.84
	0.31–0.62	4.24	0.72	0.16	0.55	0.21	0.03	0.20	0.02	0.97
	0.62–0.94	3.73	0.82	0.18	0.58	0.16	0.03	0.14	0.01	1.04
$100.0 \leq m^{e\mu}$	0.94–1.25	3.10	0.91	0.22	0.50	0.14	0.02	0.18	0.00	1.08
< 130.0 GeV	1.25–1.56	2.15	1.14	0.26	0.89	0.15	0.07	0.38	0.02	1.53
	1.56–1.88	1.19	1.71	0.40	1.01	0.35	0.07	0.62	0.04	2.14
	1.88–2.19	0.50	2.90	0.66	1.81	0.73	0.10	1.13	0.08	3.74
	2.19–2.50	0.09	7.54	1.92	4.18	1.02	0.37	2.77	0.12	9.32
	0.00–0.31	2.56	0.60	0.13	0.52	0.21	0.04	0.19	0.01	0.85
	0.31–0.62	2.42	0.62	0.14	0.78	0.18	0.03	0.20	0.01	1.05
	0.62–0.94	2.09	0.69	0.16	0.50	0.14	0.04	0.29	0.00	0.93
$130.0 \leq m^{e\mu}$	0.94–1.25	1.58	0.83	0.19	1.07	0.16	0.06	0.34	0.01	1.42
< 200.0 GeV	1.25–1.56	1.01	1.10	0.25	1.70	0.22	0.07	0.22	0.03	2.07
	1.56–1.88	0.53	1.66	0.38	1.96	0.62	0.10	0.38	0.06	2.70
	1.88–2.19	0.19	3.26	0.76	2.20	1.23	0.08	0.71	0.10	4.25
	2.19–2.50	0.038	9.42	2.36	9.26	1.84	0.25	2.92	0.18	13.86
	0.00–0.31	0.20	0.75	0.17	0.83	0.42	0.08	1.32	0.02	1.79
	0.31–0.62	0.18	0.77	0.18	1.12	0.47	0.08	1.47	0.02	2.07
	0.62–0.94	0.14	0.87	0.21	0.31	0.54	0.07	1.43	0.03	1.80
$200.0 \leq m^{e\mu}$	0.94–1.25	0.10	1.14	0.27	1.60	0.70	0.09	1.41	0.04	2.54
$< 800.0+$ GeV	1.25–1.56	0.056	1.70	0.37	2.57	1.01	0.12	1.03	0.06	3.43
	1.56–1.88	0.024	2.73	0.76	2.92	1.49	0.17	1.62	0.11	4.63
	1.88–2.19	0.0063	6.52	1.56	5.43	2.29	0.30	1.36	0.18	9.04
	2.19–2.50	0.00070	20.92	7.42	23.90	3.57	1.30	3.72	0.27	33.05

Table 26. Normalised double-differential cross-section for $|y^{e\mu}| : m^{e\mu}$. The cross-section measured in the last region includes events with an invariant mass greater than 800 GeV.

JHEP07(2023)141

$\lvert\Delta\phi^{e\mu}\rvert \times m^{e\mu}$ bins [rad]		$1/\sigma\ d^2\sigma/d\lvert\Delta\phi^{e\mu}\rvert dm^{e\mu}$ $\times 10^{-3}$ [1/rad GeV]	Data stat. [%]	MC stat. [%]	$t\bar{t}$ mod. [%]	Lep. [%]	Jets/ b-tag. [%]	Bkg. [%]	Lumi + E_{beam} [%]	Total unc. [%]
	0.00–0.39	2.06	0.66	0.15	1.02	0.12	0.10	0.40	0.01	1.30
	0.39–0.79	2.02	0.64	0.14	0.54	0.12	0.08	0.47	0.01	0.98
	0.79–1.18	1.80	0.69	0.16	0.66	0.15	0.05	0.61	0.01	1.16
$0.0 \leq m^{e\mu}$	1.18–1.57	1.31	0.81	0.20	0.63	0.28	0.05	0.68	0.01	1.28
< 70.0 GeV	1.57–1.96	0.75	1.12	0.39	0.50	0.33	0.09	0.63	0.01	1.47
	1.96–2.36	0.39	1.72	0.81	1.24	0.47	0.27	0.96	0.03	2.53
	2.36–2.75	0.24	2.32	1.30	2.54	0.50	0.38	1.47	0.03	4.01
	2.75–3.14	0.16	2.59	1.75	1.35	0.69	0.45	1.82	0.06	3.95
	0.00–0.39	0.91	1.50	0.33	0.59	0.16	0.11	0.66	0.01	1.79
	0.39–0.79	1.14	1.26	0.29	0.74	0.14	0.08	0.21	0.01	1.51
	0.79–1.18	1.78	1.05	0.24	1.08	0.15	0.13	0.20	0.01	1.55
$70.0 \leq m^{e\mu}$	1.18–1.57	2.92	0.82	0.18	0.78	0.10	0.07	0.17	0.01	1.17
< 100.0 GeV	1.57–1.96	3.44	0.79	0.18	0.67	0.22	0.04	0.31	0.01	1.12
	1.96–2.36	3.20	0.79	0.21	0.82	0.28	0.06	0.77	0.01	1.42
	2.36–2.75	2.68	0.87	0.26	0.59	0.32	0.11	0.77	0.01	1.37
	2.75–3.14	2.38	0.97	0.29	1.14	0.31	0.23	0.68	0.01	1.72
	0.00–0.39	0.51	1.97	0.43	2.34	0.24	0.20	0.67	0.01	3.17
	0.39–0.79	0.62	1.73	0.37	1.71	0.28	0.11	0.45	0.01	2.52
	0.79–1.18	0.88	1.41	0.32	1.40	0.24	0.11	0.76	0.01	2.17
$100.0 \leq m^{e\mu}$	1.18–1.57	1.52	1.08	0.24	0.54	0.19	0.13	0.46	0.00	1.33
< 130.0 GeV	1.57–1.96	2.46	0.86	0.20	0.50	0.10	0.05	0.17	0.00	1.03
	1.96–2.36	3.13	0.78	0.18	0.93	0.21	0.04	0.24	0.01	1.27
	2.36–2.75	3.20	0.79	0.17	0.74	0.24	0.08	0.54	0.01	1.25
	2.75–3.14	3.16	0.80	0.18	0.30	0.29	0.06	0.36	0.01	0.99
	0.00–0.39	0.22	1.99	0.41	3.94	0.35	0.19	0.76	0.03	4.51
	0.39–0.79	0.25	1.88	0.40	2.86	0.31	0.13	1.14	0.02	3.64
	0.79–1.18	0.32	1.56	0.34	1.47	0.27	0.12	0.93	0.01	2.38
$130.0 \leq m^{e\mu}$	1.18–1.57	0.54	1.24	0.27	1.04	0.34	0.13	0.68	0.01	1.82
< 200.0 GeV	1.57–1.96	0.97	0.89	0.20	0.84	0.27	0.09	0.71	0.01	1.46
	1.96–2.36	1.61	0.70	0.16	0.58	0.15	0.05	0.11	0.01	0.94
	2.36–2.75	2.11	0.61	0.14	0.60	0.17	0.06	0.13	0.00	0.90
	2.75–3.14	2.26	0.60	0.14	0.39	0.20	0.08	0.24	0.00	0.79
	0.00–0.39	0.0089	3.43	0.71	3.20	0.58	0.19	2.30	0.04	5.31
	0.39–0.79	0.010	3.05	0.66	2.58	0.57	0.19	3.12	0.04	5.15
	0.79–1.18	0.014	2.57	0.58	2.22	0.65	0.13	2.44	0.03	4.28
$200.0 \leq m^{e\mu}$	1.18–1.57	0.022	2.13	0.47	1.80	0.53	0.20	2.44	0.03	3.77
$< 800.0+$ GeV	1.57–1.96	0.040	1.55	0.35	0.95	0.61	0.16	2.55	0.04	3.22
	1.96–2.36	0.085	1.07	0.23	0.89	0.60	0.12	1.81	0.03	2.38
	2.36–2.75	0.16	0.73	0.19	0.37	0.54	0.08	1.17	0.03	1.54
	2.75–3.14	0.22	0.65	0.15	0.61	0.53	0.13	0.87	0.03	1.37

Table 27. Normalised double-differential cross-section for $|\Delta\phi^{e\mu}| : m^{e\mu}$. The cross-section measured in the last region includes events with an invariant mass greater than 800 GeV.

JHEP07(2023)141

$\lvert\Delta\phi^{e\mu}\rvert \times p_{\mathrm{T}}^{e\mu}$ bins [rad]		$1/\sigma\ d^2\sigma/d\lvert\Delta\phi^{e\mu}\rvert dp_{\mathrm{T}}^{e\mu}$ $\times 10^{-3}$ [1/rad GeV]	Data stat. [%]	MC stat. [%]	$t\bar{t}$ mod. [%]	Lep. [%]	Jets/ b-tag. [%]	Bkg. [%]	Lumi + E_{beam} [%]	Total unc. [%]
$0.0 \leq p_{\mathrm{T}}^{e\mu} < 40.0$ GeV	0.00–1.65	0.0070	8.68	3.10	8.35	1.61	0.27	5.85	0.02	13.84
	1.65–2.02	0.46	2.10	0.79	2.35	0.58	0.17	1.36	0.01	3.57
	2.02–2.40	1.76	1.02	0.36	1.18	0.33	0.12	0.76	0.01	1.81
	2.40–2.77	4.43	0.60	0.17	0.28	0.32	0.12	0.48	0.01	0.90
	2.77–3.14	7.16	0.46	0.12	0.36	0.28	0.14	0.40	0.01	0.78
$40.0 \leq p_{\mathrm{T}}^{e\mu} < 65.0$ GeV	0.00–0.31	0.75	2.37	0.52	2.16	0.66	0.24	0.97	0.02	3.46
	0.31–0.63	0.96	1.99	0.42	1.09	0.56	0.13	1.05	0.03	2.60
	0.63–0.94	1.29	1.70	0.38	0.53	0.50	0.07	1.29	0.02	2.28
	0.94–1.26	1.94	1.34	0.31	1.23	0.40	0.08	0.73	0.02	2.02
	1.26–1.57	3.07	1.07	0.25	1.02	0.32	0.08	0.58	0.01	1.64
	1.57–1.88	4.41	0.86	0.22	0.80	0.28	0.05	0.32	0.01	1.27
	1.88–2.20	5.72	0.70	0.18	0.78	0.33	0.06	0.63	0.01	1.28
	2.20–2.51	6.23	0.68	0.15	0.27	0.34	0.08	0.68	0.01	1.07
	2.51–2.83	5.24	0.74	0.17	0.93	0.24	0.09	0.16	0.01	1.24
	2.83–3.14	3.69	0.88	0.21	0.91	0.22	0.11	0.21	0.01	1.32
$65.0 \leq p_{\mathrm{T}}^{e\mu} < 100.0+$ GeV	0.00–0.31	5.40	0.63	0.14	0.64	0.14	0.12	0.17	0.01	0.94
	0.31–0.63	5.42	0.62	0.13	0.28	0.14	0.09	0.16	0.01	0.73
	0.63–0.94	5.54	0.58	0.13	0.86	0.13	0.10	0.21	0.00	1.08
	0.94–1.26	5.68	0.58	0.13	0.86	0.13	0.08	0.09	0.00	1.06
	1.26–1.57	5.83	0.58	0.13	0.57	0.12	0.10	0.31	0.00	0.89
	1.57–1.88	5.59	0.60	0.13	0.47	0.15	0.08	0.53	0.01	0.95
	1.88–2.20	5.14	0.61	0.14	0.51	0.26	0.08	0.64	0.01	1.07
	2.20–2.51	4.25	0.69	0.16	0.52	0.45	0.10	0.85	0.02	1.30
	2.51–2.83	3.09	0.78	0.20	0.20	0.68	0.08	1.13	0.04	1.56
	2.83–3.14	2.44	0.94	0.23	0.90	0.80	0.17	1.55	0.04	2.20

Table 28. Normalised double-differential cross-section for $|\Delta\phi^{e\mu}| : p_{\mathrm{T}}^{e\mu}$. The cross-section measured in the last region includes events with a p_{T} greater than 100 GeV.

JHEP07(2023)141

$\lvert\Delta\phi^{e\mu}\rvert \times (E^e + E^\mu)$ bins [rad]		$1/\sigma\ d^2\sigma/d\lvert\Delta\phi^{e\mu}\rvert d(E^e+E^\mu)$ $\times 10^{-3}$ [1/rad GeV]	Data stat. [%]	MC stat. [%]	$t\bar{t}$ mod. [%]	Lep. [%]	Jets/ b-tag. [%]	Bkg. [%]	Lumi + E_{beam} [%]	Total unc. [%]
$0.0 \le E^e + E^\mu$ < 110.0 GeV	0.00–0.39	0.41	1.19	0.27	0.72	0.30	0.11	0.78	0.04	1.65
	0.39–0.79	0.42	1.12	0.24	1.68	0.30	0.08	0.83	0.03	2.22
	0.79–1.18	0.42	1.07	0.26	0.49	0.30	0.10	0.94	0.03	1.56
	1.18–1.57	0.42	1.11	0.27	0.40	0.33	0.07	0.62	0.03	1.40
	1.57–1.96	0.42	1.11	0.31	0.76	0.34	0.07	0.67	0.03	1.57
	1.96–2.36	0.40	1.15	0.44	1.23	0.35	0.19	0.53	0.03	1.86
	2.36–2.75	0.40	1.20	0.44	0.94	0.35	0.18	1.01	0.02	1.92
	2.75–3.14	0.38	1.23	0.50	1.38	0.35	0.16	0.76	0.02	2.10
$110.0 \le E^e + E^\mu$ < 140.0 GeV	0.00–0.39	1.30	1.28	0.27	1.49	0.20	0.11	0.28	0.03	2.01
	0.39–0.79	1.37	1.15	0.26	0.68	0.20	0.06	0.83	0.03	1.61
	0.79–1.18	1.48	1.13	0.24	0.51	0.22	0.05	0.48	0.02	1.37
	1.18–1.57	1.61	1.08	0.24	1.03	0.23	0.02	0.58	0.03	1.63
	1.57–1.96	1.65	1.04	0.27	0.75	0.28	0.06	0.23	0.02	1.36
	1.96–2.36	1.75	1.02	0.25	0.88	0.30	0.06	0.85	0.02	1.64
	2.36–2.75	1.70	1.07	0.26	0.64	0.32	0.08	0.81	0.02	1.54
	2.75–3.14	1.71	1.03	0.26	0.49	0.36	0.06	0.57	0.03	1.36
$140.0 \le E^e + E^\mu$ < 200.0 GeV	0.00–0.39	0.94	1.05	0.23	1.01	0.17	0.12	0.21	0.01	1.50
	0.39–0.79	1.00	0.96	0.21	0.55	0.15	0.09	0.25	0.01	1.16
	0.79–1.18	1.08	0.92	0.21	0.93	0.16	0.11	0.17	0.01	1.35
	1.18–1.57	1.29	0.86	0.19	1.21	0.15	0.06	0.28	0.01	1.53
	1.57–1.96	1.48	0.78	0.19	0.86	0.18	0.04	0.13	0.01	1.20
	1.96–2.36	1.68	0.75	0.18	0.48	0.25	0.04	0.34	0.02	1.00
	2.36–2.75	1.78	0.72	0.18	1.06	0.28	0.10	0.34	0.01	1.37
	2.75–3.14	1.78	0.72	0.18	0.71	0.30	0.08	0.43	0.01	1.15
$200.0 \le E^e + E^\mu$ < 250.0 GeV	0.00–0.39	0.55	1.57	0.33	1.04	0.24	0.18	0.29	0.01	1.96
	0.39–0.79	0.57	1.46	0.33	2.19	0.24	0.11	0.27	0.01	2.68
	0.79–1.18	0.65	1.32	0.31	0.80	0.20	0.10	0.38	0.01	1.63
	1.18–1.57	0.81	1.20	0.26	0.85	0.15	0.12	0.33	0.00	1.54
	1.57–1.96	0.97	1.11	0.25	1.21	0.14	0.05	0.18	0.00	1.67
	1.96–2.36	1.20	0.94	0.23	1.29	0.15	0.02	0.21	0.00	1.63
	2.36–2.75	1.39	0.92	0.21	0.32	0.24	0.05	0.31	0.00	1.07
	2.75–3.14	1.48	0.87	0.21	0.51	0.25	0.17	0.23	0.00	1.10
$250.0 \le E^e + E^\mu$ $< 900.0+$ GeV	0.00–0.39	0.059	1.32	0.30	1.71	0.50	0.19	1.17	0.04	2.53
	0.39–0.79	0.064	1.22	0.29	1.68	0.51	0.16	1.54	0.04	2.66
	0.79–1.18	0.077	1.16	0.26	1.15	0.47	0.11	1.11	0.04	2.05
	1.18–1.57	0.10	1.07	0.24	0.69	0.47	0.15	1.11	0.04	1.78
	1.57–1.96	0.13	0.84	0.20	0.80	0.45	0.11	1.14	0.04	1.70
	1.96–2.36	0.19	0.73	0.16	0.58	0.38	0.07	0.79	0.04	1.29
	2.36–2.75	0.25	0.57	0.15	0.49	0.38	0.06	0.76	0.04	1.15
	2.75–3.14	0.30	0.56	0.13	0.58	0.40	0.12	0.55	0.04	1.07

Table 29. Normalised double-differential cross-section for $|\Delta\phi^{e\mu}| : E^e + E^\mu$. The cross-section measured in the last region includes events with a sum of the two energies greater than 900 GeV.

Open Access. This article is distributed under the terms of the Creative Commons Attribution License (CC-BY 4.0), which permits any use, distribution and reproduction in any medium, provided the original author(s) and source are credited.

References

[1] ATLAS collaboration, *The ATLAS experiment at the CERN Large Hadron Collider*, 2008 *JINST* **3** S08003 [INSPIRE].

[2] ATLAS IBL collaboration, *Production and integration of the ATLAS Insertable B-Layer*, 2018 *JINST* **13** T05008 [arXiv:1803.00844] [INSPIRE].

[3] ATLAS collaboration, *ATLAS Insertable B-Layer: technical design report*, ATLAS-TDR-19, CERN, Geneva, Switzerland (2010).

[4] ATLAS collaboration, *Measurement of the $t\bar{t}$ production cross-section using $e\mu$ events with b-tagged jets in pp collisions at $\sqrt{s} = 7$ and 8 TeV with the ATLAS detector*, *Eur. Phys. J. C* **74** (2014) 3109 [*Addendum ibid.* **76** (2016) 642] [arXiv:1406.5375] [INSPIRE].

JHEP07(2023)141

[5] ATLAS collaboration, *Measurement of lepton differential distributions and the top quark mass in $t\bar{t}$ production in pp collisions at $\sqrt{s} = 8$ TeV with the ATLAS detector*, *Eur. Phys. J. C* **77** (2017) 804 [arXiv:1709.09407] [INSPIRE].

[6] ATLAS collaboration, *Measurement of the $t\bar{t}$ production cross-section and lepton differential distributions in $e\mu$ dilepton events from pp collisions at $\sqrt{s} = 13$ TeV with the ATLAS detector*, *Eur. Phys. J. C* **80** (2020) 528 [arXiv:1910.08819] [INSPIRE].

[7] CMS collaboration, *Measurements of $t\bar{t}$ differential cross sections in proton-proton collisions at $\sqrt{s} = 13$ TeV using events containing two leptons*, *JHEP* **02** (2019) 149 [arXiv:1811.06625] [INSPIRE].

[8] CMS collaboration, *Measurement of $t\bar{t}$ normalised multi-differential cross sections in pp collisions at $\sqrt{s} = 13$ TeV, and simultaneous determination of the strong coupling strength, top quark pole mass, and parton distribution functions*, *Eur. Phys. J. C* **80** (2020) 658 [arXiv:1904.05237] [INSPIRE].

[9] CMS collaboration, *Measurement of the top quark Yukawa coupling from $t\bar{t}$ kinematic distributions in the dilepton final state in proton-proton collisions at $\sqrt{s} = 13$ TeV*, *Phys. Rev. D* **102** (2020) 092013 [arXiv:2009.07123] [INSPIRE].

[10] ATLAS collaboration, *Luminosity determination in pp collisions at $\sqrt{s} = 13$ TeV using the ATLAS detector at the LHC*, arXiv:2212.09379 [INSPIRE].

[11] ATLAS collaboration, *The ATLAS collaboration software and firmware*, ATL-SOFT-PUB-2021-001, CERN, Geneva, Switzerland (2021).

[12] ATLAS collaboration, *Performance of the ATLAS trigger system in* 2015, *Eur. Phys. J. C* **77** (2017) 317 [arXiv:1611.09661] [INSPIRE].

[13] ATLAS collaboration, *Performance of the ATLAS muon triggers in run* 2, 2020 *JINST* **15** P09015 [arXiv:2004.13447] [INSPIRE].

[14] ATLAS collaboration, *Performance of electron and photon triggers in ATLAS during LHC run* 2, *Eur. Phys. J. C* **80** (2020) 47 [arXiv:1909.00761] [INSPIRE].

[15] ATLAS collaboration, *ATLAS data quality operations and performance for* 2015–2018 *data-taking*, 2020 *JINST* **15** P04003 [arXiv:1911.04632] [INSPIRE].

[16] ATLAS collaboration, *The ATLAS simulation infrastructure*, *Eur. Phys. J. C* **70** (2010) 823 [arXiv:1005.4568] [INSPIRE].

[17] GEANT4 collaboration, *GEANT4 — a simulation toolkit*, *Nucl. Instrum. Meth. A* **506** (2003) 250 [INSPIRE].

[18] C. ATLAS et al., *The simulation principle and performance of the ATLAS fast calorimeter simulation FastCaloSim*, ATL-PHYS-PUB-2010-013, CERN, Geneva, Switzerland (2010).

[19] T. Sjöstrand, S. Mrenna and P.Z. Skands, *A brief introduction to PYTHIA* 8.1, *Comput. Phys. Commun.* **178** (2008) 852 [arXiv:0710.3820] [INSPIRE].

[20] R.D. Ball et al., *Parton distributions with LHC data*, *Nucl. Phys. B* **867** (2013) 244 [arXiv:1207.1303] [INSPIRE].

[21] ATLAS collaboration, *The Pythia* 8 *A*3 *tune description of ATLAS minimum bias and inelastic measurements incorporating the Donnachie-Landshoff diffractive model*, ATL-PHYS-PUB-2016-017, CERN, Geneva, Switzerland (2016).

JHEP07(2023)141

[22] D.J. Lange, *The EvtGen particle decay simulation package*, *Nucl. Instrum. Meth. A* **462** (2001) 152 [INSPIRE].

[23] P. Nason, *A new method for combining NLO QCD with shower Monte Carlo algorithms*, *JHEP* **11** (2004) 040 [hep-ph/0409146] [INSPIRE].

[24] S. Frixione, P. Nason and C. Oleari, *Matching NLO QCD computations with parton shower simulations: the POWHEG method*, *JHEP* **11** (2007) 070 [arXiv:0709.2092] [INSPIRE].

[25] S. Alioli, P. Nason, C. Oleari and E. Re, *A general framework for implementing NLO calculations in shower Monte Carlo programs: the POWHEG BOX*, *JHEP* **06** (2010) 043 [arXiv:1002.2581] [INSPIRE].

[26] S. Frixione, P. Nason and G. Ridolfi, *A positive-weight next-to-leading-order Monte Carlo for heavy flavour hadroproduction*, *JHEP* **09** (2007) 126 [arXiv:0707.3088] [INSPIRE].

[27] NNPDF collaboration, *Parton distributions for the LHC run II*, *JHEP* **04** (2015) 040 [arXiv:1410.8849] [INSPIRE].

[28] T. Sjöstrand et al., *An introduction to PYTHIA* 8.2, *Comput. Phys. Commun.* **191** (2015) 159 [arXiv:1410.3012] [INSPIRE].

[29] T. Sjostrand, S. Mrenna and P.Z. Skands, *PYTHIA* 6.4 *physics and manual*, *JHEP* **05** (2006) 026 [hep-ph/0603175] [INSPIRE].

[30] ATLAS collaboration, *ATLAS Pythia* 8 *tunes to* 7 *TeV data*, ATL-PHYS-PUB-2014-021, CERN, Geneva, Switzerland (2014).

[31] ATLAS collaboration, *Studies on top-quark Monte Carlo modelling for Top*2016, ATL-PHYS-PUB-2016-020, CERN, Geneva, Switzerland (2016).

[32] ATLAS collaboration, *Improvements in $t\bar{t}$ modelling using NLO+PS Monte Carlo generators for run* 2, ATL-PHYS-PUB-2018-009, CERN, Geneva, Switzerland (2018).

[33] J. Butterworth et al., *PDF4LHC recommendations for LHC run II*, *J. Phys. G* **43** (2016) 023001 [arXiv:1510.03865] [INSPIRE].

[34] J. Gao and P. Nadolsky, *A meta-analysis of parton distribution functions*, *JHEP* **07** (2014) 035 [arXiv:1401.0013] [INSPIRE].

[35] S. Carrazza et al., *An unbiased Hessian representation for Monte Carlo PDFs*, *Eur. Phys. J. C* **75** (2015) 369 [arXiv:1505.06736] [INSPIRE].

[36] J. Alwall et al., *The automated computation of tree-level and next-to-leading order differential cross sections, and their matching to parton shower simulations*, *JHEP* **07** (2014) 079 [arXiv:1405.0301] [INSPIRE].

[37] ATLAS collaboration, *Study of top-quark pair modelling and uncertainties using ATLAS measurements at* $\sqrt{s} = 13$ *TeV*, ATL-PHYS-PUB-2020-023, CERN, Geneva, Switzerland (2020).

[38] M. Bähr et al., *Herwig++ physics and manual*, *Eur. Phys. J. C* **58** (2008) 639 [arXiv:0803.0883] [INSPIRE].

[39] J. Bellm et al., *Herwig* 7.0/*Herwig++* 3.0 *release note*, *Eur. Phys. J. C* **76** (2016) 196 [arXiv:1512.01178] [INSPIRE].

[40] S. Gieseke, C. Röhr and A. Siódmok, *Colour reconnections in Herwig++*, *Eur. Phys. J. C* **72** (2012) 2225 [arXiv:1206.0041] [INSPIRE].

JHEP07(2023)141

[41] J. Bellm et al., *Herwig* 7.1 *release note*, arXiv:1705.06919 [INSPIRE].

[42] S. Carrazza, J.I. Latorre, J. Rojo and G. Watt, *A compression algorithm for the combination of PDF sets*, *Eur. Phys. J. C* **75** (2015) 474 [arXiv:1504.06469] [INSPIRE].

[43] M. Czakon et al., *Top-pair production at the LHC through NNLO QCD and NLO EW*, *JHEP* **10** (2017) 186 [arXiv:1705.04105] [INSPIRE].

[44] S. Catani et al., *Top-quark pair production at the LHC: fully differential QCD predictions at NNLO*, *JHEP* **07** (2019) 100 [arXiv:1906.06535] [INSPIRE].

[45] ATLAS and CMS collaborations, *Treatment of top-quark backgrounds in extreme phase spaces: the "top p_{T} reweighting" and novel data-driven estimations in ATLAS and CMS*, in the proceedings of the 13$^{\mathrm{th}}$ *International Workshop on Top Quark Physics*, online, 14–18 September 2021 [arXiv:2105.03977] [INSPIRE].

[46] M. Czakon and A. Mitov, *Top++: a program for the calculation of the top-pair cross-section at hadron colliders*, *Comput. Phys. Commun.* **185** (2014) 2930 [arXiv:1112.5675] [INSPIRE].

[47] P. Bärnreuther, M. Czakon and A. Mitov, *Percent level precision physics at the Tevatron: first genuine NNLO QCD corrections to $q\bar{q} \to t\bar{t} + X$*, *Phys. Rev. Lett.* **109** (2012) 132001 [arXiv:1204.5201] [INSPIRE].

[48] M. Czakon and A. Mitov, *NNLO corrections to top-pair production at hadron colliders: the all-fermionic scattering channels*, *JHEP* **12** (2012) 054 [arXiv:1207.0236] [INSPIRE].

[49] M. Czakon and A. Mitov, *NNLO corrections to top pair production at hadron colliders: the quark-gluon reaction*, *JHEP* **01** (2013) 080 [arXiv:1210.6832] [INSPIRE].

[50] M. Czakon, P. Fiedler and A. Mitov, *Total top-quark pair-production cross section at hadron colliders through $O(\alpha_S^4)$*, *Phys. Rev. Lett.* **110** (2013) 252004 [arXiv:1303.6254] [INSPIRE].

[51] C.D. White, S. Frixione, E. Laenen and F. Maltoni, *Isolating Wt production at the LHC*, *JHEP* **11** (2009) 074 [arXiv:0908.0631] [INSPIRE].

[52] E. Re, *Single-top Wt-channel production matched with parton showers using the POWHEG method*, *Eur. Phys. J. C* **71** (2011) 1547 [arXiv:1009.2450] [INSPIRE].

[53] T. Gleisberg et al., *Event generation with SHERPA* 1.1, *JHEP* **02** (2009) 007 [arXiv:0811.4622] [INSPIRE].

[54] F. Cascioli et al., *Precise Higgs-background predictions: merging NLO QCD and squared quark-loop corrections to four-lepton + 0, 1 jet production*, *JHEP* **01** (2014) 046 [arXiv:1309.0500] [INSPIRE].

[55] SHERPA collaboration, *Event generation with Sherpa* 2.2, *SciPost Phys.* **7** (2019) 034 [arXiv:1905.09127] [INSPIRE].

[56] ATLAS collaboration, *Electron and photon performance measurements with the ATLAS detector using the* 2015–2017 *LHC proton-proton collision data*, 2019 *JINST* **14** P12006 [arXiv:1908.00005] [INSPIRE].

[57] ATLAS collaboration, *Reconstruction of primary vertices at the ATLAS experiment in run* 1 *proton-proton collisions at the LHC*, *Eur. Phys. J. C* **77** (2017) 332 [arXiv:1611.10235] [INSPIRE].

[58] ATLAS collaboration, *Muon reconstruction and identification efficiency in ATLAS using the full run* 2 *pp collision data set at $\sqrt{s} = 13$ TeV*, *Eur. Phys. J. C* **81** (2021) 578 [arXiv:2012.00578] [INSPIRE].

JHEP07(2023)141

[59] ATLAS collaboration, *Topological cell clustering in the ATLAS calorimeters and its performance in LHC run* 1, *Eur. Phys. J. C* **77** (2017) 490 [arXiv:1603.02934] [INSPIRE].

[60] M. Cacciari, G.P. Salam and G. Soyez, *The anti-k_t jet clustering algorithm*, *JHEP* **04** (2008) 063 [arXiv:0802.1189] [INSPIRE].

[61] M. Cacciari, G.P. Salam and G. Soyez, *FastJet user manual*, *Eur. Phys. J. C* **72** (2012) 1896 [arXiv:1111.6097] [INSPIRE].

[62] ATLAS collaboration, *Jet energy scale and resolution measured in proton-proton collisions at $\sqrt{s} = 13$ TeV with the ATLAS detector*, *Eur. Phys. J. C* **81** (2021) 689 [arXiv:2007.02645] [INSPIRE].

[63] ATLAS collaboration, *Performance of pile-up mitigation techniques for jets in pp collisions at $\sqrt{s} = 8$ TeV using the ATLAS detector*, *Eur. Phys. J. C* **76** (2016) 581 [arXiv:1510.03823] [INSPIRE].

[64] ATLAS collaboration, *Measurements of b-jet tagging efficiency with the ATLAS detector using $t\bar{t}$ events at $\sqrt{s} = 13$ TeV*, *JHEP* **08** (2018) 089 [arXiv:1805.01845] [INSPIRE].

[65] ATLAS collaboration, *Measurements of the production cross-section for a Z boson in association with b-jets in proton-proton collisions at $\sqrt{s} = 13$ TeV with the ATLAS detector*, *JHEP* **07** (2020) 044 [arXiv:2003.11960] [INSPIRE].

[66] PARTICLE DATA GROUP collaboration, *Review of particle physics*, *PTEP* **2020** (2020) 083C01 [INSPIRE].

[67] G. Bohm and G. Zech, *Introduction to statistics and measurement analysis for physicists*, 3rd revised edition, Verlag Deutsches Elektronen-Synchrotron, Hamburg, Germany (2005) [DOI:10.3204/PUBDB-2017-08987] [INSPIRE].

[68] ATLAS collaboration, *Evaluation of theoretical uncertainties for simplified template cross section measurements of V-associated production of the Higgs boson*, ATL-PHYS-PUB-2018-035, CERN, Geneva, Switzerland (2018).

[69] ATLAS collaboration, *Jet energy scale measurements and their systematic uncertainties in proton-proton collisions at $\sqrt{s} = 13$ TeV with the ATLAS detector*, *Phys. Rev. D* **96** (2017) 072002 [arXiv:1703.09665] [INSPIRE].

[70] ATLAS collaboration, *Measurements of b-jet tagging efficiency with the ATLAS detector using $t\bar{t}$ events at $\sqrt{s} = 13$ TeV*, *JHEP* **08** (2018) 089 [arXiv:1805.01845] [INSPIRE].

[71] N. Kidonakis, *Two-loop soft anomalous dimensions for single top quark associated production with a W^- or H^-*, *Phys. Rev. D* **82** (2010) 054018 [arXiv:1005.4451] [INSPIRE].

[72] ATLAS collaboration, *Measurement of $W^\pm Z$ production cross sections and gauge boson polarisation in pp collisions at $\sqrt{s} = 13$ TeV with the ATLAS detector*, *Eur. Phys. J. C* **79** (2019) 535 [arXiv:1902.05759] [INSPIRE].

[73] ATLAS collaboration, *Measurement of the $t\bar{t}Z$ and $t\bar{t}W$ cross sections in proton-proton collisions at $\sqrt{s} = 13$ TeV with the ATLAS detector*, *Phys. Rev. D* **99** (2019) 072009 [arXiv:1901.03584] [INSPIRE].

[74] G. Avoni et al., *The new LUCID-2 detector for luminosity measurement and monitoring in ATLAS*, 2018 *JINST* **13** P07017 [INSPIRE].

[75] E. Todesco and J. Wenninger, *Large Hadron Collider momentum calibration and accuracy*, *Phys. Rev. Accel. Beams* **20** (2017) 081003 [INSPIRE].

JHEP07(2023)141

[76] A. Buckley et al., *LHAPDF6: parton density access in the LHC precision era*, *Eur. Phys. J. C* **75** (2015) 132 [arXiv:1412.7420] [INSPIRE].

[77] ATLAS collaboration, *Measurements of top-quark pair spin correlations in the eμ channel at $\sqrt{s} = 13$ TeV using pp collisions in the ATLAS detector*, *Eur. Phys. J. C* **80** (2020) 754 [arXiv:1903.07570] [INSPIRE].

[78] ATLAS collaboration, *ATLAS computing acknowledgements*, ATL-SOFT-PUB-2021-003, CERN, Geneva, Switzerland (2021).

JHEP07(2023)141

The ATLAS collaboration

G. Aad[102], B. Abbott[120], D.C. Abbott[103], K. Abeling[55], S.H. Abidi[29], A. Aboulhorma[35e], H. Abramowicz[151], H. Abreu[150], Y. Abulaiti[117], A.C. Abusleme Hoffman[137a], B.S. Acharya[69a,69b,p], C. Adam Bourdarios[4], L. Adamczyk[85a], L. Adamek[155], S.V. Addepalli[26], J. Adelman[115], A. Adiguzel[21c], S. Adorni[56], T. Adye[134], A.A. Affolder[136], Y. Afik[36], M.N. Agaras[13], J. Agarwala[73a,73b], A. Aggarwal[100], C. Agheorghiesei[27c], J.A. Aguilar-Saavedra[130f], A. Ahmad[36], F. Ahmadov[38,z], W.S. Ahmed[104], S. Ahuja[95], X. Ai[48], G. Aielli[76a,76b], M. Ait Tamlihat[35e], B. Aitbenchikh[35a], I. Aizenberg[169], M. Akbiyik[100], T.P.A. Åkesson[98], A.V. Akimov[37], K. Al Khoury[41], G.L. Alberghi[23b], J. Albert[165], P. Albicocco[53], S. Alderweireldt[52], M. Aleksa[36], I.N. Aleksandrov[38], C. Alexa[27b], T. Alexopoulos[10], A. Alfonsi[114], F. Alfonsi[23b], M. Alhroob[120], B. Ali[132], S. Ali[148], M. Aliev[37], G. Alimonti[71a], W. Alkakhi[55], C. Allaire[66], B.M.M. Allbrooke[146], C.A. Allendes Flores[137f], P.P. Allport[20], A. Aloisio[72a,72b], F. Alonso[90], C. Alpigiani[138], M. Alvarez Estevez[99], A. Alvarez Fernandez[100], M.G. Alviggi[72a,72b], M. Aly[101], Y. Amaral Coutinho[82b], A. Ambler[104], C. Amelung[36], M. Amerl[1], C.G. Ames[109], D. Amidei[106], S.P. Amor Dos Santos[130a], K.R. Amos[163], V. Ananiev[125], C. Anastopoulos[139], T. Andeen[11], J.K. Anders[36], S.Y. Andrean[47a,47b], A. Andreazza[71a,71b], S. Angelidakis[9], A. Angerami[41,ab], A.V. Anisenkov[37], A. Annovi[74a], C. Antel[56], M.T. Anthony[139], E. Antipov[121], M. Antonelli[53], D.J.A. Antrim[17a], F. Anulli[75a], M. Aoki[83], T. Aoki[153], J.A. Aparisi Pozo[163], M.A. Aparo[146], L. Aperio Bella[48], C. Appelt[18], N. Aranzabal[36], V. Araujo Ferraz[82a], C. Arcangeletti[53], A.T.H. Arce[51], E. Arena[92], J-F. Arguin[108], S. Argyropoulos[54], J.-H. Arling[48], A.J. Armbruster[36], O. Arnaez[155], H. Arnold[114], Z.P. Arrubarrena Tame[109], G. Artoni[75a,75b], H. Asada[111], K. Asai[118], S. Asai[153], N.A. Asbah[61], J. Assahsah[35d], K. Assamagan[29], R. Astalos[28a], R.J. Atkin[33a], M. Atkinson[162], N.B. Atlay[18], H. Atmani[62b], P.A. Atmasiddha[106], K. Augsten[132], S. Auricchio[72a,72b], A.D. Auriol[20], V.A. Austrup[171], G. Avner[150], G. Avolio[36], K. Axiotis[56], G. Azuelos[108,ad], D. Babal[28a], H. Bachacou[135], K. Bachas[152,r], A. Bachiu[34], F. Backman[47a,47b], A. Badea[61], P. Bagnaia[75a,75b], M. Bahmani[18], A.J. Bailey[163], V.R. Bailey[162], J.T. Baines[134], C. Bakalis[10], O.K. Baker[172], P.J. Bakker[114], E. Bakos[15], D. Bakshi Gupta[8], S. Balaji[147], R. Balasubramanian[114], E.M. Baldin[37], P. Balek[133], E. Ballabene[71a,71b], F. Balli[135], L.M. Baltes[63a], W.K. Balunas[32], J. Balz[100], E. Banas[86], M. Bandieramonte[129], A. Bandyopadhyay[24], S. Bansal[24], L. Barak[151], E.L. Barberio[105], D. Barberis[57b,57a], M. Barbero[102], G. Barbour[96], K.N. Barends[33a], T. Barillari[110], M-S. Barisits[36], T. Barklow[143], R.M. Barnett[17a], P. Baron[122], D.A. Baron Moreno[101], A. Baroncelli[62a], G. Barone[29], A.J. Barr[126], L. Barranco Navarro[47a,47b], F. Barreiro[99], J. Barreiro Guimarães da Costa[14a], U. Barron[151], M.G. Barros Teixeira[130a], S. Barsov[37], F. Bartels[63a], R. Bartoldus[143], A.E. Barton[91], P. Bartos[28a], A. Basalaev[48], A. Basan[100], M. Baselga[49], I. Bashta[77a,77b], A. Bassalat[66,b], M.J. Basso[155], C.R. Basson[101], R.L. Bates[59], S. Batlamous[35e], J.R. Batley[32], B. Batool[141],

JHEP07(2023)141

M. Battaglia[136], D. Battulga[18], M. Bauce[75a,75b], P. Bauer[24], J.B. Beacham[51], T. Beau[127], P.H. Beauchemin[158], F. Becherer[54], P. Bechtle[24], H.P. Beck[19,q], K. Becker[167], A.J. Beddall[21d], V.A. Bednyakov[38], C.P. Bee[145], L.J. Beemster[15], T.A. Beermann[36], M. Begalli[82d,82d], M. Begel[29], A. Behera[145], J.K. Behr[48], C. Beirao Da Cruz E Silva[36], J.F. Beirer[55,36], F. Beisiegel[24], M. Belfkir[159], G. Bella[151], L. Bellagamba[23b], A. Bellerive[34], P. Bellos[20], K. Beloborodov[37], K. Belotskiy[37], N.L. Belyaev[37], D. Benchekroun[35a], F. Bendebba[35a], Y. Benhammou[151], D.P. Benjamin[29], M. Benoit[29], J.R. Bensinger[26], S. Bentvelsen[114], L. Beresford[36], M. Beretta[53], E. Bergeaas Kuutmann[161], N. Berger[4], B. Bergmann[132], J. Beringer[17a], S. Berlendis[7], G. Bernardi[5], C. Bernius[143], F.U. Bernlochner[24], T. Berry[95], P. Berta[133], A. Berthold[50], I.A. Bertram[91], S. Bethke[110], A. Betti[75a,75b], A.J. Bevan[94], M. Bhamjee[33c], S. Bhatta[145], D.S. Bhattacharya[166], P. Bhattarai[26], V.S. Bhopatkar[121], R. Bi[29,ag], R.M. Bianchi[129], O. Biebel[109], R. Bielski[123], M. Biglietti[77a], T.R.V. Billoud[132], M. Bindi[55], A. Bingul[21b], C. Bini[75a,75b], A. Biondini[92], C.J. Birch-sykes[101], G.A. Bird[20,134], M. Birman[169], M. Biros[133], T. Bisanz[36], E. Bisceglie[43b,43a], D. Biswas[170], A. Bitadze[101], K. Bjørke[125], I. Bloch[48], C. Blocker[26], A. Blue[59], U. Blumenschein[94], J. Blumenthal[100], G.J. Bobbink[114], V.S. Bobrovnikov[37], M. Boehler[54], D. Bogavac[36], A.G. Bogdanchikov[37], C. Bohm[47a], V. Boisvert[95], P. Bokan[48], T. Bold[85a], M. Bomben[5], M. Bona[94], M. Boonekamp[135], C.D. Booth[95], A.G. Borbély[59], H.M. Borecka-Bielska[108], L.S. Borgna[96], G. Borissov[91], D. Bortoletto[126], D. Boscherini[23b], M. Bosman[13], J.D. Bossio Sola[36], K. Bouaouda[35a], N. Bouchhar[163], J. Boudreau[129], E.V. Bouhova-Thacker[91], D. Boumediene[40], R. Bouquet[5], A. Boveia[119], J. Boyd[36], D. Boye[29], I.R. Boyko[38], J. Bracinik[20], N. Brahimi[62d], G. Brandt[171], O. Brandt[32], F. Braren[48], B. Brau[103], J.E. Brau[123], K. Brendlinger[48], R. Brener[169], L. Brenner[114], R. Brenner[161], S. Bressler[169], D. Britton[59], D. Britzger[110], I. Brock[24], G. Brooijmans[41], W.K. Brooks[137f], E. Brost[29], L.M. Brown[165], T.L. Bruckler[126], P.A. Bruckman de Renstrom[86], B. Brüers[48], D. Bruncko[28b,*], A. Bruni[23b], G. Bruni[23b], M. Bruschi[23b], N. Bruscino[75a,75b], T. Buanes[16], Q. Buat[138], P. Buchholz[141], A.G. Buckley[59], I.A. Budagov[38,*], M.K. Bugge[125], O. Bulekov[37], B.A. Bullard[143], S. Burdin[92], C.D. Burgard[49], A.M. Burger[40], B. Burghgrave[8], J.T.P. Burr[32], C.D. Burton[11], J.C. Burzynski[142], E.L. Busch[41], V. Büscher[100], P.J. Bussey[59], J.M. Butler[25], C.M. Buttar[59], J.M. Butterworth[96], W. Buttinger[134], C.J. Buxo Vazquez[107], A.R. Buzykaev[37], G. Cabras[23b], S. Cabrera Urbán[163], D. Caforio[58], H. Cai[129], Y. Cai[14a,14d], V.M.M. Cairo[36], O. Cakir[3a], N. Calace[36], P. Calafiura[17a], G. Calderini[127], P. Calfayan[68], G. Callea[59], L.P. Caloba[82b], D. Calvet[40], S. Calvet[40], T.P. Calvet[102], M. Calvetti[74a,74b], R. Camacho Toro[127], S. Camarda[36], D. Camarero Munoz[26], P. Camarri[76a,76b], M.T. Camerlingo[72a,72b], D. Cameron[125], C. Camincher[165], M. Campanelli[96], A. Camplani[42], V. Canale[72a,72b], A. Canesse[104], M. Cano Bret[80], J. Cantero[163], Y. Cao[162], F. Capocasa[26], M. Capua[43b,43a], A. Carbone[71a,71b], R. Cardarelli[76a], J.C.J. Cardenas[8], F. Cardillo[163], T. Carli[36], G. Carlino[72a], J.I. Carlotto[13], B.T. Carlson[129,s], E.M. Carlson[165,156a], L. Carminati[71a,71b], M. Carnesale[75a,75b], S. Caron[113], E. Carquin[137f], S. Carrá[71a,71b],

JHEP07(2023)141

G. Carratta[23b,23a], F. Carrio Argos[33g], J.W.S. Carter[155], T.M. Carter[52], M.P. Casado[13,j], A.F. Casha[155], E.G. Castiglia[172], F.L. Castillo[63a], L. Castillo Garcia[13], V. Castillo Gimenez[163], N.F. Castro[130a,130e], A. Catinaccio[36], J.R. Catmore[125], V. Cavaliere[29], N. Cavalli[23b,23a], V. Cavasinni[74a,74b], E. Celebi[21a], F. Celli[126], M.S. Centonze[70a,70b], K. Cerny[122], A.S. Cerqueira[82a], A. Cerri[146], L. Cerrito[76a,76b], F. Cerutti[17a], A. Cervelli[23b], S.A. Cetin[21d], Z. Chadi[35a], D. Chakraborty[115], M. Chala[130f], J. Chan[170], W.Y. Chan[153], J.D. Chapman[32], B. Chargeishvili[149b], D.G. Charlton[20], T.P. Charman[94], M. Chatterjee[19], S. Chekanov[6], S.V. Chekulaev[156a], G.A. Chelkov[38,a], A. Chen[106], B. Chen[151], B. Chen[165], H. Chen[14c], H. Chen[29], J. Chen[62c], J. Chen[142], S. Chen[153], S.J. Chen[14c], X. Chen[62c], X. Chen[14b,ac], Y. Chen[62a], C.L. Cheng[170], H.C. Cheng[64a], S. Cheong[143], A. Cheplakov[38], E. Cheremushkina[48], E. Cherepanova[114], R. Cherkaoui El Moursli[35e], E. Cheu[7], K. Cheung[65], L. Chevalier[135], V. Chiarella[53], G. Chiarelli[74a], N. Chiedde[102], G. Chiodini[70a], A.S. Chisholm[20], A. Chitan[27b], M. Chitishvili[163], Y.H. Chiu[165], M.V. Chizhov[38], K. Choi[11], A.R. Chomont[75a,75b], Y. Chou[103], E.Y.S. Chow[114], T. Chowdhury[33g], L.D. Christopher[33g], K.L. Chu[64a], M.C. Chu[64a], X. Chu[14a,14d], J. Chudoba[131], J.J. Chwastowski[86], D. Cieri[110], K.M. Ciesla[85a], V. Cindro[93], A. Ciocio[17a], F. Cirotto[72a,72b], Z.H. Citron[169,m], M. Citterio[71a], D.A. Ciubotaru[27b], B.M. Ciungu[155], A. Clark[56], P.J. Clark[52], J.M. Clavijo Columbie[48], S.E. Clawson[101], C. Clement[47a,47b], J. Clercx[48], L. Clissa[23b,23a], Y. Coadou[102], M. Cobal[69a,69c], A. Coccaro[57b], R.F. Coelho Barrue[130a], R. Coelho Lopes De Sa[103], S. Coelli[71a], H. Cohen[151], A.E.C. Coimbra[71a,71b], B. Cole[41], J. Collot[60], P. Conde Muiño[130a,130g], M.P. Connell[33c], S.H. Connell[33c], I.A. Connelly[59], E.I. Conroy[126], F. Conventi[72a,ae], H.G. Cooke[20], A.M. Cooper-Sarkar[126], F. Cormier[164], L.D. Corpe[36], M. Corradi[75a,75b], E.E. Corrigan[98], F. Corriveau[104,x], A. Cortes-Gonzalez[18], M.J. Costa[163], F. Costanza[4], D. Costanzo[139], B.M. Cote[119], G. Cowan[95], J.W. Cowley[32], K. Cranmer[117], S. Crépé-Renaudin[60], F. Crescioli[127], M. Cristinziani[141], M. Cristoforetti[78a,78b,d], V. Croft[158], G. Crosetti[43b,43a], A. Cueto[36], T. Cuhadar Donszelmann[160], H. Cui[14a,14d], Z. Cui[7], W.R. Cunningham[59], F. Curcio[43b,43a], P. Czodrowski[36], M.M. Czurylo[63b], M.J. Da Cunha Sargedas De Sousa[62a], J.V. Da Fonseca Pinto[82b], C. Da Via[101], W. Dabrowski[85a], T. Dado[49], S. Dahbi[33g], T. Dai[106], C. Dallapiccola[103], M. Dam[42], G. D'amen[29], V. D'Amico[109], J. Damp[100], J.R. Dandoy[128], M.F. Daneri[30], M. Danninger[142], V. Dao[36], G. Darbo[57b], S. Darmora[6], S.J. Das[29,ag], S. D'Auria[71a,71b], C. David[156b], T. Davidek[133], D.R. Davis[51], B. Davis-Purcell[34], I. Dawson[94], K. De[8], R. De Asmundis[72a], M. De Beurs[114], N. De Biase[48], S. De Castro[23b,23a], N. De Groot[113], P. de Jong[114], H. De la Torre[107], A. De Maria[14c], A. De Salvo[75a], U. De Sanctis[76a,76b], A. De Santo[146], J.B. De Vivie De Regie[60], D.V. Dedovich[38], J. Degens[114], A.M. Deiana[44], F. Del Corso[23b,23a], J. Del Peso[99], F. Del Rio[63a], F. Deliot[135], C.M. Delitzsch[49], M. Della Pietra[72a,72b], D. Della Volpe[56], A. Dell'Acqua[36], L. Dell'Asta[71a,71b], M. Delmastro[4], P.A. Delsart[60], S. Demers[172], M. Demichev[38], S.P. Denisov[37], L. D'Eramo[115], D. Derendarz[86], F. Derue[127], P. Dervan[92], K. Desch[24], K. Dette[155], C. Deutsch[24], F.A. Di Bello[57b,57a], A. Di Ciaccio[76a,76b], L. Di Ciaccio[4], A. Di Domenico[75a,75b], C. Di Donato[72a,72b],

JHEP07(2023)141

A. Di Girolamo[36], G. Di Gregorio[5], A. Di Luca[78a,78b], B. Di Micco[77a,77b], R. Di Nardo[77a,77b], C. Diaconu[102], F.A. Dias[114], T. Dias Do Vale[142], M.A. Diaz[137a,137b], F.G. Diaz Capriles[24], M. Didenko[163], E.B. Diehl[106], L. Diehl[54], S. Díez Cornell[48], C. Diez Pardos[141], C. Dimitriadi[24,161], A. Dimitrievska[17a], J. Dingfelder[24], I-M. Dinu[27b], S.J. Dittmeier[63b], F. Dittus[36], F. Djama[102], T. Djobava[149b], J.I. Djuvsland[16], C. Doglioni[101,98], J. Dolejsi[133], Z. Dolezal[133], M. Donadelli[82c], B. Dong[107], J. Donini[40], A. D'Onofrio[77a,77b], M. D'Onofrio[92], J. Dopke[134], A. Doria[72a], M.T. Dova[90], A.T. Doyle[59], M.A. Draguet[126], E. Drechsler[142], E. Dreyer[169], I. Drivas-koulouris[10], A.S. Drobac[158], M. Drozdova[56], D. Du[62a], T.A. du Pree[114], F. Dubinin[37], M. Dubovsky[28a], E. Duchovni[169], G. Duckeck[109], O.A. Ducu[27b], D. Duda[110], A. Dudarev[36], E.R. Duden[26], M. D'uffizi[101], L. Duflot[66], M. Dührssen[36], C. Dülsen[171], A.E. Dumitriu[27b], M. Dunford[63a], S. Dungs[49], K. Dunne[47a,47b], A. Duperrin[102], H. Duran Yildiz[3a], M. Düren[58], A. Durglishvili[149b], B.L. Dwyer[115], G.I. Dyckes[17a], M. Dyndal[85a], S. Dysch[101], B.S. Dziedzic[86], Z.O. Earnshaw[146], B. Eckerova[28a], S. Eggebrecht[55], M.G. Eggleston[51], E. Egidio Purcino De Souza[127], L.F. Ehrke[56], G. Eigen[16], K. Einsweiler[17a], T. Ekelof[161], P.A. Ekman[98], Y. El Ghazali[35b], H. El Jarrari[35e,148], A. El Moussaouy[35a], V. Ellajosyula[161], M. Ellert[161], F. Ellinghaus[171], A.A. Elliot[94], N. Ellis[36], J. Elmsheuser[29], M. Elsing[36], D. Emeliyanov[134], A. Emerman[41], Y. Enari[153], I. Ene[17a], S. Epari[13], J. Erdmann[49], P.A. Erland[86], M. Errenst[171], M. Escalier[66], C. Escobar[163], E. Etzion[151], G. Evans[130a], H. Evans[68], M.O. Evans[146], A. Ezhilov[37], S. Ezzarqtouni[35a], F. Fabbri[59], L. Fabbri[23b,23a], G. Facini[96], V. Fadeyev[136], R.M. Fakhrutdinov[37], S. Falciano[75a], L.F. Falda Ulhoa Coelho[36], P.J. Falke[24], S. Falke[36], J. Faltova[133], Y. Fan[14a], Y. Fang[14a,14d], G. Fanourakis[46], M. Fanti[71a,71b], M. Faraj[69a,69b], Z. Farazpay[97], A. Farbin[8], A. Farilla[77a], T. Farooque[107], S.M. Farrington[52], F. Fassi[35e], D. Fassouliotis[9], M. Faucci Giannelli[76a,76b], W.J. Fawcett[32], L. Fayard[66], P. Federicova[131], O.L. Fedin[37,a], G. Fedotov[37], M. Feickert[170], L. Feligioni[102], A. Fell[139], D.E. Fellers[123], C. Feng[62b], M. Feng[14b], Z. Feng[114], M.J. Fenton[160], A.B. Fenyuk[37], L. Ferencz[48], R.A.M. Ferguson[91], S.I. Fernandez Luengo[137f], J. Ferrando[48], A. Ferrari[161], P. Ferrari[114,113], R. Ferrari[73a], D. Ferrere[56], C. Ferretti[106], F. Fiedler[100], A. Filipčič[93], E.K. Filmer[1], F. Filthaut[113], M.C.N. Fiolhais[130a,130c,c], L. Fiorini[163], F. Fischer[141], W.C. Fisher[107], T. Fitschen[101], I. Fleck[141], P. Fleischmann[106], T. Flick[171], L. Flores[128], M. Flores[33d], L.R. Flores Castillo[64a], F.M. Follega[78a,78b], N. Fomin[16], J.H. Foo[155], B.C. Forland[68], A. Formica[135], A.C. Forti[101], E. Fortin[102], A.W. Fortman[61], M.G. Foti[17a], L. Fountas[9,k], D. Fournier[66], H. Fox[91], P. Francavilla[74a,74b], S. Francescato[61], S. Franchellucci[56], M. Franchini[23b,23a], S. Franchino[63a], D. Francis[36], L. Franco[113], L. Franconi[19], M. Franklin[61], G. Frattari[26], A.C. Freegard[94], P.M. Freeman[20], W.S. Freund[82b], N. Fritzsche[50], A. Froch[54], D. Froidevaux[36], J.A. Frost[126], Y. Fu[62a], M. Fujimoto[118], E. Fullana Torregrosa[163,*], J. Fuster[163], A. Gabrielli[23b,23a], A. Gabrielli[155], P. Gadow[48], G. Gagliardi[57b,57a], L.G. Gagnon[17a], G.E. Gallardo[126], E.J. Gallas[126], B.J. Gallop[134], R. Gamboa Goni[94], K.K. Gan[119], S. Ganguly[153], J. Gao[62a], Y. Gao[52],

JHEP07(2023)141

F.M. Garay Walls[137a,137b], B. Garcia[29,ag], C. García[163], J.E. García Navarro[163], M. Garcia-Sciveres[17a], R.W. Gardner[39], D. Garg[80], R.B. Garg[143,al], C.A. Garner[155], V. Garonne[29], S.J. Gasiorowski[138], P. Gaspar[82b], G. Gaudio[73a], V. Gautam[13], P. Gauzzi[75a,75b], I.L. Gavrilenko[37], A. Gavrilyuk[37], C. Gay[164], G. Gaycken[48], E.N. Gazis[10], A.A. Geanta[27b,27e], C.M. Gee[136], J. Geisen[98], C. Gemme[57b], M.H. Genest[60], S. Gentile[75a,75b], S. George[95], W.F. George[20], T. Geralis[46], L.O. Gerlach[55], P. Gessinger-Befurt[36], M.E. Geyik[171], M. Ghasemi Bostanabad[165], M. Ghneimat[141], K. Ghorbanian[94], A. Ghosal[141], A. Ghosh[160], A. Ghosh[7], B. Giacobbe[23b], S. Giagu[75a,75b], P. Giannetti[74a], A. Giannini[62a], S.M. Gibson[95], M. Gignac[136], D.T. Gil[85b], A.K. Gilbert[85a], B.J. Gilbert[41], D. Gillberg[34], G. Gilles[114], N.E.K. Gillwald[48], L. Ginabat[127], D.M. Gingrich[2,ad], M.P. Giordani[69a,69c], P.F. Giraud[135], G. Giugliarelli[69a,69c], D. Giugni[71a], F. Giuli[36], I. Gkialas[9,k], L.K. Gladilin[37], C. Glasman[99], G.R. Gledhill[123], M. Glisic[123], I. Gnesi[43b,g], Y. Go[29,ag], M. Goblirsch-Kolb[26], B. Gocke[49], D. Godin[108], B. Gokturk[21a], S. Goldfarb[105], T. Golling[56], M.G.D. Gololo[33g], D. Golubkov[37], J.P. Gombas[107], A. Gomes[130a,130b], G. Gomes Da Silva[141], A.J. Gomez Delegido[163], R. Goncalves Gama[55], R. Gonçalo[130a,130c], G. Gonella[123], L. Gonella[20], A. Gongadze[38], F. Gonnella[20], J.L. Gonski[41], R.Y. González Andana[52], S. González de la Hoz[163], S. Gonzalez Fernandez[13], R. Gonzalez Lopez[92], C. Gonzalez Renteria[17a], R. Gonzalez Suarez[161], S. Gonzalez-Sevilla[56], G.R. Gonzalvo Rodriguez[163], L. Goossens[36], N.A. Gorasia[20], P.A. Gorbounov[37], B. Gorini[36], E. Gorini[70a,70b], A. Gorišek[93], A.T. Goshaw[51], M.I. Gostkin[38], S. Goswami[121], C.A. Gottardo[36], M. Gouighri[35b], V. Goumarre[48], A.G. Goussiou[138], N. Govender[33c], C. Goy[4], I. Grabowska-Bold[85a], K. Graham[34], E. Gramstad[125], S. Grancagnolo[18], M. Grandi[146], V. Gratchev[37,*], P.M. Gravila[27f], F.G. Gravili[70a,70b], H.M. Gray[17a], M. Greco[70a,70b], C. Grefe[24], I.M. Gregor[48], P. Grenier[143], C. Grieco[13], A.A. Grillo[136], K. Grimm[31,n], S. Grinstein[13,u], J.-F. Grivaz[66], E. Gross[169], J. Grosse-Knetter[55], C. Grud[106], J.C. Grundy[126], L. Guan[106], W. Guan[170], C. Gubbels[164], J.G.R. Guerrero Rojas[163], G. Guerrieri[69a,69b], F. Guescini[110], R. Gugel[100], J.A.M. Guhit[106], A. Guida[48], T. Guillemin[4], E. Guilloton[167,134], S. Guindon[36], F. Guo[14a,14d], J. Guo[62c], L. Guo[66], Y. Guo[106], R. Gupta[48], S. Gurbuz[24], S.S. Gurdasani[54], G. Gustavino[36], M. Guth[56], P. Gutierrez[120], L.F. Gutierrez Zagazeta[128], C. Gutschow[96], C. Guyot[135], C. Gwenlan[126], C.B. Gwilliam[92], E.S. Haaland[125], A. Haas[117], M. Habedank[48], C. Haber[17a], H.K. Hadavand[8], A. Hadef[100], S. Hadzic[110], E.H. Haines[96], M. Haleem[166], J. Haley[121], J.J. Hall[139], G.D. Hallewell[102], L. Halser[19], K. Hamano[165], H. Hamdaoui[35e], M. Hamer[24], G.N. Hamity[52], J. Han[62b], K. Han[62a], L. Han[14c], L. Han[62a], S. Han[17a], Y.F. Han[155], K. Hanagaki[83], M. Hance[136], D.A. Hangal[41,ab], H. Hanif[142], M.D. Hank[39], R. Hankache[101], J.B. Hansen[42], J.D. Hansen[42], P.H. Hansen[42], K. Hara[157], D. Harada[56], T. Harenberg[171], S. Harkusha[37], Y.T. Harris[126], N.M. Harrison[119], P.F. Harrison[167], N.M. Hartman[143], N.M. Hartmann[109], Y. Hasegawa[140], A. Hasib[52], S. Haug[19], R. Hauser[107], M. Havranek[132], C.M. Hawkes[20], R.J. Hawkings[36], S. Hayashida[111], D. Hayden[107], C. Hayes[106], R.L. Hayes[164], C.P. Hays[126], J.M. Hays[94], H.S. Hayward[92], F. He[62a],

JHEP07(2023)141

Y. He[154], Y. He[127], M.P. Heath[52], N.B. Heatley[94], V. Hedberg[98], A.L. Heggelund[125], N.D. Hehir[94], C. Heidegger[54], K.K. Heidegger[54], W.D. Heidorn[81], J. Heilman[34], S. Heim[48], T. Heim[17a], J.G. Heinlein[128], J.J. Heinrich[123], L. Heinrich[110,aj], J. Hejbal[131], L. Helary[48], A. Held[170], S. Hellesund[125], C.M. Helling[164], S. Hellman[47a,47b], C. Helsens[36], R.C.W. Henderson[91], L. Henkelmann[32], A.M. Henriques Correia[36], H. Herde[98], Y. Hernández Jiménez[145], L.M. Herrmann[24], T. Herrmann[50], G. Herten[54], R. Hertenberger[109], L. Hervas[36], N.P. Hessey[156a], H. Hibi[84], E. Higón-Rodriguez[163], S.J. Hillier[20], I. Hinchliffe[17a], F. Hinterkeuser[24], M. Hirose[124], S. Hirose[157], D. Hirschbuehl[171], T.G. Hitchings[101], B. Hiti[93], J. Hobbs[145], R. Hobincu[27e], N. Hod[169], M.C. Hodgkinson[139], B.H. Hodkinson[32], A. Hoecker[36], J. Hofer[48], D. Hohn[54], T. Holm[24], M. Holzbock[110], L.B.A.H. Hommels[32], B.P. Honan[101], J. Hong[62c], T.M. Hong[129], J.C. Honig[54], B.H. Hooberman[162], W.H. Hopkins[6], Y. Horii[111], S. Hou[148], A.S. Howard[93], J. Howarth[59], J. Hoya[6], M. Hrabovsky[122], A. Hrynevich[48], T. Hryn'ova[4], P.J. Hsu[65], S.-C. Hsu[138], Q. Hu[41], Y.F. Hu[14a,14d,af], D.P. Huang[96], S. Huang[64b], X. Huang[14c], Y. Huang[62a], Y. Huang[14a], Z. Huang[101], Z. Hubacek[132], M. Huebner[24], F. Huegging[24], T.B. Huffman[126], M. Huhtinen[36], S.K. Huiberts[16], R. Hulsken[104], N. Huseynov[12,a], J. Huston[107], J. Huth[61], R. Hyneman[143], S. Hyrych[28a], G. Iacobucci[56], G. Iakovidis[29], I. Ibragimov[141], L. Iconomidou-Fayard[66], P. Iengo[72a,72b], R. Ignazzi[42], R. Iguchi[153], T. Iizawa[56], Y. Ikegami[83], A. Ilg[19], N. Ilic[155], H. Imam[35a], T. Ingebretsen Carlson[47a,47b], G. Introzzi[73a,73b], M. Iodice[77a], V. Ippolito[75a,75b], M. Ishino[153], W. Islam[170], C. Issever[18,48], S. Istin[21a,ak], H. Ito[168], J.M. Iturbe Ponce[64a], R. Iuppa[78a,78b], A. Ivina[169], J.M. Izen[45], V. Izzo[72a], P. Jacka[131,132], P. Jackson[1], R.M. Jacobs[48], B.P. Jaeger[142], C.S. Jagfeld[109], P. Jain[54], G. Jäkel[171], K. Jakobs[54], T. Jakoubek[169], J. Jamieson[59], K.W. Janas[85a], G. Jarlskog[98], A.E. Jaspan[92], M. Javurkova[103], F. Jeanneau[135], L. Jeanty[123], J. Jejelava[149a,aa], P. Jenni[54,h], C.E. Jessiman[34], S. Jézéquel[4], C. Jia[62b], J. Jia[145], X. Jia[61], X. Jia[14a,14d], Z. Jia[14c], Y. Jiang[62a], S. Jiggins[52], J. Jimenez Pena[110], S. Jin[14c], A. Jinaru[27b], O. Jinnouchi[154], P. Johansson[139], K.A. Johns[7], J.W. Johnson[136], D.M. Jones[32], E. Jones[167], P. Jones[32], R.W.L. Jones[91], T.J. Jones[92], R. Joshi[119], J. Jovicevic[15], X. Ju[17a], J.J. Junggeburth[36], T. Junkermann[63a], A. Juste Rozas[13,u], S. Kabana[137e], A. Kaczmarska[86], M. Kado[75a,75b], H. Kagan[119], M. Kagan[143], A. Kahn[41], A. Kahn[128], C. Kahra[100], T. Kaji[168], E. Kajomovitz[150], N. Kakati[169], C.W. Kalderon[29], A. Kamenshchikov[155], S. Kanayama[154], N.J. Kang[136], D. Kar[33g], K. Karava[126], M.J. Kareem[156b], E. Karentzos[54], I. Karkanias[152,f], S.N. Karpov[38], Z.M. Karpova[38], V. Kartvelishvili[91], A.N. Karyukhin[37], E. Kasimi[152,f], C. Kato[62d], J. Katzy[48], S. Kaur[34], K. Kawade[140], K. Kawagoe[89], T. Kawamoto[135], G. Kawamura[55], E.F. Kay[165], F.I. Kaya[158], S. Kazakos[13], V.F. Kazanin[37], Y. Ke[145], J.M. Keaveney[33a], R. Keeler[165], G.V. Kehris[61], J.S. Keller[34], A.S. Kelly[96], D. Kelsey[146], J.J. Kempster[146], K.E. Kennedy[41], P.D. Kennedy[100], O. Kepka[131], B.P. Kerridge[167], S. Kersten[171], B.P. Kerševan[93], S. Keshri[66], L. Keszeghova[28a], S. Ketabchi Haghighat[155], M. Khandoga[127], A. Khanov[121], A.G. Kharlamov[37], T. Kharlamova[37], E.E. Khoda[138],

JHEP07(2023)141

T.J. Khoo[18], G. Khoriauli[166], J. Khubua[149b], Y.A.R. Khwaira[66], M. Kiehn[36], A. Kilgallon[123], D.W. Kim[47a,47b], E. Kim[154], Y.K. Kim[39], N. Kimura[96], A. Kirchhoff[55], D. Kirchmeier[50], C. Kirfel[24], J. Kirk[134], A.E. Kiryunin[110], T. Kishimoto[153], D.P. Kisliuk[155], C. Kitsaki[10], O. Kivernyk[24], M. Klassen[63a], C. Klein[34], L. Klein[166], M.H. Klein[106], M. Klein[92], S.B. Klein[56], U. Klein[92], P. Klimek[36], A. Klimentov[29], F. Klimpel[110], T. Klioutchnikova[36], P. Kluit[114], S. Kluth[110], E. Kneringer[79], T.M. Knight[155], A. Knue[54], D. Kobayashi[89], R. Kobayashi[87], M. Kocian[143], P. Kodyš[133], D.M. Koeck[146], P.T. Koenig[24], T. Koffas[34], M. Kolb[135], I. Koletsou[4], T. Komarek[122], K. Köneke[54], A.X.Y. Kong[1], T. Kono[118], N. Konstantinidis[96], B. Konya[98], R. Kopeliansky[68], S. Koperny[85a], K. Korcyl[86], K. Kordas[152,f], G. Koren[151], A. Korn[96], S. Korn[55], I. Korolkov[13], N. Korotkova[37], B. Kortman[114], O. Kortner[110], S. Kortner[110], W.H. Kostecka[115], V.V. Kostyukhin[141], A. Kotsokechagia[135], A. Kotwal[51], A. Koulouris[36], A. Kourkoumeli-Charalampidi[73a,73b], C. Kourkoumelis[9], E. Kourlitis[6], O. Kovanda[146], R. Kowalewski[165], W. Kozanecki[135], A.S. Kozhin[37], V.A. Kramarenko[37], G. Kramberger[93], P. Kramer[100], M.W. Krasny[127], A. Krasznahorkay[36], J.A. Kremer[100], T. Kresse[50], J. Kretzschmar[92], K. Kreul[18], P. Krieger[155], S. Krishnamurthy[103], M. Krivos[133], K. Krizka[17a], K. Kroeninger[49], H. Kroha[110], J. Kroll[131], J. Kroll[128], K.S. Krowpman[107], U. Kruchonak[38], H. Krüger[24], N. Krumnack[81], M.C. Kruse[51], J.A. Krzysiak[86], O. Kuchinskaia[37], S. Kuday[3a], D. Kuechler[48], J.T. Kuechler[48], S. Kuehn[36], R. Kuesters[54], T. Kuhl[48], V. Kukhtin[38], Y. Kulchitsky[37,a], S. Kuleshov[137d,137b], M. Kumar[33g], N. Kumari[102], A. Kupco[131], T. Kupfer[49], A. Kupich[37], O. Kuprash[54], H. Kurashige[84], L.L. Kurchaninov[156a], Y.A. Kurochkin[37], A. Kurova[37], M. Kuze[154], A.K. Kvam[103], J. Kvita[122], T. Kwan[104], K.W. Kwok[64a], N.G. Kyriacou[106], L.A.O. Laatu[102], C. Lacasta[163], F. Lacava[75a,75b], H. Lacker[18], D. Lacour[127], N.N. Lad[96], E. Ladygin[38], B. Laforge[127], T. Lagouri[137e], S. Lai[55], I.K. Lakomiec[85a], N. Lalloue[60], J.E. Lambert[120], S. Lammers[68], W. Lampl[7], C. Lampoudis[152,f], A.N. Lancaster[115], E. Lançon[29], U. Landgraf[54], M.P.J. Landon[94], V.S. Lang[54], R.J. Langenberg[103], A.J. Lankford[160], F. Lanni[36], K. Lantzsch[24], A. Lanza[73a], A. Lapertosa[57b,57a], J.F. Laporte[135], T. Lari[71a], F. Lasagni Manghi[23b], M. Lassnig[36], V. Latonova[131], A. Laudrain[100], A. Laurier[150], S.D. Lawlor[95], Z. Lawrence[101], M. Lazzaroni[71a,71b], B. Le[101], B. Leban[93], A. Lebedev[81], M. LeBlanc[36], T. LeCompte[6], F. Ledroit-Guillon[60], A.C.A. Lee[96], G.R. Lee[16], S.C. Lee[148], S. Lee[47a,47b], T.F. Lee[92], L.L. Leeuw[33c], H.P. Lefebvre[95], M. Lefebvre[165], C. Leggett[17a], K. Lehmann[142], G. Lehmann Miotto[36], M. Leigh[56], W.A. Leight[103], A. Leisos[152,t], M.A.L. Leite[82c], C.E. Leitgeb[48], R. Leitner[133], K.J.C. Leney[44], T. Lenz[24], S. Leone[74a], C. Leonidopoulos[52], A. Leopold[144], C. Leroy[108], R. Les[107], C.G. Lester[32], M. Levchenko[37], J. Levêque[4], D. Levin[106], L.J. Levinson[169], M.P. Lewicki[86], D.J. Lewis[4], A. Li[5], B. Li[62b], C. Li[62a], C-Q. Li[62c], H. Li[62a], H. Li[62b], H. Li[14c], H. Li[62b], J. Li[62c], K. Li[138], L. Li[62c], M. Li[14a,14d], Q.Y. Li[62a], S. Li[14a,14d], S. Li[62d,62c,e], T. Li[62b], X. Li[104], Z. Li[62b], Z. Li[126], Z. Li[104], Z. Li[92], Z. Li[14a,14d], Z. Liang[14a], M. Liberatore[48], B. Liberti[76a], K. Lie[64c], J. Lieber Marin[82b], H. Lien[68], K. Lin[107], R.A. Linck[68], R.E. Lindley[7], J.H. Lindon[2],

JHEP07(2023)141

A. Linss[48], E. Lipeles[128], A. Lipniacka[16], A. Lister[164], J.D. Little[4], B. Liu[14a], B.X. Liu[142], D. Liu[62d,62c], J.B. Liu[62a], J.K.K. Liu[32], K. Liu[62d,62c], M. Liu[62a], M.Y. Liu[62a], P. Liu[14a], Q. Liu[62d,138,62c], X. Liu[62a], Y. Liu[14c,14d], Y.L. Liu[106], Y.W. Liu[62a], M. Livan[73a,73b], J. Llorente Merino[142], S.L. Lloyd[94], E.M. Lobodzinska[48], P. Loch[7], S. Loffredo[76a,76b], T. Lohse[18], K. Lohwasser[139], M. Lokajicek[131], J.D. Long[162], I. Longarini[160], L. Longo[70a,70b], R. Longo[162], I. Lopez Paz[67], A. Lopez Solis[48], J. Lorenz[109], N. Lorenzo Martinez[4], A.M. Lory[109], X. Lou[47a,47b], X. Lou[14a,14d], A. Lounis[66], J. Love[6], P.A. Love[91], J.J. Lozano Bahilo[163], G. Lu[14a,14d], M. Lu[80], S. Lu[128], Y.J. Lu[65], H.J. Lubatti[138], C. Luci[75a,75b], F.L. Lucio Alves[14c], A. Lucotte[60], F. Luehring[68], I. Luise[145], O. Lukianchuk[66], O. Lundberg[144], B. Lund-Jensen[144], N.A. Luongo[123], M.S. Lutz[151], D. Lynn[29], H. Lyons[92], R. Lysak[131], E. Lytken[98], F. Lyu[14a], V. Lyubushkin[38], T. Lyubushkina[38], M.M. Lyukova[145], H. Ma[29], L.L. Ma[62b], Y. Ma[96], D.M. Mac Donell[165], G. Maccarrone[53], J.C. MacDonald[139], R. Madar[40], W.F. Mader[50], J. Maeda[84], T. Maeno[29], M. Maerker[50], H. Maguire[139], D.J. Mahon[41], A. Maio[130a,130b,130d], K. Maj[85a], O. Majersky[48], S. Majewski[123], N. Makovec[66], V. Maksimovic[15], B. Malaescu[127], Pa. Malecki[86], V.P. Maleev[37], F. Malek[60], D. Malito[43b,43a], U. Mallik[80], C. Malone[32], S. Maltezos[10], S. Malyukov[38], J. Mamuzic[13], G. Mancini[53], G. Manco[73a,73b], J.P. Mandalia[94], I. Mandić[93], L. Manhaes de Andrade Filho[82a], I.M. Maniatis[169], J. Manjarres Ramos[50], D.C. Mankad[169], A. Mann[109], B. Mansoulie[135], S. Manzoni[36], A. Marantis[152,t], G. Marchiori[5], M. Marcisovsky[131], C. Marcon[71a,71b], M. Marinescu[20], M. Marjanovic[120], E.J. Marshall[91], Z. Marshall[17a], S. Marti-Garcia[163], T.A. Martin[167], V.J. Martin[52], B. Martin dit Latour[16], L. Martinelli[75a,75b], M. Martinez[13,u], P. Martinez Agullo[163], V.I. Martinez Outschoorn[103], P. Martinez Suarez[13], S. Martin-Haugh[134], V.S. Martoiu[27b], A.C. Martyniuk[96], A. Marzin[36], S.R. Maschek[110], D. Mascione[78a,78b], L. Masetti[100], T. Mashimo[153], J. Masik[101], A.L. Maslennikov[37], L. Massa[23b], P. Massarotti[72a,72b], P. Mastrandrea[74a,74b], A. Mastroberardino[43b,43a], T. Masubuchi[153], T. Mathisen[161], N. Matsuzawa[153], J. Maurer[27b], B. Maček[93], D.A. Maximov[37], R. Mazini[148], I. Maznas[152,f], M. Mazza[107], S.M. Mazza[136], C. Mc Ginn[29], J.P. Mc Gowan[104], S.P. Mc Kee[106], E.F. McDonald[105], A.E. McDougall[114], J.A. Mcfayden[146], G. Mchedlidze[149b], R.P. Mckenzie[33g], T.C. Mclachlan[48], D.J. Mclaughlin[96], K.D. McLean[165], S.J. McMahon[134], P.C. McNamara[105], C.M. Mcpartland[92], R.A. McPherson[165,x], T. Megy[40], S. Mehlhase[109], A. Mehta[92], B. Meirose[45], D. Melini[150], B.R. Mellado Garcia[33g], A.H. Melo[55], F. Meloni[48], E.D. Mendes Gouveia[130a], A.M. Mendes Jacques Da Costa[20], H.Y. Meng[155], L. Meng[91], S. Menke[110], M. Mentink[36], E. Meoni[43b,43a], C. Merlassino[126], L. Merola[72a,72b], C. Meroni[71a], G. Merz[106], O. Meshkov[37], J. Metcalfe[6], A.S. Mete[6], C. Meyer[68], J-P. Meyer[135], M. Michetti[18], R.P. Middleton[134], L. Mijović[52], G. Mikenberg[169], M. Mikestikova[131], M. Mikuž[93], H. Mildner[139], A. Milic[36], C.D. Milke[44], D.W. Miller[39], L.S. Miller[34], A. Milov[169], D.A. Milstead[47a,47b], T. Min[14c], A.A. Minaenko[37], I.A. Minashvili[149b], L. Mince[59], A.I. Mincer[117], B. Mindur[85a], M. Mineev[38], Y. Mino[87], L.M. Mir[13], M. Miralles Lopez[163], M. Mironova[126],

JHEP07(2023)141

M.C. Missio[113], T. Mitani[168], A. Mitra[167], V.A. Mitsou[163], O. Miu[155], P.S. Miyagawa[94], Y. Miyazaki[89], A. Mizukami[83], J.U. Mjörnmark[98], T. Mkrtchyan[63a], M. Mlinarevic[96], T. Mlinarevic[96], M. Mlynarikova[36], T. Moa[47a,47b], S. Mobius[55], K. Mochizuki[108], P. Moder[48], P. Mogg[109], A.F. Mohammed[14a,14d], S. Mohapatra[41], G. Mokgatitswane[33g], B. Mondal[141], S. Mondal[132], K. Mönig[48], E. Monnier[102], L. Monsonis Romero[163], J. Montejo Berlingen[83], M. Montella[119], F. Monticelli[90], N. Morange[66], A.L. Moreira De Carvalho[130a], M. Moreno Llácer[163], C. Moreno Martinez[56], P. Morettini[57b], S. Morgenstern[167], M. Morii[61], M. Morinaga[153], A.K. Morley[36], F. Morodei[75a,75b], L. Morvaj[36], P. Moschovakos[36], B. Moser[36], M. Mosidze[149b], T. Moskalets[54], P. Moskvitina[113], J. Moss[31,o], E.J.W. Moyse[103], O. Mtintsilana[33g], S. Muanza[102], J. Mueller[129], D. Muenstermann[91], R. Müller[19], G.A. Mullier[161], J.J. Mullin[128], D.P. Mungo[155], J.L. Munoz Martinez[13], D. Munoz Perez[163], F.J. Munoz Sanchez[101], M. Murin[101], W.J. Murray[167,134], A. Murrone[71a,71b], J.M. Muse[120], M. Muškinja[17a], C. Mwewa[29], A.G. Myagkov[37,a], A.J. Myers[8], A.A. Myers[129], G. Myers[68], M. Myska[132], B.P. Nachman[17a], O. Nackenhorst[49], A. Nag[50], K. Nagai[126], K. Nagano[83], J.L. Nagle[29,ag], E. Nagy[102], A.M. Nairz[36], Y. Nakahama[83], K. Nakamura[83], H. Nanjo[124], R. Narayan[44], E.A. Narayanan[112], I. Naryshkin[37], M. Naseri[34], C. Nass[24], G. Navarro[22a], J. Navarro-Gonzalez[163], R. Nayak[151], A. Nayaz[18], P.Y. Nechaeva[37], F. Nechansky[48], L. Nedic[126], T.J. Neep[20], A. Negri[73a,73b], M. Negrini[23b], C. Nellist[113], C. Nelson[104], K. Nelson[106], S. Nemecek[131], M. Nessi[36,i], M.S. Neubauer[162], F. Neuhaus[100], J. Neundorf[48], R. Newhouse[164], P.R. Newman[20], C.W. Ng[129], Y.S. Ng[18], Y.W.Y. Ng[48], B. Ngair[35e], H.D.N. Nguyen[108], R.B. Nickerson[126], R. Nicolaidou[135], J. Nielsen[136], M. Niemeyer[55], N. Nikiforou[36], V. Nikolaenko[37,a], I. Nikolic-Audit[127], K. Nikolopoulos[20], P. Nilsson[29], I. Ninca[48], H.R. Nindhito[56], G. Ninio[151], A. Nisati[75a], N. Nishu[2], R. Nisius[110], J-E. Nitschke[50], E.K. Nkadimeng[33g], S.J. Noacco Rosende[90], T. Nobe[153], D.L. Noel[32], Y. Noguchi[87], T. Nommensen[147], M.A. Nomura[29], M.B. Norfolk[139], R.R.B. Norisam[96], B.J. Norman[34], J. Novak[93], T. Novak[48], O. Novgorodova[50], L. Novotny[132], R. Novotny[112], L. Nozka[122], K. Ntekas[160], N.M.J. Nunes De Moura Junior[82b], E. Nurse[96], F.G. Oakham[34,ad], J. Ocariz[127], A. Ochi[84], I. Ochoa[130a], S. Oerdek[161], J.T. Offermann[39], A. Ogrodnik[85a], A. Oh[101], C.C. Ohm[144], H. Oide[83], R. Oishi[153], M.L. Ojeda[48], Y. Okazaki[87], M.W. O'Keefe[92], Y. Okumura[153], A. Olariu[27b], L.F. Oleiro Seabra[130a], S.A. Olivares Pino[137e], D. Oliveira Damazio[29], D. Oliveira Goncalves[82a], J.L. Oliver[160], M.J.R. Olsson[160], A. Olszewski[86], J. Olszowska[86,*], Ö.O. Öncel[54], D.C. O'Neil[142], A.P. O'Neill[19], A. Onofre[130a,130e], P.U.E. Onyisi[11], M.J. Oreglia[39], G.E. Orellana[90], D. Orestano[77a,77b], N. Orlando[13], R.S. Orr[155], V. O'Shea[59], R. Ospanov[62a], G. Otero y Garzon[30], H. Otono[89], P.S. Ott[63a], G.J. Ottino[17a], M. Ouchrif[35d], J. Ouellette[29,ag], F. Ould-Saada[125], M. Owen[59], R.E. Owen[134], K.Y. Oyulmaz[21a], V.E. Ozcan[21a], N. Ozturk[8], S. Ozturk[21d], J. Pacalt[122], H.A. Pacey[32], K. Pachal[51], A. Pacheco Pages[13], C. Padilla Aranda[13], G. Padovano[75a,75b], S. Pagan Griso[17a], G. Palacino[68], A. Palazzo[70a,70b], S. Palestini[36], J. Pan[172], T. Pan[64a], D.K. Panchal[11], C.E. Pandini[114], J.G. Panduro Vazquez[95], H. Pang[14b], P. Pani[48],

JHEP07(2023)141

G. Panizzo[69a,69c], L. Paolozzi[56], C. Papadatos[108], S. Parajuli[44], A. Paramonov[6], C. Paraskevopoulos[10], D. Paredes Hernandez[64b], T.H. Park[155], M.A. Parker[32], F. Parodi[57b,57a], E.W. Parrish[115], V.A. Parrish[52], J.A. Parsons[41], U. Parzefall[54], B. Pascual Dias[108], L. Pascual Dominguez[151], V.R. Pascuzzi[17a], F. Pasquali[114], E. Pasqualucci[75a], S. Passaggio[57b], F. Pastore[95], P. Pasuwan[47a,47b], P. Patel[86], J.R. Pater[101], T. Pauly[36], J. Pearkes[143], M. Pedersen[125], R. Pedro[130a], S.V. Peleganchuk[37], O. Penc[36], E.A. Pender[52], C. Peng[64b], H. Peng[62a], K.E. Penski[109], M. Penzin[37], B.S. Peralva[82d,82d], A.P. Pereira Peixoto[60], L. Pereira Sanchez[47a,47b], D.V. Perepelitsa[29,ag], E. Perez Codina[156a], M. Perganti[10], L. Perini[71a,71b,*], H. Pernegger[36], S. Perrella[36], A. Perrevoort[113], O. Perrin[40], K. Peters[48], R.F.Y. Peters[101], B.A. Petersen[36], T.C. Petersen[42], E. Petit[102], V. Petousis[132], C. Petridou[152,f], A. Petrukhin[141], M. Pettee[17a], N.E. Pettersson[36], A. Petukhov[37], K. Petukhova[133], A. Peyaud[135], R. Pezoa[137f], L. Pezzotti[36], G. Pezzullo[172], T.M. Pham[170], T. Pham[105], P.W. Phillips[134], M.W. Phipps[162], G. Piacquadio[145], E. Pianori[17a], F. Piazza[71a,71b], R. Piegaia[30], D. Pietreanu[27b], A.D. Pilkington[101], M. Pinamonti[69a,69c], J.L. Pinfold[2], B.C. Pinheiro Pereira[130a], C. Pitman Donaldson[96], D.A. Pizzi[34], L. Pizzimento[76a,76b], A. Pizzini[114], M.-A. Pleier[29], V. Plesanovs[54], V. Pleskot[133], E. Plotnikova[38], G. Poddar[4], R. Poettgen[98], L. Poggioli[127], I. Pogrebnyak[107], D. Pohl[24], I. Pokharel[55], S. Polacek[133], G. Polesello[73a], A. Poley[142,156a], R. Polifka[132], A. Polini[23b], C.S. Pollard[167], Z.B. Pollock[119], V. Polychronakos[29], E. Pompa Pacchi[75a,75b], D. Ponomarenko[113], L. Pontecorvo[36], S. Popa[27a], G.A. Popeneciu[27d], D.M. Portillo Quintero[156a], S. Pospisil[132], P. Postolache[27c], K. Potamianos[126], P.P. Potepa[85a], I.N. Potrap[38], C.J. Potter[32], H. Potti[1], T. Poulsen[48], J. Poveda[163], M.E. Pozo Astigarraga[36], A. Prades Ibanez[163], M.M. Prapa[46], J. Pretel[54], D. Price[101], M. Primavera[70a], M.A. Principe Martin[99], R. Privara[122], M.L. Proffitt[138], N. Proklova[128], K. Prokofiev[64c], G. Proto[76a,76b], S. Protopopescu[29], J. Proudfoot[6], M. Przybycien[85a], J.E. Puddefoot[139], D. Pudzha[37], P. Puzo[66], D. Pyatiizbyantseva[37], J. Qian[106], D. Qichen[101], Y. Qin[101], T. Qiu[94], A. Quadt[55], M. Queitsch-Maitland[101], G. Quetant[56], G. Rabanal Bolanos[61], D. Rafanoharana[54], F. Ragusa[71a,71b], J.L. Rainbolt[39], J.A. Raine[56], S. Rajagopalan[29], E. Ramakoti[37], K. Ran[48,14d], N.P. Rapheeha[33g], V. Raskina[127], D.F. Rassloff[63a], S. Rave[100], B. Ravina[55], I. Ravinovich[169], M. Raymond[36], A.L. Read[125], N.P. Readioff[139], D.M. Rebuzzi[73a,73b], G. Redlinger[29], K. Reeves[45], J.A. Reidelsturz[171], D. Reikher[151], A. Rej[141], C. Rembser[36], A. Renardi[48], M. Renda[27b], M.B. Rendel[110], F. Renner[48], A.G. Rennie[59], S. Resconi[71a], M. Ressegotti[57b,57a], E.D. Resseguie[17a], S. Rettie[36], J.G. Reyes Rivera[107], B. Reynolds[119], E. Reynolds[17a], M. Rezaei Estabragh[171], O.L. Rezanova[37], P. Reznicek[133], N. Ribaric[91], E. Ricci[78a,78b], R. Richter[110], S. Richter[47a,47b], E. Richter-Was[85b], M. Ridel[127], S. Ridouani[35d], P. Rieck[117], P. Riedler[36], M. Rijssenbeek[145], A. Rimoldi[73a,73b], M. Rimoldi[48], L. Rinaldi[23b,23a], T.T. Rinn[29], M.P. Rinnagel[109], G. Ripellino[144], I. Riu[13], P. Rivadeneira[48], J.C. Rivera Vergara[165], F. Rizatdinova[121], E. Rizvi[94], C. Rizzi[56], B.A. Roberts[167], B.R. Roberts[17a], S.H. Robertson[104,x], M. Robin[48], D. Robinson[32], C.M. Robles Gajardo[137f], M. Robles Manzano[100], A. Robson[59], A. Rocchi[76a,76b],

JHEP07(2023)141

C. Roda[74a,74b], S. Rodriguez Bosca[63a], Y. Rodriguez Garcia[22a], A. Rodriguez Rodriguez[54], A.M. Rodríguez Vera[156b], S. Roe[36], J.T. Roemer[160], A.R. Roepe-Gier[120], J. Roggel[171], O. Røhne[125], R.A. Rojas[103], B. Roland[54], C.P.A. Roland[68], J. Roloff[29], A. Romaniouk[37], E. Romano[73a,73b], M. Romano[23b], A.C. Romero Hernandez[162], N. Rompotis[92], L. Roos[127], S. Rosati[75a], B.J. Rosser[39], E. Rossi[4], E. Rossi[72a,72b], L.P. Rossi[57b], L. Rossini[48], R. Rosten[119], M. Rotaru[27b], B. Rottler[54], C. Rougier[102,ai], D. Rousseau[66], D. Rousso[32], G. Rovelli[73a,73b], A. Roy[162], S. Roy-Garand[155], A. Rozanov[102], Y. Rozen[150], X. Ruan[33g], A. Rubio Jimenez[163], A.J. Ruby[92], V.H. Ruelas Rivera[18], T.A. Ruggeri[1], F. Rühr[54], A. Ruiz-Martinez[163], A. Rummler[36], Z. Rurikova[54], N.A. Rusakovich[38], H.L. Russell[165], J.P. Rutherfoord[7], K. Rybacki[91], M. Rybar[133], E.B. Rye[125], A. Ryzhov[37], J.A. Sabater Iglesias[56], P. Sabatini[163], L. Sabetta[75a,75b], H.F-W. Sadrozinski[136], F. Safai Tehrani[75a], B. Safarzadeh Samani[146], M. Safdari[143], S. Saha[104], M. Sahinsoy[110], M. Saimpert[135], M. Saito[153], T. Saito[153], D. Salamani[36], G. Salamanna[77a,77b], A. Salnikov[143], J. Salt[163], A. Salvador Salas[13], D. Salvatore[43b,43a], F. Salvatore[146], A. Salzburger[36], D. Sammel[54], D. Sampsonidis[152,f], D. Sampsonidou[62d,62c], J. Sánchez[163], A. Sanchez Pineda[4], V. Sanchez Sebastian[163], H. Sandaker[125], C.O. Sander[48], J.A. Sandesara[103], M. Sandhoff[171], C. Sandoval[22b], D.P.C. Sankey[134], T. Sano[87], A. Sansoni[53], L. Santi[75a,75b], C. Santoni[40], H. Santos[130a,130b], S.N. Santpur[17a], A. Santra[169], K.A. Saoucha[139], J.G. Saraiva[130a,130d], J. Sardain[7], O. Sasaki[83], K. Sato[157], C. Sauer[63b], F. Sauerburger[54], E. Sauvan[4], P. Savard[155,ad], R. Sawada[153], C. Sawyer[134], L. Sawyer[97], I. Sayago Galvan[163], C. Sbarra[23b], A. Sbrizzi[23b,23a], T. Scanlon[96], J. Schaarschmidt[138], P. Schacht[110], D. Schaefer[39], U. Schäfer[100], A.C. Schaffer[66,44], D. Schaile[109], R.D. Schamberger[145], E. Schanet[109], C. Scharf[18], M.M. Schefer[19], V.A. Schegelsky[37], D. Scheirich[133], F. Schenck[18], M. Schernau[160], C. Scheulen[55], C. Schiavi[57b,57a], Z.M. Schillaci[26], E.J. Schioppa[70a,70b], M. Schioppa[43b,43a], B. Schlag[100,al], K.E. Schleicher[54], S. Schlenker[36], J. Schmeing[171], M.A. Schmidt[171], K. Schmieden[100], C. Schmitt[100], S. Schmitt[48], L. Schoeffel[135], A. Schoening[63b], P.G. Scholer[54], E. Schopf[126], M. Schott[100], J. Schovancova[36], S. Schramm[56], F. Schroeder[171], H-C. Schultz-Coulon[63a], M. Schumacher[54], B.A. Schumm[136], Ph. Schune[135], H.R. Schwartz[136], A. Schwartzman[143], T.A. Schwarz[106], Ph. Schwemling[135], R. Schwienhorst[107], A. Sciandra[136], G. Sciolla[26], F. Scuri[74a], F. Scutti[105], C.D. Sebastiani[92], K. Sedlaczek[49], P. Seema[18], S.C. Seidel[112], A. Seiden[136], B.D. Seidlitz[41], C. Seitz[48], J.M. Seixas[82b], G. Sekhniaidze[72a], S.J. Sekula[44], L. Selem[4], N. Semprini-Cesari[23b,23a], S. Sen[51], D. Sengupta[56], V. Senthilkumar[163], L. Serin[66], L. Serkin[69a,69b], M. Sessa[77a,77b], H. Severini[120], F. Sforza[57b,57a], A. Sfyrla[56], E. Shabalina[55], R. Shaheen[144], J.D. Shahinian[128], D. Shaked Renous[169], L.Y. Shan[14a], M. Shapiro[17a], A. Sharma[36], A.S. Sharma[164], P. Sharma[80], S. Sharma[48], P.B. Shatalov[37], K. Shaw[146], S.M. Shaw[101], Q. Shen[62c,5], P. Sherwood[96], L. Shi[96], C.O. Shimmin[172], Y. Shimogama[168], J.D. Shinner[95], I.P.J. Shipsey[126], S. Shirabe[60], M. Shiyakova[38,am], J. Shlomi[169], M.J. Shochet[39], J. Shojaii[105], D.R. Shope[125], S. Shrestha[119,ah], E.M. Shrif[33g], M.J. Shroff[165],

JHEP07(2023)141

P. Sicho[131], A.M. Sickles[162], E. Sideras Haddad[33g], A. Sidoti[23b], F. Siegert[50], Dj. Sijacki[15], R. Sikora[85a], F. Sili[90], J.M. Silva[20], M.V. Silva Oliveira[36], S.B. Silverstein[47a], S. Simion[66], R. Simoniello[36], E.L. Simpson[59], H. Simpson[146], L.R. Simpson[106], N.D. Simpson[98], S. Simsek[21d], S. Sindhu[55], P. Sinervo[155], S. Singh[142], S. Singh[155], S. Sinha[48], S. Sinha[33g], M. Sioli[23b,23a], I. Siral[36], S.Yu. Sivoklokov[37,*], J. Sjölin[47a,47b], A. Skaf[55], E. Skorda[98], P. Skubic[120], M. Slawinska[86], V. Smakhtin[169], B.H. Smart[134], J. Smiesko[36], S.Yu. Smirnov[37], Y. Smirnov[37], L.N. Smirnova[37,a], O. Smirnova[98], A.C. Smith[41], E.A. Smith[39], H.A. Smith[126], J.L. Smith[92], R. Smith[143], M. Smizanska[91], K. Smolek[132], A. Smykiewicz[86], A.A. Snesarev[37], H.L. Snoek[114], S. Snyder[29], R. Sobie[165,x], A. Soffer[151], C.A. Solans Sanchez[36], E.Yu. Soldatov[37], U. Soldevila[163], A.A. Solodkov[37], S. Solomon[54], A. Soloshenko[38], K. Solovieva[54], O.V. Solovyanov[40], V. Solovyev[37], P. Sommer[36], A. Sonay[13], W.Y. Song[156b], J.M. Sonneveld[114], A. Sopczak[132], A.L. Sopio[96], F. Sopkova[28b], V. Sothilingam[63a], S. Sottocornola[68], R. Soualah[116b], Z. Soumaimi[35e], D. South[48], S. Spagnolo[70a,70b], M. Spalla[110], F. Spanò[95], D. Sperlich[54], G. Spigo[36], M. Spina[146], S. Spinali[91], D.P. Spiteri[59], M. Spousta[133], E.J. Staats[34], A. Stabile[71a,71b], R. Stamen[63a], M. Stamenkovic[114], A. Stampekis[20], M. Standke[24], E. Stanecka[86], M.V. Stange[50], B. Stanislaus[17a], M.M. Stanitzki[48], M. Stankaityte[126], B. Stapf[48], E.A. Starchenko[37], G.H. Stark[136], J. Stark[102,ai], D.M. Starko[156b], P. Staroba[131], P. Starovoitov[63a], S. Stärz[104], R. Staszewski[86], G. Stavropoulos[46], J. Steentoft[161], P. Steinberg[29], A.L. Steinhebel[123], B. Stelzer[142,156a], H.J. Stelzer[129], O. Stelzer-Chilton[156a], H. Stenzel[58], T.J. Stevenson[146], G.A. Stewart[36], M.C. Stockton[36], G. Stoicea[27b], M. Stolarski[130a], S. Stonjek[110], A. Straessner[50], J. Strandberg[144], S. Strandberg[47a,47b], M. Strauss[120], T. Strebler[102], P. Strizenec[28b], R. Ströhmer[166], D.M. Strom[123], L.R. Strom[48], R. Stroynowski[44], A. Strubig[47a,47b], S.A. Stucci[29], B. Stugu[16], J. Stupak[120], N.A. Styles[48], D. Su[143], S. Su[62a], W. Su[62d,138,62c], X. Su[62a,66], K. Sugizaki[153], V.V. Sulin[37], M.J. Sullivan[92], D.M.S. Sultan[78a,78b], L. Sultanaliyeva[37], S. Sultansoy[3b], T. Sumida[87], S. Sun[106], S. Sun[170], O. Sunneborn Gudnadottir[161], M.R. Sutton[146], M. Svatos[131], M. Swiatlowski[156a], T. Swirski[166], I. Sykora[28a], M. Sykora[133], T. Sykora[133], D. Ta[100], K. Tackmann[48,v], A. Taffard[160], R. Tafirout[156a], J.S. Tafoya Vargas[66], R.H.M. Taibah[127], R. Takashima[88], K. Takeda[84], E.P. Takeva[52], Y. Takubo[83], M. Talby[102], A.A. Talyshev[37], K.C. Tam[64b], N.M. Tamir[151], A. Tanaka[153], J. Tanaka[153], R. Tanaka[66], M. Tanasini[57b,57a], J. Tang[62c], Z. Tao[164], S. Tapia Araya[137f], S. Tapprogge[100], A. Tarek Abouelfadl Mohamed[107], S. Tarem[150], K. Tariq[62b], G. Tarna[102,27b], G.F. Tartarelli[71a], P. Tas[133], M. Tasevsky[131], E. Tassi[43b,43a], A.C. Tate[162], G. Tateno[153], Y. Tayalati[35e,w], G.N. Taylor[105], W. Taylor[156b], H. Teagle[92], A.S. Tee[170], R. Teixeira De Lima[143], P. Teixeira-Dias[95], J.J. Teoh[155], K. Terashi[153], J. Terron[99], S. Terzo[13], M. Testa[53], R.J. Teuscher[155,x], A. Thaler[79], O. Theiner[56], N. Themistokleous[52], T. Theveneaux-Pelzer[18], O. Thielmann[171], D.W. Thomas[95], J.P. Thomas[20], E.A. Thompson[17a], P.D. Thompson[20], E. Thomson[128], E.J. Thorpe[94], Y. Tian[55], V. Tikhomirov[37,a], Yu.A. Tikhonov[37], S. Timoshenko[37], E.X.L. Ting[1], P. Tipton[172], S. Tisserant[102], S.H. Tlou[33g], A. Tnourji[40], K. Todome[23b,23a], S. Todorova-Nova[133],

JHEP07(2023)141

S. Todt[50], M. Togawa[83], J. Tojo[89], S. Tokár[28a], K. Tokushuku[83], O. Toldaiev[68], R. Tombs[32], M. Tomoto[83,111], L. Tompkins[143,al], K.W. Topolnicki[85b], P. Tornambe[103], E. Torrence[123], H. Torres[50,ai], E. Torró Pastor[163], M. Toscani[30], C. Tosciri[39], M. Tost[11], D.R. Tovey[139], A. Traeet[16], I.S. Trandafir[27b], T. Trefzger[166], A. Tricoli[29], I.M. Trigger[156a], S. Trincaz-Duvoid[127], D.A. Trischuk[26], B. Trocmé[60], C. Troncon[71a], L. Truong[33c], M. Trzebinski[86], A. Trzupek[86], F. Tsai[145], M. Tsai[106], A. Tsiamis[152,f], P.V. Tsiareshka[37], S. Tsigaridas[156a], A. Tsirigotis[152,t], V. Tsiskaridze[145], E.G. Tskhadadze[149a], M. Tsopoulou[152,f], Y. Tsujikawa[87], I.I. Tsukerman[37], V. Tsulaia[17a], S. Tsuno[83], O. Tsur[150], D. Tsybychev[145], Y. Tu[64b], A. Tudorache[27b], V. Tudorache[27b], A.N. Tuna[36], S. Turchikhin[38], I. Turk Cakir[3a], R. Turra[71a], T. Turtuvshin[38,y], P.M. Tuts[41], S. Tzamarias[152,f], P. Tzanis[10], E. Tzovara[100], K. Uchida[153], F. Ukegawa[157], P.A. Ulloa Poblete[137c], E.N. Umaka[29], G. Unal[36], M. Unal[11], A. Undrus[29], G. Unel[160], J. Urban[28b], P. Urquijo[105], G. Usai[8], R. Ushioda[154], M. Usman[108], Z. Uysal[21b], L. Vacavant[102], V. Vacek[132], B. Vachon[104], K.O.H. Vadla[125], T. Vafeiadis[36], A. Vaitkus[96], C. Valderanis[109], E. Valdes Santurio[47a,47b], M. Valente[156a], S. Valentinetti[23b,23a], A. Valero[163], A. Vallier[102,ai], J.A. Valls Ferrer[163], D.R. Van Arneman[114], T.R. Van Daalen[138], P. Van Gemmeren[6], M. Van Rijnbach[125,36], S. Van Stroud[96], I. Van Vulpen[114], M. Vanadia[76a,76b], W. Vandelli[36], M. Vandenbroucke[135], E.R. Vandewall[121], D. Vannicola[151], L. Vannoli[57b,57a], R. Vari[75a], E.W. Varnes[7], C. Varni[17a], T. Varol[148], D. Varouchas[66], L. Varriale[163], K.E. Varvell[147], M.E. Vasile[27b], L. Vaslin[40], G.A. Vasquez[165], F. Vazeille[40], T. Vazquez Schroeder[36], J. Veatch[31], V. Vecchio[101], M.J. Veen[103], I. Veliscek[126], L.M. Veloce[155], F. Veloso[130a,130c], S. Veneziano[75a], A. Ventura[70a,70b], A. Verbytskyi[110], M. Verducci[74a,74b], C. Vergis[24], M. Verissimo De Araujo[82b], W. Verkerke[114], J.C. Vermeulen[114], C. Vernieri[143], P.J. Verschuuren[95], M. Vessella[103], M.C. Vetterli[142,ad], A. Vgenopoulos[152,f], N. Viaux Maira[137f], T. Vickey[139], O.E. Vickey Boeriu[139], G.H.A. Viehhauser[126], L. Vigani[63b], M. Villa[23b,23a], M. Villaplana Perez[163], E.M. Villhauer[52], E. Vilucchi[53], M.G. Vincter[34], G.S. Virdee[20], A. Vishwakarma[52], C. Vittori[36], I. Vivarelli[146], V. Vladimirov[167], E. Voevodina[110], F. Vogel[109], P. Vokac[132], J. Von Ahnen[48], E. Von Toerne[24], B. Vormwald[36], V. Vorobel[133], K. Vorobev[37], M. Vos[163], K. Voss[141], J.H. Vossebeld[92], M. Vozak[114], L. Vozdecky[94], N. Vranjes[15], M. Vranjes Milosavljevic[15], M. Vreeswijk[114], R. Vuillermet[36], O. Vujinovic[100], I. Vukotic[39], S. Wada[157], C. Wagner[103], W. Wagner[171], S. Wahdan[171], H. Wahlberg[90], R. Wakasa[157], M. Wakida[111], V.M. Walbrecht[110], J. Walder[134], R. Walker[109], W. Walkowiak[141], A.M. Wang[61], A.Z. Wang[170], C. Wang[100], C. Wang[62c], H. Wang[17a], J. Wang[64a], R.-J. Wang[100], R. Wang[61], R. Wang[6], S.M. Wang[148], S. Wang[62b], T. Wang[62a], W.T. Wang[80], X. Wang[14c], X. Wang[162], X. Wang[62c], Y. Wang[62d], Y. Wang[14c], Z. Wang[106], Z. Wang[62d,51,62c], Z. Wang[106], A. Warburton[104], R.J. Ward[20], N. Warrack[59], A.T. Watson[20], H. Watson[59], M.F. Watson[20], G. Watts[138], B.M. Waugh[96], A.F. Webb[11], C. Weber[29], H.A. Weber[18], M.S. Weber[19], S.M. Weber[63a], C. Wei[62a], Y. Wei[126], A.R. Weidberg[126], J. Weingarten[49], M. Weirich[100], C. Weiser[54], C.J. Wells[48], T. Wenaus[29],

JHEP07(2023)141

B. Wendland[49], T. Wengler[36], N.S. Wenke[110], N. Wermes[24], M. Wessels[63a], K. Whalen[123], A.M. Wharton[91], A.S. White[61], A. White[8], M.J. White[1], D. Whiteson[160], L. Wickremasinghe[124], W. Wiedenmann[170], C. Wiel[50], M. Wielers[134], C. Wiglesworth[42], L.A.M. Wiik-Fuchs[54], D.J. Wilbern[120], H.G. Wilkens[36], D.M. Williams[41], H.H. Williams[128], S. Williams[32], S. Willocq[103], P.J. Windischhofer[126], F. Winklmeier[123], B.T. Winter[54], J.K. Winter[101], M. Wittgen[143], M. Wobisch[97], R. Wölker[126], J. Wollrath[160], M.W. Wolter[86], H. Wolters[130a,130c], V.W.S. Wong[164], A.F. Wongel[48], S.D. Worm[48], B.K. Wosiek[86], K.W. Woźniak[86], K. Wraight[59], J. Wu[14a,14d], M. Wu[64a], M. Wu[113], S.L. Wu[170], X. Wu[56], Y. Wu[62a], Z. Wu[135,62a], J. Wuerzinger[126], T.R. Wyatt[101], B.M. Wynne[52], S. Xella[42], L. Xia[14c], M. Xia[14b], J. Xiang[64c], X. Xiao[106], M. Xie[62a], X. Xie[62a], S. Xin[14a,14d], J. Xiong[17a], I. Xiotidis[146], D. Xu[14a], H. Xu[62a], H. Xu[62a], L. Xu[62a], R. Xu[128], T. Xu[106], W. Xu[106], Y. Xu[14b], Z. Xu[62b], Z. Xu[14a], B. Yabsley[147], S. Yacoob[33a], N. Yamaguchi[89], Y. Yamaguchi[154], H. Yamauchi[157], T. Yamazaki[17a], Y. Yamazaki[84], J. Yan[62c], S. Yan[126], Z. Yan[25], H.J. Yang[62c,62d], H.T. Yang[62a], S. Yang[62a], T. Yang[64c], X. Yang[62a], X. Yang[14a], Y. Yang[44], Y. Yang[62a], Z. Yang[62a,106], W-M. Yao[17a], Y.C. Yap[48], H. Ye[14c], H. Ye[55], J. Ye[44], S. Ye[29], X. Ye[62a], Y. Yeh[96], I. Yeletskikh[38], B.K. Yeo[17a], M.R. Yexley[91], P. Yin[41], K. Yorita[168], S. Younas[27b], C.J.S. Young[54], C. Young[143], Y. Yu[62a], M. Yuan[106], R. Yuan[62b,l], L. Yue[96], X. Yue[63a], M. Zaazoua[35e], B. Zabinski[86], E. Zaid[52], T. Zakareishvili[149b], N. Zakharchuk[34], S. Zambito[56], J.A. Zamora Saa[137d,137b], J. Zang[153], D. Zanzi[54], O. Zaplatilek[132], S.V. Zeißner[49], C. Zeitnitz[171], J.C. Zeng[162], D.T. Zenger Jr[26], O. Zenin[37], T. Ženiš[28a], S. Zenz[94], S. Zerradi[35a], D. Zerwas[66], M. Zhai[14a,14d], B. Zhang[14c], D.F. Zhang[139], J. Zhang[62b], J. Zhang[6], K. Zhang[14a,14d], L. Zhang[14c], P. Zhang[14a,14d], R. Zhang[170], S. Zhang[106], T. Zhang[153], X. Zhang[62c], X. Zhang[62b], Y. Zhang[62c,5], Z. Zhang[17a], Z. Zhang[66], H. Zhao[138], P. Zhao[51], T. Zhao[62b], Y. Zhao[136], Z. Zhao[62a], A. Zhemchugov[38], X. Zheng[62a], Z. Zheng[143], D. Zhong[162], B. Zhou[106], C. Zhou[170], H. Zhou[7], N. Zhou[62c], Y. Zhou[7], C.G. Zhu[62b], C. Zhu[14a,14d], H.L. Zhu[62a], H. Zhu[14a], J. Zhu[106], Y. Zhu[62c], Y. Zhu[62a], X. Zhuang[14a], K. Zhukov[37], V. Zhulanov[37], N.I. Zimine[38], J. Zinsser[63b], M. Ziolkowski[141], L. Živković[15], A. Zoccoli[23b,23a], K. Zoch[56], T.G. Zorbas[139], O. Zormpa[46], W. Zou[41], L. Zwalinski[36]

[1] *Department of Physics, University of Adelaide, Adelaide; Australia*
[2] *Department of Physics, University of Alberta, Edmonton AB; Canada*
[3] [(a)] *Department of Physics, Ankara University, Ankara;* [(b)] *Division of Physics, TOBB University of Economics and Technology, Ankara; Türkiye*
[4] *LAPP, Université Savoie Mont Blanc, CNRS/IN2P3, Annecy; France*
[5] *APC, Université Paris Cité, CNRS/IN2P3, Paris; France*
[6] *High Energy Physics Division, Argonne National Laboratory, Argonne IL; United States of America*
[7] *Department of Physics, University of Arizona, Tucson AZ; United States of America*
[8] *Department of Physics, University of Texas at Arlington, Arlington TX; United States of America*
[9] *Physics Department, National and Kapodistrian University of Athens, Athens; Greece*
[10] *Physics Department, National Technical University of Athens, Zografou; Greece*
[11] *Department of Physics, University of Texas at Austin, Austin TX; United States of America*

JHEP07(2023)141

[12] Institute of Physics, Azerbaijan Academy of Sciences, Baku; Azerbaijan
[13] Institut de Física d'Altes Energies (IFAE), Barcelona Institute of Science and Technology, Barcelona; Spain
[14] [(a)] Institute of High Energy Physics, Chinese Academy of Sciences, Beijing; [(b)] Physics Department, Tsinghua University, Beijing; [(c)] Department of Physics, Nanjing University, Nanjing; [(d)] University of Chinese Academy of Science (UCAS), Beijing; China
[15] Institute of Physics, University of Belgrade, Belgrade; Serbia
[16] Department for Physics and Technology, University of Bergen, Bergen; Norway
[17] [(a)] Physics Division, Lawrence Berkeley National Laboratory, Berkeley CA; [(b)] University of California, Berkeley CA; United States of America
[18] Institut für Physik, Humboldt Universität zu Berlin, Berlin; Germany
[19] Albert Einstein Center for Fundamental Physics and Laboratory for High Energy Physics, University of Bern, Bern; Switzerland
[20] School of Physics and Astronomy, University of Birmingham, Birmingham; United Kingdom
[21] [(a)] Department of Physics, Bogazici University, Istanbul; [(b)] Department of Physics Engineering, Gaziantep University, Gaziantep; [(c)] Department of Physics, Istanbul University, Istanbul; [(d)] Istinye University, Sariyer, Istanbul; Türkiye
[22] [(a)] Facultad de Ciencias y Centro de Investigaciónes, Universidad Antonio Nariño, Bogotá; [(b)] Departamento de Física, Universidad Nacional de Colombia, Bogotá; Colombia
[23] [(a)] Dipartimento di Fisica e Astronomia A. Righi, Università di Bologna, Bologna; [(b)] INFN Sezione di Bologna; Italy
[24] Physikalisches Institut, Universität Bonn, Bonn; Germany
[25] Department of Physics, Boston University, Boston MA; United States of America
[26] Department of Physics, Brandeis University, Waltham MA; United States of America
[27] [(a)] Transilvania University of Brasov, Brasov; [(b)] Horia Hulubei National Institute of Physics and Nuclear Engineering, Bucharest; [(c)] Department of Physics, Alexandru Ioan Cuza University of Iasi, Iasi; [(d)] National Institute for Research and Development of Isotopic and Molecular Technologies, Physics Department, Cluj-Napoca; [(e)] University Politehnica Bucharest, Bucharest; [(f)] West University in Timisoara, Timisoara; [(g)] Faculty of Physics, University of Bucharest, Bucharest; Romania
[28] [(a)] Faculty of Mathematics, Physics and Informatics, Comenius University, Bratislava; [(b)] Department of Subnuclear Physics, Institute of Experimental Physics of the Slovak Academy of Sciences, Kosice; Slovak Republic
[29] Physics Department, Brookhaven National Laboratory, Upton NY; United States of America
[30] Universidad de Buenos Aires, Facultad de Ciencias Exactas y Naturales, Departamento de Física, y CONICET, Instituto de Física de Buenos Aires (IFIBA), Buenos Aires; Argentina
[31] California State University, CA; United States of America
[32] Cavendish Laboratory, University of Cambridge, Cambridge; United Kingdom
[33] [(a)] Department of Physics, University of Cape Town, Cape Town; [(b)] iThemba Labs, Western Cape; [(c)] Department of Mechanical Engineering Science, University of Johannesburg, Johannesburg; [(d)] National Institute of Physics, University of the Philippines Diliman, Philippines; [(e)] University of South Africa, Department of Physics, Pretoria; [(f)] University of Zululand, KwaDlangezwa; [(g)] School of Physics, University of the Witwatersrand, Johannesburg; South Africa
[34] Department of Physics, Carleton University, Ottawa ON; Canada
[35] [(a)] Faculté des Sciences Ain Chock, Réseau Universitaire de Physique des Hautes Energies — Université Hassan II, Casablanca; [(b)] Faculté des Sciences, Université Ibn-Tofail, Kénitra; [(c)] Faculté des Sciences Semlalia, Université Cadi Ayyad, LPHEA-Marrakech; [(d)] LPMR, Faculté des Sciences, Université Mohamed Premier, Oujda; [(e)] Faculté des sciences, Université Mohammed V, Rabat; [(f)] Institute of Applied Physics, Mohammed VI Polytechnic University, Ben Guerir; Morocco
[36] CERN, Geneva; Switzerland
[37] Affiliated with an institute covered by a cooperation agreement with CERN
[38] Affiliated with an international laboratory covered by a cooperation agreement with CERN
[39] Enrico Fermi Institute, University of Chicago, Chicago IL; United States of America

JHEP07(2023)141

[40] LPC, Université Clermont Auvergne, CNRS/IN2P3, Clermont-Ferrand; France
[41] Nevis Laboratory, Columbia University, Irvington NY; United States of America
[42] Niels Bohr Institute, University of Copenhagen, Copenhagen; Denmark
[43] [(a)] Dipartimento di Fisica, Università della Calabria, Rende;[(b)] INFN Gruppo Collegato di Cosenza, Laboratori Nazionali di Frascati; Italy
[44] Physics Department, Southern Methodist University, Dallas TX; United States of America
[45] Physics Department, University of Texas at Dallas, Richardson TX; United States of America
[46] National Centre for Scientific Research "Demokritos", Agia Paraskevi; Greece
[47] [(a)] Department of Physics, Stockholm University;[(b)] Oskar Klein Centre, Stockholm; Sweden
[48] Deutsches Elektronen-Synchrotron DESY, Hamburg and Zeuthen; Germany
[49] Fakultät Physik, Technische Universität Dortmund, Dortmund; Germany
[50] Institut für Kern- und Teilchenphysik, Technische Universität Dresden, Dresden; Germany
[51] Department of Physics, Duke University, Durham NC; United States of America
[52] SUPA — School of Physics and Astronomy, University of Edinburgh, Edinburgh; United Kingdom
[53] INFN e Laboratori Nazionali di Frascati, Frascati; Italy
[54] Physikalisches Institut, Albert-Ludwigs-Universität Freiburg, Freiburg; Germany
[55] II. Physikalisches Institut, Georg-August-Universität Göttingen, Göttingen; Germany
[56] Département de Physique Nucléaire et Corpusculaire, Université de Genève, Genève; Switzerland
[57] [(a)] Dipartimento di Fisica, Università di Genova, Genova;[(b)] INFN Sezione di Genova; Italy
[58] II. Physikalisches Institut, Justus-Liebig-Universität Giessen, Giessen; Germany
[59] SUPA — School of Physics and Astronomy, University of Glasgow, Glasgow; United Kingdom
[60] LPSC, Université Grenoble Alpes, CNRS/IN2P3, Grenoble INP, Grenoble; France
[61] Laboratory for Particle Physics and Cosmology, Harvard University, Cambridge MA; United States of America
[62] [(a)] Department of Modern Physics and State Key Laboratory of Particle Detection and Electronics, University of Science and Technology of China, Hefei;[(b)] Institute of Frontier and Interdisciplinary Science and Key Laboratory of Particle Physics and Particle Irradiation (MOE), Shandong University, Qingdao;[(c)] School of Physics and Astronomy, Shanghai Jiao Tong University, Key Laboratory for Particle Astrophysics and Cosmology (MOE), SKLPPC, Shanghai;[(d)] Tsung-Dao Lee Institute, Shanghai; China
[63] [(a)] Kirchhoff-Institut für Physik, Ruprecht-Karls-Universität Heidelberg, Heidelberg;[(b)] Physikalisches Institut, Ruprecht-Karls-Universität Heidelberg, Heidelberg; Germany
[64] [(a)] Department of Physics, Chinese University of Hong Kong, Shatin, N.T., Hong Kong;[(b)] Department of Physics, University of Hong Kong, Hong Kong;[(c)] Department of Physics and Institute for Advanced Study, Hong Kong University of Science and Technology, Clear Water Bay, Kowloon, Hong Kong; China
[65] Department of Physics, National Tsing Hua University, Hsinchu; Taiwan
[66] IJCLab, Université Paris-Saclay, CNRS/IN2P3, 91405, Orsay; France
[67] Centro Nacional de Microelectrónica (IMB-CNM-CSIC), Barcelona; Spain
[68] Department of Physics, Indiana University, Bloomington IN; United States of America
[69] [(a)] INFN Gruppo Collegato di Udine, Sezione di Trieste, Udine;[(b)] ICTP, Trieste;[(c)] Dipartimento Politecnico di Ingegneria e Architettura, Università di Udine, Udine; Italy
[70] [(a)] INFN Sezione di Lecce;[(b)] Dipartimento di Matematica e Fisica, Università del Salento, Lecce; Italy
[71] [(a)] INFN Sezione di Milano;[(b)] Dipartimento di Fisica, Università di Milano, Milano; Italy
[72] [(a)] INFN Sezione di Napoli;[(b)] Dipartimento di Fisica, Università di Napoli, Napoli; Italy
[73] [(a)] INFN Sezione di Pavia;[(b)] Dipartimento di Fisica, Università di Pavia, Pavia; Italy
[74] [(a)] INFN Sezione di Pisa;[(b)] Dipartimento di Fisica E. Fermi, Università di Pisa, Pisa; Italy
[75] [(a)] INFN Sezione di Roma;[(b)] Dipartimento di Fisica, Sapienza Università di Roma, Roma; Italy
[76] [(a)] INFN Sezione di Roma Tor Vergata;[(b)] Dipartimento di Fisica, Università di Roma Tor Vergata, Roma; Italy
[77] [(a)] INFN Sezione di Roma Tre;[(b)] Dipartimento di Matematica e Fisica, Università Roma Tre, Roma; Italy

JHEP07(2023)141

[78] [(a)] INFN-TIFPA;[(b)] Università degli Studi di Trento, Trento; Italy
[79] Universität Innsbruck, Department of Astro and Particle Physics, Innsbruck; Austria
[80] University of Iowa, Iowa City IA; United States of America
[81] Department of Physics and Astronomy, Iowa State University, Ames IA; United States of America
[82] [(a)] Departamento de Engenharia Elétrica, Universidade Federal de Juiz de Fora (UFJF), Juiz de Fora;[(b)] Universidade Federal do Rio De Janeiro COPPE/EE/IF, Rio de Janeiro;[(c)] Instituto de Física, Universidade de São Paulo, São Paulo;[(d)] Rio de Janeiro State University, Rio de Janeiro; Brazil
[83] KEK, High Energy Accelerator Research Organization, Tsukuba; Japan
[84] Graduate School of Science, Kobe University, Kobe; Japan
[85] [(a)] AGH University of Science and Technology, Faculty of Physics and Applied Computer Science, Krakow;[(b)] Marian Smoluchowski Institute of Physics, Jagiellonian University, Krakow; Poland
[86] Institute of Nuclear Physics Polish Academy of Sciences, Krakow; Poland
[87] Faculty of Science, Kyoto University, Kyoto; Japan
[88] Kyoto University of Education, Kyoto; Japan
[89] Research Center for Advanced Particle Physics and Department of Physics, Kyushu University, Fukuoka; Japan
[90] Instituto de Física La Plata, Universidad Nacional de La Plata and CONICET, La Plata; Argentina
[91] Physics Department, Lancaster University, Lancaster; United Kingdom
[92] Oliver Lodge Laboratory, University of Liverpool, Liverpool; United Kingdom
[93] Department of Experimental Particle Physics, Jožef Stefan Institute and Department of Physics, University of Ljubljana, Ljubljana; Slovenia
[94] School of Physics and Astronomy, Queen Mary University of London, London; United Kingdom
[95] Department of Physics, Royal Holloway University of London, Egham; United Kingdom
[96] Department of Physics and Astronomy, University College London, London; United Kingdom
[97] Louisiana Tech University, Ruston LA; United States of America
[98] Fysiska institutionen, Lunds universitet, Lund; Sweden
[99] Departamento de Física Teorica C-15 and CIAFF, Universidad Autónoma de Madrid, Madrid; Spain
[100] Institut für Physik, Universität Mainz, Mainz; Germany
[101] School of Physics and Astronomy, University of Manchester, Manchester; United Kingdom
[102] CPPM, Aix-Marseille Université, CNRS/IN2P3, Marseille; France
[103] Department of Physics, University of Massachusetts, Amherst MA; United States of America
[104] Department of Physics, McGill University, Montreal QC; Canada
[105] School of Physics, University of Melbourne, Victoria; Australia
[106] Department of Physics, University of Michigan, Ann Arbor MI; United States of America
[107] Department of Physics and Astronomy, Michigan State University, East Lansing MI; United States of America
[108] Group of Particle Physics, University of Montreal, Montreal QC; Canada
[109] Fakultät für Physik, Ludwig-Maximilians-Universität München, München; Germany
[110] Max-Planck-Institut für Physik (Werner-Heisenberg-Institut), München; Germany
[111] Graduate School of Science and Kobayashi-Maskawa Institute, Nagoya University, Nagoya; Japan
[112] Department of Physics and Astronomy, University of New Mexico, Albuquerque NM; United States of America
[113] Institute for Mathematics, Astrophysics and Particle Physics, Radboud University/Nikhef, Nijmegen; Netherlands
[114] Nikhef National Institute for Subatomic Physics and University of Amsterdam, Amsterdam; Netherlands
[115] Department of Physics, Northern Illinois University, DeKalb IL; United States of America
[116] [(a)] New York University Abu Dhabi, Abu Dhabi;[(b)] University of Sharjah, Sharjah; United Arab Emirates
[117] Department of Physics, New York University, New York NY; United States of America
[118] Ochanomizu University, Otsuka, Bunkyo-ku, Tokyo; Japan
[119] Ohio State University, Columbus OH; United States of America

JHEP07(2023)141

[120] Homer L. Dodge Department of Physics and Astronomy, University of Oklahoma, Norman OK; United States of America
[121] Department of Physics, Oklahoma State University, Stillwater OK; United States of America
[122] Palacký University, Joint Laboratory of Optics, Olomouc; Czech Republic
[123] Institute for Fundamental Science, University of Oregon, Eugene, OR; United States of America
[124] Graduate School of Science, Osaka University, Osaka; Japan
[125] Department of Physics, University of Oslo, Oslo; Norway
[126] Department of Physics, Oxford University, Oxford; United Kingdom
[127] LPNHE, Sorbonne Université, Université Paris Cité, CNRS/IN2P3, Paris; France
[128] Department of Physics, University of Pennsylvania, Philadelphia PA; United States of America
[129] Department of Physics and Astronomy, University of Pittsburgh, Pittsburgh PA; United States of America
[130] [(a)] Laboratório de Instrumentação e Física Experimental de Partículas — LIP, Lisboa;[(b)] Departamento de Física, Faculdade de Ciências, Universidade de Lisboa, Lisboa;[(c)] Departamento de Física, Universidade de Coimbra, Coimbra;[(d)] Centro de Física Nuclear da Universidade de Lisboa, Lisboa;[(e)] Departamento de Física, Universidade do Minho, Braga;[(f)] Departamento de Física Teórica y del Cosmos, Universidad de Granada, Granada (Spain);[(g)] Departamento de Física, Instituto Superior Técnico, Universidade de Lisboa, Lisboa; Portugal
[131] Institute of Physics of the Czech Academy of Sciences, Prague; Czech Republic
[132] Czech Technical University in Prague, Prague; Czech Republic
[133] Charles University, Faculty of Mathematics and Physics, Prague; Czech Republic
[134] Particle Physics Department, Rutherford Appleton Laboratory, Didcot; United Kingdom
[135] IRFU, CEA, Université Paris-Saclay, Gif-sur-Yvette; France
[136] Santa Cruz Institute for Particle Physics, University of California Santa Cruz, Santa Cruz CA; United States of America
[137] [(a)] Departamento de Física, Pontificia Universidad Católica de Chile, Santiago;[(b)] Millennium Institute for Subatomic physics at high energy frontier (SAPHIR), Santiago;[(c)] Instituto de Investigación Multidisciplinario en Ciencia y Tecnología, y Departamento de Física, Universidad de La Serena;[(d)] Universidad Andres Bello, Department of Physics, Santiago;[(e)] Instituto de Alta Investigación, Universidad de Tarapacá, Arica;[(f)] Departamento de Física, Universidad Técnica Federico Santa María, Valparaíso; Chile
[138] Department of Physics, University of Washington, Seattle WA; United States of America
[139] Department of Physics and Astronomy, University of Sheffield, Sheffield; United Kingdom
[140] Department of Physics, Shinshu University, Nagano; Japan
[141] Department Physik, Universität Siegen, Siegen; Germany
[142] Department of Physics, Simon Fraser University, Burnaby BC; Canada
[143] SLAC National Accelerator Laboratory, Stanford CA; United States of America
[144] Department of Physics, Royal Institute of Technology, Stockholm; Sweden
[145] Departments of Physics and Astronomy, Stony Brook University, Stony Brook NY; United States of America
[146] Department of Physics and Astronomy, University of Sussex, Brighton; United Kingdom
[147] School of Physics, University of Sydney, Sydney; Australia
[148] Institute of Physics, Academia Sinica, Taipei; Taiwan
[149] [(a)] E. Andronikashvili Institute of Physics, Iv. Javakhishvili Tbilisi State University, Tbilisi;[(b)] High Energy Physics Institute, Tbilisi State University, Tbilisi;[(c)] University of Georgia, Tbilisi; Georgia
[150] Department of Physics, Technion, Israel Institute of Technology, Haifa; Israel
[151] Raymond and Beverly Sackler School of Physics and Astronomy, Tel Aviv University, Tel Aviv; Israel
[152] Department of Physics, Aristotle University of Thessaloniki, Thessaloniki; Greece
[153] International Center for Elementary Particle Physics and Department of Physics, University of Tokyo, Tokyo; Japan
[154] Department of Physics, Tokyo Institute of Technology, Tokyo; Japan
[155] Department of Physics, University of Toronto, Toronto ON; Canada

JHEP07(2023)141

[156] [(a)] TRIUMF, Vancouver BC; [(b)] Department of Physics and Astronomy, York University, Toronto ON; Canada
[157] Division of Physics and Tomonaga Center for the History of the Universe, Faculty of Pure and Applied Sciences, University of Tsukuba, Tsukuba; Japan
[158] Department of Physics and Astronomy, Tufts University, Medford MA; United States of America
[159] United Arab Emirates University, Al Ain; United Arab Emirates
[160] Department of Physics and Astronomy, University of California Irvine, Irvine CA; United States of America
[161] Department of Physics and Astronomy, University of Uppsala, Uppsala; Sweden
[162] Department of Physics, University of Illinois, Urbana IL; United States of America
[163] Instituto de Física Corpuscular (IFIC), Centro Mixto Universidad de Valencia — CSIC, Valencia; Spain
[164] Department of Physics, University of British Columbia, Vancouver BC; Canada
[165] Department of Physics and Astronomy, University of Victoria, Victoria BC; Canada
[166] Fakultät für Physik und Astronomie, Julius-Maximilians-Universität Würzburg, Würzburg; Germany
[167] Department of Physics, University of Warwick, Coventry; United Kingdom
[168] Waseda University, Tokyo; Japan
[169] Department of Particle Physics and Astrophysics, Weizmann Institute of Science, Rehovot; Israel
[170] Department of Physics, University of Wisconsin, Madison WI; United States of America
[171] Fakultät für Mathematik und Naturwissenschaften, Fachgruppe Physik, Bergische Universität Wuppertal, Wuppertal; Germany
[172] Department of Physics, Yale University, New Haven CT; United States of America

[a] Also Affiliated with an institute covered by a cooperation agreement with CERN
[b] Also at An-Najah National University, Nablus; Palestine
[c] Also at Borough of Manhattan Community College, City University of New York, New York NY; United States of America
[d] Also at Bruno Kessler Foundation, Trento; Italy
[e] Also at Center for High Energy Physics, Peking University; China
[f] Also at Center for Interdisciplinary Research and Innovation (CIRI-AUTH), Thessaloniki; Greece
[g] Also at Centro Studi e Ricerche Enrico Fermi; Italy
[h] Also at CERN, Geneva; Switzerland
[i] Also at Département de Physique Nucléaire et Corpusculaire, Université de Genève, Genève; Switzerland
[j] Also at Departament de Fisica de la Universitat Autonoma de Barcelona, Barcelona; Spain
[k] Also at Department of Financial and Management Engineering, University of the Aegean, Chios; Greece
[l] Also at Department of Physics and Astronomy, Michigan State University, East Lansing MI; United States of America
[m] Also at Department of Physics, Ben Gurion University of the Negev, Beer Sheva; Israel
[n] Also at Department of Physics, California State University, East Bay; United States of America
[o] Also at Department of Physics, California State University, Sacramento; United States of America
[p] Also at Department of Physics, King's College London, London; United Kingdom
[q] Also at Department of Physics, University of Fribourg, Fribourg; Switzerland
[r] Also at Department of Physics, University of Thessaly; Greece
[s] Also at Department of Physics, Westmont College, Santa Barbara; United States of America
[t] Also at Hellenic Open University, Patras; Greece
[u] Also at Institucio Catalana de Recerca i Estudis Avancats, ICREA, Barcelona; Spain
[v] Also at Institut für Experimentalphysik, Universität Hamburg, Hamburg; Germany
[w] Also at Institute of Applied Physics, Mohammed VI Polytechnic University, Ben Guerir; Morocco
[x] Also at Institute of Particle Physics (IPP); Canada
[y] Also at Institute of Physics and Technology, Ulaanbaatar; Mongolia
[z] Also at Institute of Physics, Azerbaijan Academy of Sciences, Baku; Azerbaijan

JHEP07(2023)141

[aa] Also at Institute of Theoretical Physics, Ilia State University, Tbilisi; Georgia
[ab] Also at Lawrence Livermore National Laboratory, Livermore; United States of America
[ac] Also at The Collaborative Innovation Center of Quantum Matter (CICQM), Beijing; China
[ad] Also at TRIUMF, Vancouver BC; Canada
[ae] Also at Università di Napoli Parthenope, Napoli; Italy
[af] Also at University of Chinese Academy of Sciences (UCAS), Beijing; China
[ag] Also at University of Colorado Boulder, Department of Physics, Colorado; United States of America
[ah] Also at Washington College, Maryland; United States of America
[ai] Also at L2IT, Université de Toulouse, CNRS/IN2P3, UPS, Toulouse, France
[aj] Also at Technical University of Munich, Munich, Germany
[ak] Also at Yeditepe University, Physics Department, Istanbul, Türkiye
[al] Also at Department of Physics, Stanford University, Stanford CA, United States of America
[am] Also at Institute for Nuclear Research and Nuclear Energy (INRNE) of the Bulgarian Academy of Sciences, Sofia; Bulgaria
[*] Deceased

JHEP07(2023)141